warwick.ac.uk/lib-publications

Optimisation and Attainability of Magnetometry with Qubit Probes

by

Jamie Francis Friel

Thesis

Submitted to the University of Warwick

for the degree of

Doctor of Philosophy in Physics

Department of Physics

January 2022

My candle burns at both ends it will
not last the night but arh my friends
and oh my foes it gives a lovely light

<hr>

Edna St. Vincent Millay

Contents

List of Figures

List of Tables

Acknowledgements

I am a profoundly lucky person to have the people in my life that I do. The only downside of this is how many people I have to thank in these acknowledgements and how many unique superlatives I need to find.

I want to start with my parents. When I was a child, I was never in want of a book and I was explicitly told my parents would make any sacrifices required for my education. As far as I am concerned, this is a greatest privilege possible to bestow on a child. My curiosity and interests in the worlds of mathematics and science were continuously stoked and supported. Their support continued from childhood and is yet to end. It is no exaggeration to say this wouldn't have happened without your support.

My partner, Cat. Thank you for listen to me ramble about cryptic calculations endlessly. You have made my life better in every aspect. I am writing this with a bowl of your French chicken soup that would rival Jacques Pepin's, you kept me going. I'm a better person, a happier one and my life is better for you in it. Is there anything else I need to add to make your importance to me clear?

Pip, "my first coauthor". I am truly indebted to Pip, he was the person that aged 13 convinced me that doing experiments with mains electricity was a poor life choice and instead to build some red stone circuits in minecraft. You are the reason I am a living theorist and not a dead experimentalist. I could write for hours on the impact Pip has had on my academic and personal development, but I hope that preventing an early electric death makes Pip's significance to my life clear.

The remaining Fromies, "the gravy", Molley, Liam, Brad, Sam and Ollie. Not sure what I did in a past life to find such a group of people aged 4 (give or take a few late joiners), but it was something pretty good. Something on the order of discovering penicillin.

Before thanking the people of Aberystwyth, I have to thank the mathematics department. My AS exams were a poor time to choose to have a teenage rebellion phase. Beyond my results, Aberystwyth University mathematics department gave

the opportunity to demonstrate my love of mathematics and physics with entrance exams, guaranteeing my continued education in the only subject I've been so deeply passionate for. Thank you Aberystwyth for allowing me to demonstrate my passion and ability for mathematics and physics.

The greatest chess team Aber has ever seen, Robbie, James and Adam. Thank you spice boys. Then and now, with or without chess, your support and friendship has meant more to me than I can express. My fellow mathematicians, Damien, Ryan, Tom and Dan. A group of people driven by competitiveness and camaraderie from whence I derived motivation the become a better mathematician than I thought I could become. It is well known fact that you cannot complete a degree without all night horror movie marathons, thank you Jemma and Ben for ensuring a fully met these requirements.

To my research group and further Warwick people, thank you, thank you. I formed probably my most productive academic relationship with Francesco at Warwick. Francesco's mentorship and long whiteboard discussion sessions were essential to my growth as a researcher. Dominic, thank you for saving my LaTeX, once a week every week for three years. My remaining office companions, Sam, Eva and Nelson, you truly kept me sane.

My first manager, Dan Cosser. Dan's incredible mentorship taught me aspects of programming I didn't know I didn't know. This has equipped me with the skills needed to take the code I developed for this thesis into something that is maintainable and useful for many years to come. I am currently and I know will continue to use the lessons you taught me on a daily basis. This is just the beginning!

My two academic supervisors, Animesh Datta and Daniel Burgarth. Daniel introduces me to quantum information theory though his courses at Aberystwyth. Beyond that, when as an undergrad I thought I had an exciting research idea (that turned out to be immediately nonsense), Daniel nurtured my curiosity and introduced me to research, instead of disregarding the rambling of an overly excitable undergrad. I was able to leave Plato's quantum cave and see the trees! I see as a key moment in my academic development, it has formed part of my motivation and inspiration this entire time. Thank you Animesh, for your guidance and supervision during my PhD. In particular your laser keen eye for finding the corners of a piece of work that can be taken and expanded into something even greater. There are two greatly important skills you taught me, how to assess research ideas, knowing where to spend our limited energy and also how to find and correct subtle errors in new work. Without these skills and supervision this thesis would be incomplete and incorrect.

Finally, I want to thank my PhD examiners, Ben Green and Mădălin Guţă. Their patient reading of this thesis has helped sculpt it into something I can be truly proud of. I am so very grateful for the time and thought that went into my PhD examination.

Declaration

This thesis is submitted to the University of Warwick in support of my application for the degree of Doctor of Philosophy. It has been composed by myself and has not been submitted in any previous application for any degree.

The work presented (including data generated and data analysis) was carried out by the author. Parts of this thesis have been published by the author:

- Chapter 4 contains work available as a pre-print as Friel, Jamie, et al. "Attainability of the Holevo-Cramér-Rao bound for two-qubit 3D magnetometry." arXiv preprint arXiv:2008.01502 (2020).

- Chapter 5 contains work available as a pre-print as Friel, Jamie, et al. "Attainability of the Holevo-Cramér-Rao bound for two-qubit 3D magnetometry." arXiv preprint arXiv:2008.01502 (2020).

- Chapter 5 contains work published as Albarelli, Francesco, Jamie F. Friel, and Animesh Datta. "Evaluating the holevo cramér-rao bound for multiparameter quantum metrology." Physical review letters 123.20 (2019): 200503.

Abbreviations

CCRB classical Cramér-Rao bound

CFI classical Fisher Infromation

CRB Cramér-Rao bound

GHZ Greenberger–Horne–Zeilinger state

HCRB Holevo-Cramér-Rao bound

JW Jordan-Wigner

MSEM mean square error matrix

NV Nitrogren Vacancy

POVM positive operator valued measure

PSD positive semi-definite

PSO particle swarm optimisation

QCRB quantum Cramér-Rao bound

QFI quantum Fisher infromation

QFIM quantum Fisher infromation matrix

RLD right logarithmic derivative

SDP semidefinite program

SLD symmetric logarithmic derivative

Abstract

Quantum enhanced metrology potentially offers a great advantage to the estimation of magnetic fields. One of the greatest hurdles to overcome in unlocking this advantage is overcoming the detrimental effects of noise. The forms the main motivation of this thesis. What are the optimal states for quantum enhanced estimation of magnetic fields? A natural secondary motivation that follows from thinking practically about the impacts of noise is, how do we generate these states?

One of the subtleties involved in the analysis of using quantum systems for magnetic field estimation is the different figures of merit available and how informative each may be. To begin we show that the intuitively optimal 3D-Greenberger–Horne–Zeilinger state is indeed optimal for large numbers of qubits. We develop a novel genetic inspired algorithm to find optimal states for low numbers of qubits.

Following this, we are dedicated to the study of the Holevo Cramér-Rao bound. This being the ultimate bound to a multiparameter quantum estimation problem. We compute the first analytic three parameter example of the Holevo Cramér-Rao bound and demonstrate that is it attainable with a projective measurement.

Moving beyond the case that can be analytically solved, we study the quantum limits of magnetometry in the presence of noise. Once we have examined the attainability of magnetometry with increasing copies of the input state, we develop another genetic inspired algorithm for the optimisation of quantum circuits to attain these limits.

To conclude, we present some preliminary investigations into using spin chains with local control and measurement on only one extremal edge for the estimation of a magnetic field with a simplified control set-up. In particular we look to utilise a sub-universal model that is simulable with linear space in the number of qubits.

Chapter 1

Introduction

> A great deal of my work is just
> playing with equations and seeing
> what they give.
>
> _____
>
> Paul Dirac

All scientific theories require experimental confirmation. Without the possibility falsification a theory can be said to be "not even wrong". As the frontiers of science push on, the demands on the precision required from such experiments is ever increasing. This is the subject matter of this thesis, how much information about a set of unknown parameters is contained within a physical system and how do we optimally extract that information.

Physics does not look at the same on all energy/length scales. We have three well established scales, the very largest where the physics of Einstein's relativity dominates, the world that we experience of Newtonian classical physics and the smallest scale, quantum physics. With quantum mechanics being the smallest scale physical model we have to date it is inevitable that we would need to perform experiments on quantum systems. What is not immediately obvious is that quantum systems are able to improve sensing performance above that of a classical probe. The reason this is perhaps unintuitive on first blush is the "fuzzy" and uncertain nature of quantum mechanics.

The non-commuting nature of observables is a fundamental difference between quantum and classical mechanics. That is to say, the order in which one measures properties of a system matters on a quantum mechanical scale. The most famous

example of this is the Heisenberg uncertainty principle,

$$\delta x \delta p \geq \frac{\hbar}{2},$$ (1.1)

where the uncertainty of measuring both position and momentum is lower bound by a quantity greater than zero. In words, the better we know the position of a particle, the worse we know its momentum and vice versa. For an intuition as to where this relationship comes from, we can imagine probing a small particle with a laser. In order to know the position of the particle accurately we would require a very high frequency laser pulse, as this increases the spacial resolution available. However, very high frequency light carries more energy and would scatter the particle, disrupting the momentum measurement. Conversely, in order to not add any more energy into the system in order to obtain a good momentum measurement we would need to use a very low frequency pulse. As a result, we would have very low resolution on the position.

On initial inspection it may appear that quantum mechanical systems only offer limitations when it comes to the estimation of observables. However, this is not the case! In fact, quantum mechanical systems offer us resources which are not available classically which when properly utilised offer advantages to estimation of observables with quantum probes. The two canonical examples of such resources are entanglement and squeezing. These uniquely quantum mechanical phenomena allow for correlations between subsystems greater than that which is possible with any classical system. It is within these correlations that we find the extra power afforded to us by quantum mechanical systems.

We should be careful to not be naive in thinking that quantum mechanical systems are immediately applicable to improving all of our sensing needs. Whilst it is true that such systems offer many advantages, there are also drawbacks. Namely, noise sensitivity. As we will later see, the states which have the best performance for sensing are also often the most sensitive to environmental noise. Useful quantum states are often difficult to experimentally prepare and even harder to maintain against the bombardment of external noise. This leads to a trade-off between tuning a state's robustness to noise and its sensitivity to the parameters of interest.

If we are to rigorously examine the performance of some proposed sensing procedures then we need a well defined figure of merit in order to effectively compare one procedure from another. Ultimately an experimentalist produces as estimate of the unknown set of parameters we are interested in. This estimate will have an associated

variance which acts as the figure of merit for the quality of estimate. Whilst some experimentalists do indeed focus on other figures of merit in this work we will focus on variance. It is common that sensitivity is also used as the figure of merit—this is a good choice when you are trying to quantify the general performance of some sensing apparatus as opposed to estimating some particular experimental parameter.

The variance of an estimate depends on the input state, parameter encoding, environmental noise (can be encapsulated into parameter encoding as system dynamics), choice of measurement, measurement outcomes and estimator. This is quite the mess of variables, especially the measurement outcomes and estimator. In this work we will assume that maximum likelihood estimation is sufficient for the problems at hand [144]. With this assumption made we can use the classical Cramér-Rao bound (CCRB) as an estimator independent figure of merit (details to be found later in chapter 2.4). This gives us the relation,

$$\delta\boldsymbol{\varphi}^2 \geq C^c(\rho_{\boldsymbol{\varphi}}, \Pi), \tag{1.2}$$

where the left side, $\delta\boldsymbol{\varphi}^2$ is the estimator variance and the right hand side is the CCRB. The CCRB depends on a state $\rho_{\boldsymbol{\varphi}}$, with the parameters $\boldsymbol{\varphi}$ encoded onto it and a measurement Π used to extract information about the parameters from the state. We make the assumption that this inequality can be made tight (equal) with enough measurements and the maximum likelihood estimator (with the additional assumptions of local asymptotic normality, more on this in chapter 2.4). Practically, this gives us a pathway to analysing the performance of a state and measurement, without concerning ourselves with the technicalities of estimator analysis. With the above Π represents the measurement used in the experiment. In practice this will depend on the input state and the true value of the parameters φ.

The fundamental measurement-independent bound that we will study in this thesis is the Holevo-Cramér-Rao bound (HCRB). We call this the fundamental bound as it fully captures the fundamental non-commutativity of quantum mechanics. As a result of this, it also gives a tighter bound. By this, we mean that the HCRB is closer to equality when compared to classical Fisher Infromation (CFI) than other Cramér-Rao bounds. Importantly the HCRB is always attainable in an asymptotic sense, that is, you may require an infinite number of copies of the input state in order to attain the bound. We will examine this behavior later. We now have the essential chain of inequalities for this thesis

$$\delta\boldsymbol{\varphi}^2 \geq C^c(\rho_{\boldsymbol{\varphi}}, \Pi) \geq C^H(\rho_{\boldsymbol{\varphi}}). \tag{1.3}$$

There is one other main bound that we will study and that is the quantum Cramér-Rao bound (QCRB). It is given by the inverse of the quantum Fisher infromation (QFI). This bound is easier to calculate both analytically and numerically, however, there is no guarantee of attainability. The QCRB is always attainable for the single parameter problem [89]. The extension to multiple parameters, relying on the quantum Fisher infromation matrix (QFIM) however, is not always attainable. Given the attainability of the HCRB, we have that it is an upper bound on the QCRB. It was shown that the HCRB and QCRB differ by no more than a factor of two [193, 36].

1.1 Summary of results

In spirit this thesis has two main driving forces. These are, *what* are the optimal states and *how* do we go about attaining their Cramér-Rao bounds. Once the mathematical foundations have been laid (in Chapter 2), we begin by examining optimal states for 3D magnetometry using the quantum Fisher information as the Cramér-Rao bound of choice. In Chapter 3 we explore the structure of optimal states for 3D magnetometry in the limit of high numbers of qubits and the low numbers of qubits ($N < 8$). Indeed, for $N \geq 8$ we show that an optimal initial state (but by no means the only) is that of the 3D-GHZ state, as one might intuit. Further, for N < 8 we develop a new genetic inspired optimisation algorithm which is capable of finding structure in the optimal states over increasing qubits. This is beneficial for further analytic work that can be done with optimal states that does not rely on numerical results.

We then move away from the QFI and look towards the HCRB, a bound that is always attainable (although, it may require many copies of the input state). Always being attainable makes this bound more informative than the QFI. However, this comes at the cost of being more difficult to calculate. The increased difficulty is both numerical and analytic. In this thesis we look at tools new and old which partially break down the barriers of difficulty, allowing new insights to be obtained.

In our first exploration, in chapter 4, of the HCRB we derive a new analytic solution to the bound for 2-qubit 3D magnetometry. We accomplish this by exploiting the particular geometric properties of 2-qubit 3D magnetometry. We then go on to show that this bound is attainable with the simplest class of measurements, projective on a single copy. There is more than one way to skin the HCRB, a fact that we use

to our advantage when proving projective attainability. Once we have exploited the geometry of the problem to simplify obtaining an analytic result we can then go back to a full-space with the solution in mind.

The next section of work, chapter 5.1.2, can be seen as a natural extension of the previous work. That is to consider the effect of an environment on sensing. In particular we will focus on the effects of dephasing along Pauli-Z axis. We motivate this as being the primary noise model from experimental works that are carried out with with the Nitrogren Vacancy (NV) center. This is natural that physical systems will have a preferential axis that noise acts along and for the NV center this is the Pauli-Z direction. After we introduce a semidefinite program (SDP) formulation of the HCRB. We use this new numerical tool to explore the information geometry of 3D magnetometry that was previously hidden from us by numerical and analytic boundaries. In this we see that the weak-commutativity condition is not a useful one when it comes to assessing the attainability of a statistical model. Continuing explorations of attainability, we examine the impact of adding multiple copies over increasing noise strength. This goes towards unpacking the asymptotic nature of the HCRB with respect to the number of copies. In this we find that at low noise values one copy is effectively the best one can do, which contrasts to high noise scenario where 2 copies attains the HCRB. Finally, we use a similarly genetic inspired algorithm as in the previous chapter to design quantum circuits with a minimal number of gates. This is with noisy-intermediate-scale-quantum devices in mind where noise is still a dominant force, but we still have access to robust quantum controls. This is achieved by parameterising the single and two-qubit gates with a binary string, as a subroutine of calculating a given circuit's quantum Fisher information we optimise the continuous single qubit gates.

Finally, in chapter 6, we change the paradigm that we consider. Instead of the typical, state preparation, parameter encoding, noise channel, measurement, we consider a scenario where we are not able to decouple the input state during preparation from the parameter encoding unitary. We move into a more typical quantum control set up, utilising a spin chain as the physical model. The key analytic tool we use is to model the time evolution of creation and annihilation operators with a linear Hessian matrix. This works for Hamiltonians quadratic in creation and annihilation operators. We show that robust and scalable controls are possible to calculate for large system sizes in this linear space. This allows us to optimise control pulses for optimal magnetic field estimation with a much greater number of qubits than would normally

be possible. This is an important step towards developing practical sensing protocols with large spin-chains.

1.2 Code availability

The code used to generate numerical results within this thesis is all available via github [64]. The Quantum Estimation Toolbox main branch will continue to be developed as an open source tool for those exploring quantum estimation theory. The branch named *thesis* will remain fixed as an accurate reflection of the code used within this thesis, for reproducibility.

Chapter 2

Mathematical background

> That is not only not right; it is not
> even wrong.
>
> ———————————————
>
> Wolfgang Pauli

Before we delve into the mathematical details of quantum information theory and metrology we must first build up from the foundations. These foundations are namely, linear algebra and statistical estimation theory. We will first introduce linear algebra, as it can be argued to be the foundation to everything we examine in this thesis. Then, once we have examined the core concepts in classical estimation theory we will be able to move onto quantum estimation theory. We will pay particular attention to the effect of external magnetic fields on qubits and quantum control theory.

2.1   Linear Algebra

It is sometimes joked in the corridors of mathematics departments that there are two branches of mathematics, linear algebra and non-linear systems that are approximated until they are linear.

Linear algebra, in a broad sense is the study of vector spaces and linear functions. Slightly more formally it concerns linear equations,

$$\alpha_1 x_1 + \alpha_2 x_2 + \ldots + \alpha_n x_n = a,$$
$$\beta_1 x_1 + \beta_2 x_2 + \ldots + \beta_n x_n = b,$$

and linear mappings,

$$x_1 + x_2 + \ldots + x_n \to \alpha_1 x_1 + \alpha_2 x_2 + \ldots + \alpha_n x_n.$$

Systems of linear equations are indeed fundamental to linear algebra, however, the study of vector spaces is far more essential to the study of quantum information theory.

In order to study vector spaces, we need only two operations, some form of vector addition (denoted +) and some form of scalar multiplication (denoted *).

Definition 2.1.1 (Vector space). A vector space over a field ($\mathcal{F}$), is a set ($\mathcal{V}$) along with two operations vector addition (+) and scalar multiplication (*) subject to the conditions for $\boldsymbol{x}, \boldsymbol{y}, \boldsymbol{z} \in \mathcal{V}$ and $\alpha, \beta \in \mathcal{F}$:

1. Associative addition: $\boldsymbol{x} + (\boldsymbol{y} + \boldsymbol{z}) = (\boldsymbol{x} + \boldsymbol{y}) + \boldsymbol{z}$

2. Commutative addition: $\boldsymbol{x} + \boldsymbol{y} = \boldsymbol{y} + \boldsymbol{x}$

3. Additive identity: $\exists$ an element $\boldsymbol{0} \in \mathcal{V}$ (the additive identity) such that $\boldsymbol{x} + \boldsymbol{0} = \boldsymbol{x}, \ \forall \boldsymbol{x} \in \mathcal{V}$

4. Distributive scalar multiplication over vector addition: $\alpha * (\boldsymbol{x} + \boldsymbol{y}) = \alpha\boldsymbol{x} + \alpha\boldsymbol{y}$

5. Distributive scalar multiplication over field addition: $(\alpha + \beta) * \boldsymbol{x} = \alpha\boldsymbol{x} + \beta\boldsymbol{x}$

6. Compatibility with scalar multiplication: $\alpha * (\beta\boldsymbol{x}) = (\alpha\beta)\boldsymbol{x}$

7. Identity element of scalar multiplication: $1 * \boldsymbol{x} = \boldsymbol{x}, \ \forall \boldsymbol{x} \in \mathcal{V}$.

2.1.1 Vectors

In order to add some context to these conditions and gain some intuition we will look at the example of $\mathbb{R}^2$. This we can think of as an infinite flat plane spanning forward, behind, left and right from us, as a point of reference. Without getting too carried away with analogies, we can imagine the *center* as being the point that we are stood on. This point is our zero vector, **0**. The two directions *left to right* and *forwards and backwards* are typically labeled x and y. A vector represents movement right or left
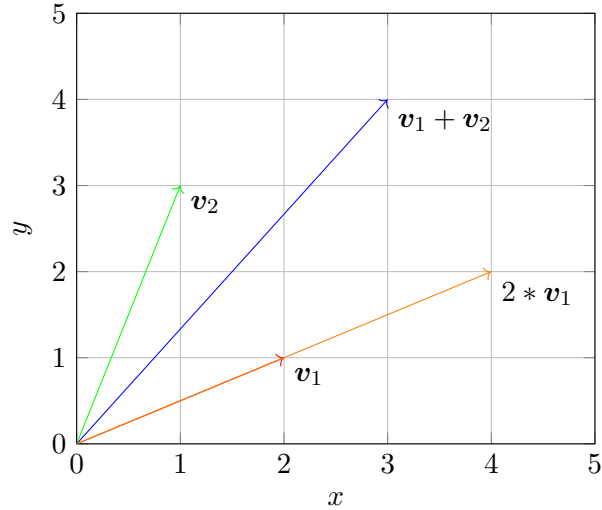
Figure 2.1: Example of vectors in $\mathbb{R}^2$

and then forward or backward by some amount. We then label an arbitrary vector,

$$\boldsymbol{v} = \begin{bmatrix} x \\ y \end{bmatrix}, \tag{2.1}$$

where $x, y \in \mathbb{R}$. Now, if we were to add two vectors together, we would be adding two x-component and y-components respectively. For arbitrary vector addition we would then have,

$$\begin{bmatrix} x_1 \\ y_1 \end{bmatrix} + \begin{bmatrix} x_2 \\ y_2 \end{bmatrix} = \begin{bmatrix} x_1 + x_2 \\ y_1 + y_2 \end{bmatrix}. \tag{2.2}$$

Similarly, for scalar multiplication, for any $\alpha \in \mathbb{R}$,

$$\alpha * \begin{bmatrix} x_1 \\ y_1 \end{bmatrix} = \begin{bmatrix} \alpha x_1 \\ \alpha y_1 \end{bmatrix}. \tag{2.3}$$

In Figure 2.1 we can see an example of vector addition and scalar multiplication. Whilst we should not get too fixated on 2-dimensional vectors, we can see that we can think of vectors as lines in space. As such it is natural for us to ask questions like, how long is a line and what is the angle between two lines?

Complex Numbers

In the next section, we will also need to move beyond the real numbers to the complex numbers. A general complex number is of the form $(a + bi)$, where $i = \sqrt{-1}$ and $(a, b) \in \mathbb{R}$.

We denote the complex conjugate of a complex number $z = (a + bi)$, as $z^* = (a - bi)$. The conjugate is one of the most useful and powerful operations in linear algebra! The first application of the conjugate is to find the size, or modulus of a complex number. For an arbitrary complex number $z = (a + ib)$, we denote the modulus $|z|$ and define it as, $|z| = \sqrt{zz^*}$. But how do we define multiplication over complex numbers?

$$(a + bi)(c + di) = ac + adi + bci + bdii, \tag{2.4}$$
$$= ac + (ad + bc)i - bd. \tag{2.5}$$

We can now expand out the modulus, by substituting $c \to a$ and $d \to -b$. Giving us $|z| = \sqrt{a^2 + b^2}$. Addition looks quite similar to vector addition on $\mathbb{R}$ that we have already seen above! Adding two complex numbers,

$$(a + bi) + (c + di) = a + c + bi + di, \tag{2.6}$$
$$= (a + c) + (a + d)i. \tag{2.7}$$

This makes it clear the difference between the real and imaginary components of a complex number. Some notation,

$$\mathrm{Re}\, z = (z + z^*)/2 = a, \tag{2.8}$$
$$\mathrm{Im}\, z = (z - z^*)/2 = b. \tag{2.9}$$

The above definitions suggest that we can represent a complex number in the same way that we represent a 2-dimensional real vector. Indeed, this is the case. Examining complex numbers plotted in $\mathbb{R}$ also allows us to gain some intuition about the operations of multiplication and addition. When it comes to complex number addition, by looking at Figure 2.2, we can see how it would be equivalent to vector addition in $\mathbb{R}^2$. In order to gain some intuition into complex numbers we look to a slightly different parameterisation. Let us first note that we can generate any unit (by
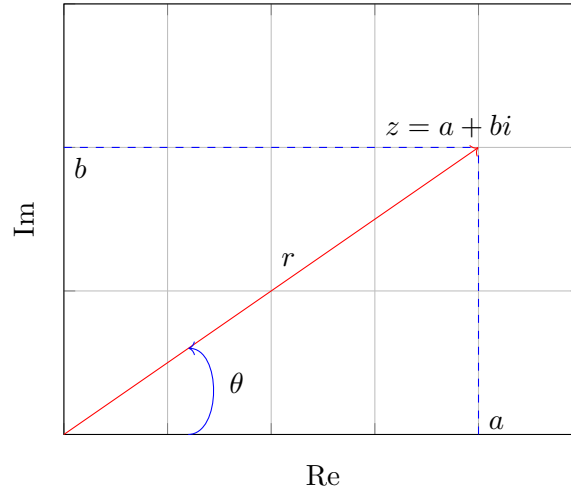
Figure 2.2: Example of complex number plotted in $\mathbb{R}^2$. For arbitrary complex number $z = a + bi$ with equivalent parameterisation $z = re^{-i\theta}$.

unit, we mean magnitude 1) complex number by,

$$z = e^{-i\theta} = \cos(\theta) + i\sin(\theta), \tag{2.10}$$

where, $e = \sum_n 1/n! \approx 2.718$, known as Euler's number. Then, all we need is to have an arbitrary modulus for the complex number and we can generate any complex number we want. In this way we have,

$$z = re^{-i\theta}, \tag{2.11}$$

for any $r \in \mathbb{R}$. We can see how these two parameterisations are equivalent in Figure 2.2. Now for complex multiplication,

$$r_1 e^{-i\theta} \cdot r_2 e^{-i\theta_2} = r_1 r_2 e^{-i\theta_1} e^{-i\theta_2}, \tag{2.12}$$

$$= r_1 r_2 e^{-i(\theta_1 + \theta_2)}. \tag{2.13}$$

In this way we can see that we are able to interpret complex multiplication as multiplying the moduli together and adding the angles. This intuition is much harder to gain in the previous (Cartesian) parameterisation. Finding the correct parameterisation is a useful skill to have in general, when it comes to solving problems more efficiently.

2.1.2   Lengths and inner products

If we want to find the length of a line on a 2D graph, then we need only invoke the old classic, Pythagoras's Theorem. For a general 2D vector,

$$\text{len}\left(\begin{bmatrix} x_1 \\ y_1 \end{bmatrix}\right) = \sqrt{x_1^2 + y_1^2}. \tag{2.14}$$

More formally, we refer to this as the Euclidean norm of a vector and generalizes Pythagoras' theorem.

When we say a vector space is over a field, that means the elements of the vectors are elements of that given field. For a complex vector of dimension n, we have,

$$\nu = \begin{bmatrix} \nu_1 \\ \nu_2 \\ \vdots \\ \nu_n \end{bmatrix}, \tag{2.15}$$

$$||\nu|| = \sqrt{\nu \cdot \nu} = \sqrt{|\nu_1|^2 + |\nu_2|^2, \ldots, |\nu_n|^2}. \tag{2.16}$$

We also refer to this as the dot product, hence $a \cdot a$. A natural question to as at this stage is what does the dot product look like between two different vectors? Roughly speaking we can think about the dot product between two different vectors as giving us, the length of one vector on another one. Or, the projection of one vector onto another. We define the dot product between two vectors to be,

---

Definition 2.1.2 (Dot product). For $x, y \in \mathbb{C}^n$ (an n-dimensional complex vector space),

$$x = \begin{bmatrix} x_1 \\ x_2 \\ \vdots \\ x_n \end{bmatrix}, \quad y = \begin{bmatrix} y_1 \\ y_2 \\ \vdots \\ y_n \end{bmatrix}. \tag{2.17}$$

We define the dot product between x and y as,

$$x \cdot y = \sum_{i=1}^{n} x_i^* y_i. \tag{2.18}$$

We will explore the intuition behind what this means for complex spaces more so when we get to the quantum portion of this chapter, section 2.2. There is not a trivial interpretation for complex vectors of magnitude other than 1. However, for real vector spaces we have a clean geometric way to view the dot product,

$$x \cdot y = ||x|| \cdot ||y|| \cos(\theta), \qquad (2.19)$$

where θ is the angle between the two vectors. In order to explain where this equality comes from, let us define a third vector $z = x - y$, which will connect the end of y to the end of x. We then have a triangle with the angle θ between x and y. By the law of cosines,

$$||z||^2 = ||x||^2 + ||y||^2 - 2||x|| * ||y|| \cos(\theta), \qquad (2.20)$$

$$(||x|| - ||y||)(||x| - ||y||) = ||x||^2 + ||y||^2 - 2||x|| * ||y|| \cos(\theta), \qquad (2.21)$$

$$||x||^2 + ||y||^2 - 2x \cdot y = ||x||^2 + ||y||^2 - 2||x|| * ||y|| \cos(\theta), \qquad (2.22)$$

$$x \cdot y = ||x|| * ||y|| \cos(\theta). \qquad (2.23)$$

2.1.3 Span, independence and basis vectors.

Now we combine the concepts of scalar multiplication and vector addition together. We do this in order to examine what it means to combine vectors in this way and how we are able to build vector spaces out of a few base vectors.

We have already seen what a linear combination is in essence, but now we more formally define it,

---

Definition 2.1.3 (Linear combination). For a set of vectors $\nu_1, \ldots, \nu_n \in \mathcal{V}$ and a corresponding set of field elements $\alpha_1, \ldots, \alpha_n \in \mathcal{F}$, the linear combination of those vectors is given by,

$$\alpha_1 \nu_1 + \ldots + \alpha_n \nu_n. \qquad (2.24)$$

The natural next step is to generalise the notion of a linear combination. By this, we mean allowing the field elements, or coefficients, as we will now call them, to be arbitrary. From this, we get the notion of a span, that is the space induced by a set of vectors and arbitrary coefficients. More formally,

Definition 2.1.4 (Span). For a set of vectors $\nu = (\nu_1, \ldots, \nu_n) \in \mathcal{V}$, then then span of ν, denoted span(ν) is,

$$span(\nu) = \{\alpha_1\nu_1 + \ldots + \alpha_n\nu_n | \alpha_i \in \mathcal{F}\}. \qquad (2.25)$$

The span is, by definition also a vector space, not only a set of vectors. If the span of a set of vectors ν is equal to a vector space $\mathcal{V}$ we say that ν spans $\mathcal{V}$. When working with spans it is useful to know if the set of vectors is as minimal as possible. This is the notion of linear dependence, is it possible to write one of the vectors in a set in terms of other vectors in the set? If it is not possible then we call that set of vectors linearly independent,

Definition 2.1.5 (Linearly independent). For a set of vectors $\nu = \nu_1, \ldots, \nu_n \in \mathcal{V}$ and a corresponding set of field elements $\alpha_1, \ldots, \alpha_n \in \mathcal{F}$. The set of vectors is said to be linearly independent when,

$$\alpha_1\nu_1 + \ldots + \alpha_n\nu_n = 0 \text{ iff } \alpha_i = 0 \forall i. \qquad (2.26)$$

In words, if the only way we are able to make a linear combination of out set of vectors is by making all their coefficients 0, then we have a linearly independent set of vectors. A linearly dependent set is one such that there is a non-zero set of coefficients such that the linear span is zero. In essence, a linear dependent set of vectors contains redundancy. This is what we mean when we say we want a minimal set of vectors, a set with no redundancy. The combination of the previous concepts brings us to the notion of a basis,

Definition 2.1.6 (Basis). The basis of a vector space $\mathcal{V}$ is a set of vectors ν that is linearly independent and spans $\mathcal{V}$.

For example, the canonical basis of $\mathbb{R}^n$ is given by,

$$\nu_1 = \begin{bmatrix} 1 \\ 0 \\ \vdots \\ 0 \end{bmatrix}, \quad \nu_2 = \begin{bmatrix} 0 \\ 1 \\ \vdots \\ 0 \end{bmatrix}, \quad \nu_n = \begin{bmatrix} 0 \\ 0 \\ \vdots \\ 1 \end{bmatrix}. \tag{2.27}$$

2.1.4 Linear maps and matrices

In this section we will see how we transform vectors through linear transformation. We will also see how these linear transformations can be represented by matrices. Linear transformations are of fundamental importance to linear algebra. They define how we may transform vectors, from one vector space into another vector space. As such, we define them promptly,

Definition 2.1.7 (Linear transformation). $T : V \rightarrow W$ (a transformation from vector space V to W), is any transformation that satisfies,

$$T(\alpha_1\nu_1 + \alpha_2\nu_2) = \alpha_1 T(\nu_1) + \alpha_2 T(\nu_2), \alpha_i \in \mathcal{F}, \nu_i \in V. \tag{2.28}$$

That is to say, a transformation which distributes over a linear combination of vectors. An important note to make is that if $V = W$, then we call the transformation a *Linear Operator*. We denote this vector space as $\mathcal{L}(V, W)$, or $\mathcal{L}(V)$ for linear operators. We can again define a transformation that takes a linear transformation and returns another. We call such transformations *superoperators*.

It is not always meaningful to define a product of linear transformations. However, for this case we do. In words, we can think of the product of linear transformations applied to a vector as performing one transformation and then the second. Formally,

Definition 2.1.8 (Product of Linear Transformations). For $T \in \mathcal{L}(V, W)$ and $S \in \mathcal{L}(W, U)$, then the product $ST \in \mathcal{V}, \mathcal{U}$ is given by,

$$(ST)\nu = S(T\nu) \tag{2.29}$$

for $\nu \in V$.

An important concept, especially for our quantum information interests, is the notion of invertibility. That is, a linear transformation that will undo the effect of another transformation. Formally,

Definition 2.1.9 (Invertible linear transformation)**.** We say a linear transformation $T \in \mathcal{L}(V, W)$ is invertible if $\exists$ a linear transformation $S \in \mathcal{L}(W, V)$ such that,

$$ST\nu = \nu \tag{2.30}$$

for $\nu \in \mathcal{V}$. We call S the multiplicative inverse, (or just inverse) of T and denote it as T^{-1}.

In order to get a sense of how we might represent a linear transformation as a matrix, we advance with an example transformation.

Example 2.1.1. Let $\nu \in \mathbb{R}^2$ be an arbitrary 2 dimensional real vector and $T_1 \in \mathcal{L}(\mathbb{R}^2)$ that acts like,

$$T_1\nu = T_1 \begin{bmatrix} x \\ y \end{bmatrix} = \begin{bmatrix} x + y \\ x - y \end{bmatrix}. \tag{2.31}$$

We can again see a visual representation of this, in Figure 2.3.

If we think about how Example 2.1.1 acts on the basis elements on $\mathbb{R}^2$, which we label,

$$\nu_1 = \begin{bmatrix} 1 \\ 0 \end{bmatrix}, \quad \nu_2 = \begin{bmatrix} 0 \\ 1 \end{bmatrix}. \tag{2.32}$$

Then we are able to example how the T_1 acts on these elements,

$$T_1\alpha\nu_1 = T_1 \begin{bmatrix} \alpha \\ 0 \end{bmatrix} = \begin{bmatrix} \alpha \\ \alpha \end{bmatrix} \tag{2.33}$$

$$T_1\beta\nu_1 = T_1 \begin{bmatrix} 0 \\ \beta \end{bmatrix} = \begin{bmatrix} \beta \\ -\beta \end{bmatrix}. \tag{2.34}$$
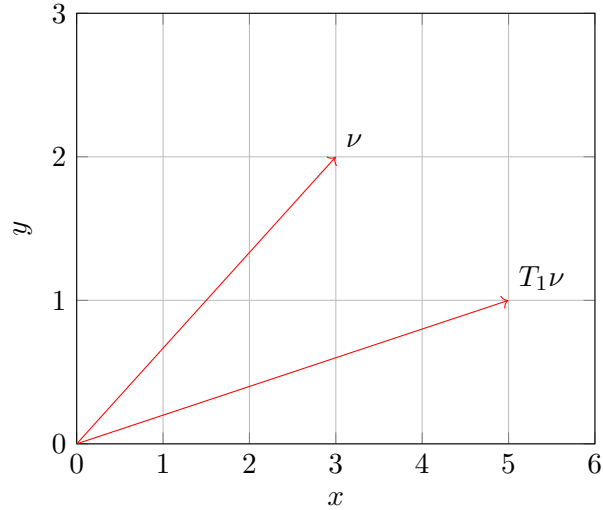
Figure 2.3: Example of the linear transformation T_1, shown in Example 2.1.1 for $\nu = (3, 2)$.

We can then define some basis elements for T_1. We define these elements as the transformation from one basis element of the vector space, to another,

$$T_{\alpha \to \alpha} = 1, \tag{2.35}$$

$$T_{\alpha \to \beta} = 1, \tag{2.36}$$

$$T_{\beta \to \beta} = 1, \tag{2.37}$$

$$T_{\beta \to \alpha} = -1. \tag{2.38}$$

As we can see, this is quite a cumbersome representation of T_1. A powerful notion in mathematics is the concept of abstraction. We take one object and "abstract" it, by finding a more useful representation with all the same properties, except for being easier to work with. In order to improve the efficiency of our representation, we introduce the concept of a matrix,

---

Definition 2.1.10 (Matrix). $M_{i,j}$, let $m, n \in \mathbb{N}$ define an m by n rectangular matrix. This is an array of elements from some field $\mathcal{F}$ that contains m rows and n columns,

$$M = \begin{bmatrix} M_{1,1} & M_{1,2} & \dots & M_{1,n} \\ M_{2,1} & M_{2,2} & \dots & M_{2,n} \\ \vdots & & \ddots & \vdots \\ M_{m,1} & M_{m,2} & \dots & M_{m,n} \end{bmatrix}. \tag{2.39}$$

Where the notation $M_{i,j}$ refers to the ith row and j^{th} column element.

The way that we have written the action of a linear transformation, visually at least, seems a lot like how we write a multiplication. This is indeed the case and we can define matrix multiplication by,

Definition 2.1.11 (Matrix multiplication)**.** For matrices A of size $m \times n$, B of size $n \times p \in \mathcal{F}$, for $m, n, p \in \mathbb{N}$, we define the multiplication of these matrices as,

$$C = AB \tag{2.40}$$

$$C_{i.j} = \sum_{k=1}^{n} A_{i,k} B_{k,j}, \tag{2.41}$$

where $A_{i,k} B_{k,j}$, is the typical scalar multiplication on the field $\mathcal{F}$.

Here we can also see that vectors can be considered as a special case of a matrix where one dimension is set to 1. Bringing all the elements above together we can now build up a *matrix representation* of the linear operator T_1,

$$T_1 = \begin{bmatrix} T_{\alpha \to \alpha} & T_{\alpha \to \beta} \\ T_{\beta \to \beta} & T_{\beta \to \alpha} \end{bmatrix} = \begin{bmatrix} 1 & 1 \\ 1 & -1 \end{bmatrix}. \tag{2.42}$$

We will see this matrix again later, it is quite important in quantum information theory and is commonly known as the *Hadamard matrix*. More generally we can build up the matrix representation of a linear operator by setting $M_{i,j}$ as the linear transformation's basis element between the ith vector basis element and the jth one.

2.1.5 Eigen decomposition and rank

For the remainder of this chapter (and indeed thesis), we will restrict ourselves to linear operators. Typically, a linear operator (referred to as just operator) will transform a given vector to something completely different to the original one. Indeed, we will later come across the notion of a *universal* set of operators, that is a set of operators

that allows us to transform one vector into any other vector in a given vector space. However, we now study vectors that are invariant (up to a scalar factor) under the operation of linear transform. More formally,

---

Definition 2.1.12 (Eigenvalue). Let $\nu \in \mathcal{V}$ and some operator $T \in \mathcal{L}(\mathcal{V})$. We define the eigenvalues of an operator T as the set of field elements $\lambda \in \mathcal{F}$, which for some vector $\nu \neq 0$ satisfies,

$$T\nu = \lambda\nu. \tag{2.43}$$

We define the identity operator $\mathbb{1} \in \mathcal{L}(V)$, such that $\mathbb{1}\nu = \nu$ for $\nu \in V$. This 'do nothing' operator is actually far more useful than it first appears. We are able to use this in order to find our eigenvalues. We re-write the eigenvalue equation as,

$$T\nu = \lambda\nu, \tag{2.44}$$

$$T\nu = \lambda\mathbb{1}\nu, \tag{2.45}$$

$$T\nu - \lambda\mathbb{1}\nu = 0, \tag{2.46}$$

$$(T - \lambda\mathbb{1})\nu = 0. \tag{2.47}$$

$$\tag{2.48}$$

The matrix $(T - \lambda\mathbb{1})$ is key to the eigenvalue problem. What is the first thing we can say? If we relabel it $\Lambda = (T - \lambda\mathbb{1})$, then it is easy for us to see immediately that this matrix is not invertible. If it was that would imply that there exists an inverse such that $\Lambda^{-1}\Lambda\nu = \nu$. However, remember that $\Lambda\nu = 0$. This would imply that $\Lambda^{-1}0 = \nu$. There are many reasons that this is impossible. The simplest being that the linear nature of operators will not allow it. For some operator T,

$$T(0) = T(0 + 0) = T(0) + T(0), \tag{2.49}$$

$$T(0) = T(0) + T(0), \tag{2.50}$$

$$T(0) - T(0) = T(0) + T(0) - T(0), \tag{2.51}$$

$$0 = T(0). \tag{2.52}$$

Simply put, once we reach the zero vector, there is no getting out via means of operator. In the next chapter we will see in more detail what the determinant is (given their tight

relationship there is much debate in the pedagogy of linear algebra as to the order the concepts should be introduced), but for now accepting the fact that the determinant of a non-invertible matrix is 0. This gives us a convenient way to find the eigenvalues,

$$\det(T - \lambda \mathbb{1}) = 0. \tag{2.53}$$

The eigenvector is the complementary concept to the eigenvalue. That is,

---

Definition 2.1.13 (Eigenvector)**.** Let $\nu \in \mathcal{V}$ and some operator $T \in \mathcal{L}(\mathcal{V})$. We define the eigenvectors of an operator T the set of vectors $\nu \neq 0$ satisfying,

$$T\nu = \lambda \nu, \tag{2.54}$$

for some $\lambda \in \mathcal{F}$.

The sets $\{\lambda_i\}$ along with the paired set $\{\nu\}$ form the *spectrum* of an operator. The eigenvectors and eigenvalues give us a sense of characteristics of an operator. Especially when the operator of interest is *complete*. By which, we mean,

---

Definition 2.1.14 (Complete matrix)**.** Is a square matrix of dimension $n \times n$ belonging to some field $\mathcal{F}$ such that the eigenvectors of the matrix form a basis of $\mathcal{F}^n$.

In other words, a matrix that has n-independent eigenvectors is complete. This is quite a powerful notion, because it means that we are able to write the action of a matrix that is complete on some vector by its effect on the span of its eigenvectors. This stems from the linearity of the operator. Let ν_1 and ν_2 be eigenvectors of some complex $n \times n$ matrix with corresponding eigenvalue λ_1 and λ_2, then we see that,

$$A(\alpha_1 \nu_1 + \alpha_2 \nu_2) = A(\alpha_1 \nu_1) + A(\alpha_2 \nu_2), \tag{2.55}$$
$$= \alpha_1 A(\nu_1) + \alpha_2 A(\nu_2), \tag{2.56}$$
$$= \alpha_1 \lambda_1 \nu_1 + \alpha_2 \lambda_1 \nu_2. \tag{2.57}$$

From this we can see that in essence eigenvalues give a sense of scale of transformation

and eigenvectors, a sense of direction. Further, eigenvalues can be 0 and the number of 0 eigenvalues is of great significance! The number of 0 valued eigenvalues is known as the *nullity*. Conversely, the *rank* of matrix is equal to the maximal number of linearly independent columns. If a matrix of dimension $n \times n$ has n linearly independent columns, then we call it *full-rank*. If a matrix has one or more zero valued eigenvalues then we call it *singular* or *rank-deficient*. As an insight into the everyday workings of a linear algebra practitioner there are many more results for rank 1 matrices and full-rank matrices than those that fall somewhere in the middle. Rank 1 matrices have the advantage of effectively being a vector, whilst full-rank matrices have many guaranteed results that become murky and unclear at lower ranks. This brings us nicely onto a topic closely tied to completeness of a matrix and that is *diagonalisability*. Formally,

---

Definition 2.1.15 (Diagonalisable matrix). Let A be an $n \times n$ complex matrix. If there exists an invertible matrix P and a diagonal matrix D (that is a matrix whose only non-zero elements are on the diagonal), such that,

$$A = PDP^{-1}. \tag{2.58}$$

If the matrix P is formed by stacking the eigenvectors of A and the diagonal elements of D are the eigenvalues of A, then A is also a complete matrix, because an invertible matrix has linearly independent rows [14] (implying all the eigenvectors are linearly independent too). The class of matrices that is most important for quantum information theory is the *Hermitian matrices*. Most importantly, these matrices are always diagonalisable [14]. These are complex matrices such that

$$A = A^{\dagger}, \tag{2.59}$$

where $A^{\dagger}$ is the conjugate transpose of the matrix A. The conjugate transpose of a matrix is the complex conjugate of all the elements and flipped across the main diagonal. That is $A_{i,j} \to A^*_{j,i}$. This imparts a lot of structure onto the matrix and we see this structure reflected in the spectrum of the matrix. Firstly, we are able to restrict the eigenvalues of a Hermitian matrix to be real. To see this, let A be some Hermitian

matrix along with an eigenvalue-vector pair ν, λ,

$$A\nu = \lambda\nu, \tag{2.60}$$

$$(A\nu)^\dagger = (\lambda\nu)^\dagger, \tag{2.61}$$

$$\nu^\dagger A^\dagger = \lambda^\star \nu^\dagger, \tag{2.62}$$

$$\nu^\dagger A = \lambda^\star \nu^\dagger, \tag{2.63}$$

$$\nu^\dagger A\nu = \lambda^\star \nu^\dagger \nu, \tag{2.64}$$

$$\lambda\nu^\dagger \nu = \lambda^\star \nu^\dagger \nu, \tag{2.65}$$

$$\lambda = \lambda^\star. \tag{2.66}$$

In order for $\lambda = \lambda^\star$ to be true $\text{Im}\,\lambda = 0$ must also be true or we would allow $-a = a$. That gives us an invaluable structure over the eigenvalues. Is there further structure to be extracted from the eigenvectors? Let ν_1, ν_2 be eigenvectors for distinct eigenvectors for eigenvalues λ_1, λ_2 of matrix A. Then we can see that,

$$\lambda_1 \nu_1^\dagger \nu_2 = (A\nu_1)^\dagger \nu_2, \tag{2.67}$$

$$= \nu_1^\dagger A^\dagger \nu_2 = \nu_1^\dagger \nu_2, \tag{2.68}$$

$$= \lambda_2 \nu_1^\dagger \nu_2, \tag{2.69}$$

$$\implies (\lambda_1 - \lambda_2)\nu_1^\dagger \nu_2 = 0. \tag{2.70}$$

Note that because $\lambda_1 \neq \lambda_2$ the only way the final equality is true, is for $\nu_1^\dagger \nu_2 = 0$. Here, we have also used the fact that $(AB)^\dagger = B^\dagger A^\dagger$ [14]. From all this above, we can see that Hermitian matrices' spectrum induces a *complete-orthonormal basis*, by this we mean a complete basis, where the elements are orthogonal (we can perform Gram-Schmidt on the cases when the eigenvalues are the same) and normalised. By normalised, we mean $\nu^\dagger \nu = 1$, this is just a scaling factor that we are free to set.

2.1.6 Determinant, trace and norms

In this and the following section we focus on studying the properties of matrices and these properties can tell us about the linear transformations they induce. One thing we lose when we move from scalars to matrices is the notion of a unique magnitude, or less clearly put, only scalars have a unique scalar value. However, the multiple scalar values that can be derived from a matrix can indeed be useful. They can give us information about many different properties and effects on vectors. Why all the

focus on scalar values? Only scalar values have a complete ordering as far as we are concerned. If we want to properly compare by order two non-scalar valued properties then we need to define some scalar.

We begin with the *determinant*, this is the scalar value that can be seen as giving us the *volume* scaling factor for the linear transform. The sign of the determinant indicates whether or not it flips the orientation of the vector space it acts on. It is worth noting that the determinant is commonly interpreted as the volume of the n-dimensional parallelepiped spanned by the columns of the matrix, gives us less of a sense on its impact on a vector transformation but will be useful as a mental image later.

The definition of determinant is a little involved so we start with a small example. The determinant of a matrix A is denoted $\det(A)$ or $|A|$. So for a general 2×2 matrix A,

$$\det(A) = \det\begin{pmatrix} a & b \\ c & d \end{pmatrix}, \tag{2.71}$$

$$= a * d - c * d. \tag{2.72}$$

The determinant is a very useful metric that comes up often in linear algebra. Firstly we point out that a matrix is invertible iff its determinant is non-zero. For an intuition, if we see the determinant as the volume of the transformation, if there is no volume change, then we cannot 'undo' it, hence no inverse. We have already previously seen the utility of the determinant when it comes to calculating eigenvalues, but now we know how to solve for the eigenvalues too!

The general definition for an $n \times n$ matrix A,

Definition 2.1.16 (Determinant). The determinant of $n \times n$ matrix A is given by,

$$\det(A) = \sum_{\sigma \in S_n} (\mathrm{sgn}(\sigma)\Pi_{i=1}^n A_{i,\sigma_i}). \tag{2.73}$$

The sum over $\sigma \in S_n$ is the set of all permutations of the set $\{1, 2, \ldots, n\}$. The function sgn(.) takes value +1 when the reordering of σ can be generated by an even number of swaps from the original set and -1 when it can be generated by an odd number of swaps.

The determinant has useful properties, which we will list and not prove here. For proofs see [5].

1. $\det(\mathbb{1}) = 1$

2. $\det(A^T) = \det(A)$

3. $\det(A^{-1}) = \det(A)^{-1}$

4. $\det(AB) = \det(A)\det(B)$

5. $\det(\alpha A) = \alpha^n A$

6. $\det(e^A) = e^{\text{trace}(A)}$.

Before we continue with one more useful result we must first note that we are able to generate a unitary matrix by the exponential of a hermitian matrix. We will see much more of Hermitian matrices in section 2.2, as they are one of the fundamental structures for unitary matrices, which drive dynamics in quantum systems. That is to say, for some unitary matrix U such that $U^{-1} = U^\dagger$, there exists a matrix H such that,

$$U = e^{-iH}, \tag{2.74}$$

for H, $H^\dagger = H$. We will see the trace in more detail soon, but we define the trace to be the sum of the diagonal elements. If we recall the diagonal decomposition of some matrix A, by a unitary matrix of eigenvectors P and a diagonal matrix of eigenvalues $D_{i,i} = \lambda_i$, then we have,

$$\det(A) = \det(PDP^\dagger) \tag{2.75}$$
$$= \det(P)\det(D)\det(P^\dagger) \tag{2.76}$$
$$= \det(e^{-iH_1})\det(D)\det(e^{-iH_2}) \tag{2.77}$$
$$= (e^{\text{trace}(-iH_1)})\det(D)e^{\text{trace}(-iH_2)} \tag{2.78}$$
$$= (e^0)\det(D)(e^0) \tag{2.79}$$
$$= (1)\det(D)(1) \tag{2.80}$$
$$= \prod_i \lambda_i. \tag{2.81}$$

From this we can see that for a square complex matrix, the determinant is equal to the product of the eigenvalues. Recall that in section 2.1 we mentioned that a matrix

is only invertible if its determinant is not 0. Combining these two facts we conclude that only full-rank matrices are invertible. We have mentioned the trace a few times in this discussion on determinant, this makes a natural transition into a more detailed look at the trace.

We begin immediately with the definition,

Definition 2.1.17 (Trace). The trace of an $n \times n$ matrix A is given by,

$$\text{Tr}(A) = \sum_{i=1}^{n} A_{i,i}. \tag{2.82}$$

In words, the trace is the sum of the main diagonal elements. The useful properties of trace,

1. $\text{Tr}(A + B) = \text{Tr}(A) + \text{Tr}(B)$

2. $\text{Tr}(\alpha A) = \alpha \, \text{Tr}(A)$

3. $\text{Tr}(AB) = \text{Tr}(BA)$

4. $\text{Tr}(ABC) = \text{Tr}(BCA)$

5. $\text{Tr}(A \otimes B) = \text{Tr}(A) \, \text{Tr}(B),$

where $\otimes$ is the *Kronecker product*, defined,

Definition 2.1.18 (Kronecker product). For an $n \times m$ matrix A and $o \times p$ matrix B, the Kronecker product gives an $on \times mp$ block matrix given by,

$$A \otimes B = \begin{bmatrix} A_{1,1}B & \dots & A_{1,m}B \\ \vdots & \ddots & \vdots \\ A_{n,1}B & \dots & A_{n,m}B. \end{bmatrix} \tag{2.83}$$

We will see more of the Kronecker product in the section 2.2 as it is the matrix operation that 'brings together' multiple quantum systems. As we have done before,

let us return to the diagonalisation of a diagonalisable complex $n \times n$ matrix A with unitary makes of eigenvectors P and diagonal matrix of eigenvalues $D_{i,i} = \lambda_i$ and take its trace,

$$\text{Tr}(A) = \text{Tr}(PDP^{-1}) \tag{2.84}$$

$$= \text{Tr}(DP^{-1}P) \tag{2.85}$$

$$= \text{Tr}(D) \tag{2.86}$$

$$= \sum_i \lambda_i. \tag{2.87}$$

We can therefore see that the trace is the sum of the eigenvalues. From this single value that scales with some property of the matrix we can get a sense of *how large* a given matrix is.

In fact, this notion of a scalar value giving a sense of the size of a matrix can be generalised. If we instead think about *how far* from some notion of 0 a given matrix is, then we can build more general frameworks. We call this a norm,

---

Definition 2.1.19 (Matrix norm)**.** Any function acting on arbitrary matrix A onto the reals, $||.|| : A \to \mathbb{R}$ satisfying the following,

1. $||\alpha A|| = |\alpha| ||A||$

2. $||A + B|| \leq ||A|| + ||B||$

3. $||A|| \geq 0$

4. $||A|| = 0$ iff $A = 0$.

Not only does this give us a sense of how far an individual matrix is from 0, but also the distance between two matrices. The norm induces this idea of distance by taking the difference of two matrices, i.e., $||A - B||$. There is no unique sene of a norm, but one particularly important family of norms over Hilbert spaces is known as a *Schatten norm*.

Definition 2.1.20 (Schatten Norm)**.** Let $\mathcal{H}_1$, $\mathcal{H}_2$ be Hilbert spaces, and A a linear bounded operator from $\mathcal{H}_1$ to $\mathcal{H}_2$. For $p \in [1, \infty)$, we define the Schatten p-norm

---

of A as,

$$||A||_p = (\text{Tr}[|A|^p])^{\frac{1}{p}}. \tag{2.88}$$

A particularly important norm is known as the *Frobenius-norm*,

$$||A||_F = \sqrt{\text{Tr}[AA^\dagger]}. \tag{2.89}$$

The Frobenius norm is an upper bound to the $p = 2$ Schatten norm and gives us an intuition into the total distortion induced by a linear transform. In general these above norms are known in general as an *operator norm* and give a measure of the size of an operator.

This notion becomes particularly powerful when combined with a vector space. Although not necessarily always being induced by a norm, but commonly so, a vector space with an associated *inner-product* is known as an inner-product space. This equips a vector space with a rigorous geometric meaning, as we have seen previously with vector inner products it gives us a sense of angle and distance with a vector space.

This section has now equipped us with the fundamental linear algebra requirements needed to proceed with our understanding of quantum information theory.

2.2 Quantum Information Theory

Information theory concerns itself with the quantification, processing and communication of digital information. Quantum information theory is the study of information as it relates to the state of a quantum system. As with classical information, quantum information can be transmitted, processed and utilised for our advantage.

2.2.1 Quantum bits

We relabel a complex unit vector by a "ket",

$$|\psi\rangle = \begin{bmatrix} \psi_1 \\ \psi_2 \\ \vdots \\ \psi_n \end{bmatrix} \tag{2.90}$$

and a "bra" but its hermitian conjugate,

$$\langle\psi| = |\psi\rangle^\dagger.$$ (2.91)

This notation can simply be seen as "syntax sugar" in as much as it does not fundamentally change anything that we do, it simple abstracts a vector in quite a useful way. By unit vector, we mean that it has inner product of 1. We introduce a new definition of the inner product,

$$\langle\psi|\psi\rangle = 1.$$ (2.92)

Which induces a norm,

$$|| \,|\psi\rangle\, || = \sqrt{\langle\psi|\psi\rangle}.$$ (2.93)

We will now build up the machinery required to define a Hilbert space, that will be complete with respect to this norm. We call this vector, $|\psi\rangle$ a 'state'. Before defining the vector space for quantum states we must also define the notion of a complex metric space. Loosely, a complete metric space, is a vector space with the notion of a distance whereby every sequence that has a diminishing distance in the vector space, converges within the vector space. More formally, we start with a metric space,

---

Definition 2.2.1 (Metric space). A metric space consists of an ordered pair (X, d), where X is a set and d is a metric on X. A metric is a function mapping $d : X \times X \to \mathbb{R}$ which satisfies the following, for $x, y, z \in X$:

1. Non-negativity: $d(x, y) \geq 0$

2. Non degeneracy: $d(x, y) = 0 \iff x = y$

3. Symmetry: $d(x, y) = d(y, x)$

4. Triangle inequality: $d(x, z) \leq d(x, y) + d(y, z)$.

Roughly speaking, this gives us the notion of a vector space with a sense of

distance. Next we define a Cauchy sequence,

Definition 2.2.2 (Cauchy sequence). Let $\varepsilon > 0$ be given. For a metric space (X, d), we say that a sequence $\{x_n\}_{n \in \mathbb{N}} \subseteq X$ is Cauchy if $\forall \ \varepsilon \ \exists \ N_\varepsilon \in \mathbb{N}$ such that $\forall \ n, m \geq N_\varepsilon, \ d(x_n, x_m) < \varepsilon$.

In words, a Cauchy sequence is one such that the further down the sequence we go, the closer the points in the sequence get, where the distance is given by the metric of our space. From these definitions we can now define a complete metric space,

Definition 2.2.3 (Complete metric space). Let (X, d) be a metric space and $\{x_n\}_{n \in \mathbb{N}} \subseteq X$ be a Cauchy sequence. We say a metric space is complete if for every Cauchy sequence $\{x_n\}_{n \in \mathbb{N}}$, $\exists x \in X$ such that $\lim_{n \to \infty} d(x_n, x) = 0$.

Having a complete metric space imbues a vector space with many important properties [209]. It gives us the uniqueness of the adjoint, which further gives us complete set of eigenstates as well as guaranteeing an orthonormal basis, essential elements required for our description of quantum information theory [209]. When we later look at time evolution of quantum states, we will see that completeness also assures the convergence of time evolution operators within the Hilbert space, preserving the probabilistic interpretation of quantum states. The vector space for quantum states is known as a Hilbert space, defined by,

Definition 2.2.4 (Hilbert Space, $\mathcal{H}$). A complete complex vector space, along with the dot product that is also a complete metric space with respect to the distance induced by the given inner product. For vectors $|x\rangle, |y\rangle, |z\rangle \in \mathcal{H}$, they must satisfy the following conditions:

1. Symmetric inner product wrt conjugation: $\langle x|y\rangle = \overline{\langle y|x\rangle}$

2. Linear in the first argument: $\forall \alpha, \beta \in \mathbb{C}, \ \langle \alpha x + \beta y|z\rangle = \alpha \langle x|z\rangle + \beta \langle y|z\rangle$

3. Postitive semi-definite inner product: $\langle x|x\rangle \geq 0$ and $\langle x|x\rangle = 0$ iff $x = 0$.

For infinite dimensional quantum systems there are more technical requirements, but for the purposes of this thesis we will stick with finite dimensional systems. Further, for most of this thesis we will be focused on spin-1/2 particles. Without delving into the details of physics, for our purposes that is a system that can be accurately described as being equivalent to an electron with an *up* and *down* spin. As we saw previously in section 2.1 vector spaces can be decomposed into basis vectors. Here, our basis vectors have physical meaning, one being the *up* basis vector and the other being the *down*. A more physical interpretation of up and down is to think of down as being the ground state of our system and up being the first excited state. Mathematically,

$$|\text{up}\rangle = |1\rangle = \begin{bmatrix} 0 \\ 1 \end{bmatrix}, \tag{2.94}$$

$$|\text{down}\rangle = |0\rangle = \begin{bmatrix} 1 \\ 0 \end{bmatrix}. \tag{2.95}$$

We can now build up a general spin-1/2 quantum state from a linear combination of these two basis states,

$$|\psi\rangle = \alpha |0\rangle + \beta |1\rangle , \tag{2.96}$$

subject to $|\alpha|^2 + |\beta|^2 = 1$ and $\alpha, \beta \in \mathbb{C}$.

The term $|\alpha|^2$ corresponds to the probability that the quantum state is in $|0\rangle$ visa versa with $|\beta|^2$ and $|1\rangle$. We therefore refer to α and β as the probability amplitudes for $|0\rangle$ and $|1\rangle$ respectively. The complex nature of the probability amplitudes is essential, as it not only encodes the probability of a given state, but also the relative phase of our two basis states. It is this relative phase that gives rise some uniquely quantum effects like the double slit experiment [210] and Rabi oscillations [159]. Another important note is that the overall global phase of a quantum state has no physical meaning, as it cannot be measured experimentally and so has no observable impact. A result of this fact is that a common parameterisation is $\alpha = \cos(\theta/2), \beta = e^{i\phi}\sin(\theta/2)$. This factors out any imaginary component of α into the global phase. Reducing one degree of freedom should never be underestimated!

This forms the fundamental unit of quantum information, a quantum-bit if you will, much in the same way that the bit, which takes values either 0 or 1 is the classical unit of information. This is why we call this a qubit (quantum-bit). Formally,

Definition 2.2.5 (Pure State Qubit). Are defined to be $|\psi_q\rangle \in \mathbb{C}^2$, vector $\langle\psi|\psi\rangle = 1$.

2.2.2 Multi-qubit systems

Whilst it is true that one qubit (or one bit for its defence) is in itself a very interesting object to study, we must also look at multi-qubit systems. We looked at the coefficients, that we refer to as *probability amplitudes* of a single qubit as deriving the probabilities of finding the state in a given state. Then, if we take two states,

$$|\varphi_1\rangle = \begin{bmatrix} a \\ b \end{bmatrix} \tag{2.97}$$

$$|\varphi_2\rangle = \begin{bmatrix} c \\ d \end{bmatrix}, \tag{2.98}$$

where a, c and b, d are the probability amplitudes of finding the respective state in $|0\rangle$ or $|1\rangle$ respectively. When we take a joint system of the two qubits we need to represent the probability of finding (0 and 0) or (1 and 1) or (1 and 0) or (0 and 1), we can write these probability amplitudes as a vector,

$$|\varphi_1\rangle \text{ and } |\varphi_2\rangle = \begin{bmatrix} ac \\ ad \\ bc \\ bd \end{bmatrix}. \tag{2.99}$$

This is a definition we have seen previously, the Kronecker product,

$$|\varphi_1\rangle \text{ and } |\varphi_2\rangle = |\varphi_1\rangle \otimes |\varphi_2\rangle. \tag{2.100}$$

It is important that we are careful here, there is no general inner product on a product tensor space. There is however an extension over a Hilbert space. If we let $|\varphi_1\rangle, |\varphi_2\rangle$ belong to a hilbert space $\mathcal{H}_1$ and $|\psi_1\rangle, |\psi_2\rangle$ belong to a hilbert space $\mathcal{H}_2$, with respective inner products $\langle .|. \rangle_1$ and $\langle .|. \rangle_2$. Then we are able to define the inner product
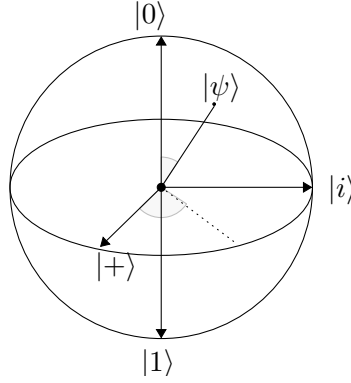
Figure 2.4: Representation of the Bloch sphere.

between the state $|\varphi_1\rangle \otimes |\psi_1\rangle$ and $|\varphi_2\rangle \otimes |\psi_2\rangle$,

$$\langle \varphi_1 \otimes \psi_1 | \varphi_2 \otimes \psi_2 \rangle = \langle \varphi_1 | \varphi_2 \rangle_1 \langle \psi_1 | \psi_2 \rangle_2. \tag{2.101}$$

In terms dimensions, for a system of n qubits, we will have a 2^n dimensional vector state.

2.2.3 Unitary transformations and Pauli matrices

Preserving the norm of these vectors is vital if we want to maintain a consistent interpretation of what our vectors represent. How might we represent this? We have a 3-dimensional vector with a fixed norm one. That sounds like moving around surface of a sphere! To see this, we begin by introducing a new representation of a single qubit state,

$$|\psi\rangle = \cos\left(\frac{\theta}{2}\right)|0\rangle + e^{-i\phi}\sin\left(\frac{\theta}{2}\right), \tag{2.102}$$

where $0 \leq \theta \leq \pi$ and $0 \leq \phi \leq 2\pi$. We can now reinterpret these two parameters θ and ϕ as spherical coordinates,

$$\boldsymbol{\alpha} = (\sin(\theta)\cos(\phi), \sin(\theta)\sin(\phi), \cos(\theta)), \tag{2.103}$$

on a sphere of radius 1 over $\mathbb{R}^3$. We call $\boldsymbol{\alpha}$ the *Bloch vector*. A visual representation of this can be found in Figure 2.4 and we call this the *Bloch sphere*.

We define a matrix U to be a *unitary matrix* if, $U^\dagger U = \mathbb{1}$. From this definition we can demonstrate that a unitary matrix is norm preserving. Explicitly, for some unitary

matrix U,

$$|| U \, |\varphi\rangle \, ||^2 = \langle\varphi|U^\dagger U|\varphi\rangle \tag{2.104}$$

$$= \langle\varphi|\mathbb{1}|\varphi\rangle \tag{2.105}$$

$$= \langle\varphi|\varphi\rangle = || \, |\varphi\rangle \, ||^2. \tag{2.106}$$

As we have already seen in equation 5.17 this is the definition of a *unitary operator*. We have also previously seen how we can define an arbitrary unitary operation,

$$U = e^{-itH}, \tag{2.107}$$

where t is the time we allow our transformation to operate on the state vector and H is the Hermitian transformation matrix, known as a *Hamiltonian*. The Hamiltonian is the driver of a quantum state's dynamics.

Definition 2.2.6 (Schrödinger equation)**.** For a time evolving quantum state $|\varphi(t)\rangle$, the Hamiltonian drives the state's dynamics described by the Schrödinger equation (we already work in units such that physical constants are set to one, i.e., $\hbar = 1$.),

$$H \, |\varphi(t)\rangle = i\frac{\partial}{\partial t} \, |\varphi(t)\rangle , \tag{2.108}$$

for a time-independent Hamiltonian, for some initial state $|\varphi(0)\rangle$ and time $t = 0$,

$$|\varphi(t)\rangle = e^{-iHt} \, |\varphi(0)\rangle . \tag{2.109}$$

The canonical basis of Hermitian matrices that will be used extensively throughout this thesis are the *Pauli matrices*.

Definition 2.2.7 (Pauli matrices)**.** The three Pauli matrices, denoted σ_x, σ_y and

σ_z are defined by,

$$\sigma_x = \begin{bmatrix} 0 & 1 \\ 1 & 0 \end{bmatrix}, \tag{2.110}$$

$$\sigma_y = \begin{bmatrix} 0 & -i \\ i & 0 \end{bmatrix}, \tag{2.111}$$

$$\sigma_z = \begin{bmatrix} 1 & 0 \\ 0 & -1 \end{bmatrix}. \tag{2.112}$$

These matrices from a basis of the traceless Hermitian Hamiltonians over the field of real values. In the same way that we did for qubits in section 2.2.1, we will first briefly examine the structure of single-body systems before moving onto multiple-body systems where we will spend most of our time. As previously shown in equation 2.107, we find a unitary operator by taking the exponential of a Hamiltonian. In this way we can generate dynamics for quantum states from the Pauli matrices. We start with a real valued vector $\boldsymbol{\alpha}$, of dimension 3 and norm 1, i.e., $|\boldsymbol{\alpha}| = 1$, along with a vector of the Pauli matrices $\boldsymbol{\sigma} = (\sigma_x, \sigma_y, \sigma_z)$. The dot product of which defines some Hamiltonian,

$$\hat{H} = (\boldsymbol{\alpha} \cdot \boldsymbol{\sigma}). \tag{2.113}$$

There are two distinct cases for powers of this Hamiltonian, an odd power $2n + 1$ and an even power $2n$ for $n \in \mathbb{N}$. For an even power we have,

$$(\boldsymbol{\alpha} \cdot \boldsymbol{\sigma})^{2n} = \mathbb{1}. \tag{2.114}$$

To show this we begin with $n = 1$,

$$(\boldsymbol{\alpha} \cdot \boldsymbol{\sigma})^2 = (\boldsymbol{\alpha} \cdot \boldsymbol{\sigma}) \cdot (\boldsymbol{\alpha} \cdot \boldsymbol{\sigma}) \tag{2.115}$$

$$= \alpha_1^2 \sigma_x \sigma_x + \alpha_1 \alpha_2 \sigma_x \sigma_y + \alpha_2 \alpha_1 \sigma_y \sigma_x + \ldots \tag{2.116}$$

$$= \alpha_1^2 \sigma_x \sigma_x + \alpha_1 \alpha_2 \sigma_x \sigma_y - \alpha_1 \alpha_2 \sigma_x \sigma_y + \ldots \tag{2.117}$$

$$= \alpha_1^2 \sigma_x \sigma_x + \alpha_2^2 \sigma_y \sigma_y + \alpha_3^2 \sigma_z \sigma_z \tag{2.118}$$

$$= (\alpha_1^2 + \alpha_2^2 + \alpha_3^2)\mathbb{1} \tag{2.119}$$

$$= \mathbb{1}, \tag{2.120}$$

where we have used the fact that we have a norm 1 vector $|\boldsymbol{\alpha}| = 1$, a Pauli matrix is its own inverse $\sigma_i \sigma_i = \mathbb{1}$ and the Pauli matrices anti-commute, $\sigma_i \sigma_j = -\sigma_j \sigma_i$. We now take $n > 2$ to be given. We can can take $(\boldsymbol{\alpha} \cdot \boldsymbol{\sigma})^{2n}$, to be $((\boldsymbol{\alpha} \cdot \boldsymbol{\sigma})^2)^n$, giving us $\mathbb{1}^n = \mathbb{1}$. Given this result we can now compute the odd power case,

$$(\boldsymbol{\alpha} \cdot \boldsymbol{\sigma})^{2n+1} = (\boldsymbol{\alpha} \cdot \boldsymbol{\sigma})^{2n}(\boldsymbol{\alpha} \cdot \boldsymbol{\sigma}) \tag{2.121}$$

$$= \mathbb{1}(\boldsymbol{\alpha} \cdot \boldsymbol{\sigma}) \tag{2.122}$$

$$= (\boldsymbol{\alpha} \cdot \boldsymbol{\sigma}). \tag{2.123}$$

We can now compute a general unitary evolution for a single qubit Hamiltonian,

$$e^{-it\hat{H}} = \sum_{n=0}^{\infty} \frac{i^n t^n (\boldsymbol{\alpha} \cdot \boldsymbol{\sigma})^n}{n!} \tag{2.124}$$

$$= \sum_{n=0}^{\infty} \frac{i^{2n} t^{2n} (\boldsymbol{\alpha} \cdot \boldsymbol{\sigma})^{(2n)}}{(2n)!} + \sum_{n=0}^{\infty} \frac{i^{2n+1} t^{2n+1} (\boldsymbol{\alpha} \cdot \boldsymbol{\sigma})^{(2n+1)}}{(2n+1)!} \tag{2.125}$$

$$= \sum_{n=0}^{\infty} \frac{-1^n t^{2n}}{(2n)!} \mathbb{1} + i^{(2n+1)} \sum_{n=0}^{\infty} \frac{-1^n t^{2n+1}}{(2n+1)!} (\boldsymbol{\alpha} \cdot \boldsymbol{\sigma}) \tag{2.126}$$

$$= \cos(t)\mathbb{1} + i\sin(t)(\boldsymbol{\alpha} \cdot \boldsymbol{\sigma}). \tag{2.127}$$

This is without loss of generality in the case that $\boldsymbol{\alpha}$ is not of norm 1, as the norm of the vector can be absorbed into t.

We saw previously in section 2.2.2 how to build up a many qubit system through the Kronecker product of qubits. For Hamiltonians this structure remains, that is to say if we want our Hamiltonian to act with the Pauli X rotation on the first qubit and do nothing to the second qubit our Hamiltonian is simply $\sigma_x \otimes \mathbb{1}$.

Here we examined the foundation of manipulating quantum state. The hidden assumption has been that we are under ideal conditions, with no external environment negativity impacting our quantum state. We now move onto building the mathematical framework to model such environmental impacts.

2.2.4 Quantum noise

Unfortunately, unwanted interaction with the environment is part and parcel of real world quantum systems. It would be a grave mistake to omit this fact entirely in our analysis.

The dynamics of a closed quantum system are given by a unitary evolution. In

a closed system, information is preserved and evolution reversible. As we have seen, we can consider a quantum system as being composed of various smaller sub-systems. When two such systems are entangled, they are correlated such that complete knowledge of one sub-system requires complete knowledge of the other as well. In this sense, if we only observe one of the sub-systems then it would appear that we have lost information regarding its state. The sub-system will now be in a state of classical uncertainty, being dependent on the state of its entangled partner.

In this way we can build up a picture of how quantum states interact with their surrounding environment. We have the main *system* (ρ_s) that we are interesting in, as well as some *environment* (ρ_e). Here, we assume that these two states begin in a product state. Noting, quantum systems are continuously interacting with their environment, but this assumption holds for key noise models and simple environments. This assumption is particularly justified by our emphasis on experimental work. At the beginning of each experiment, the experimentalist is able to remove almost all correlations with the initial state and environment. As seen in Figure 2.5, in general once a quantum system has undergone a joint evolution with some environment it will no longer be unitarily related to its initial state.

$$
\begin{array}{c}
\rho_s \quad \boxed{U_{\varphi,\gamma}} \quad \mathcal{E}(\rho_s) \\
\rho_e \qquad\qquad \boxed{Discard}
\end{array}
$$
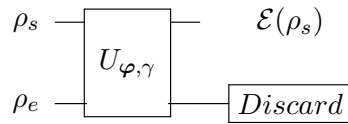
Figure 2.5: Model of environmental interaction and its effect on an input state. The unitary dynamics is parameterised by some value on the system φ and a noise strength γ (this is the typical parameterisation we will work with). The final state of the system $\mathcal{E}(\rho_s)$ represents the non-unitary *quantum channel* the system state undergoes.

An analytic form to the channel $\mathcal{E}(\rho_s)$ is still required for meaningful calculations. For this, we turn to the *partial trace*. When tracing over a sub-system, you eliminate all aspects of the state which pertain to that particular sub-system, leaving only the other. In this way, we can examine only the main system's state whilst taking into account the impact an environment has on it. Formally,

Definition 2.2.8 (Partial trace Tr_b)**.** A mapping from a global state composed of two sub-systems a and b, ρ_{ab} over a composite Hilbert space $\mathcal{H}_a \otimes \mathcal{H}_b$ onto the

Hilbert space $\mathcal{H}_a$ along with its corresponding density matrix ρ_a.

Let the set $\{\alpha_i\}$ and $\{\beta_i\}$ be some orthonormal basis states for the Hilbert space $\mathcal{H}_a$ and $\mathcal{H}_b$ respectively. Note that any state on the joint Hilbert space $\mathcal{H}_a \otimes \mathcal{H}_b$ can be expressed,

$$\rho_{ab} = \Sigma_{ijkl}\eta_{ijkl} \, |\alpha_i\rangle \, \langle\alpha_j| \, |\beta_k\rangle \, \langle\beta_l| . \tag{2.128}$$

Then the partial trace is given by,

$$\mathrm{Tr}_b \, \rho_{ab} = \Sigma_{ijkl}\eta_{ijkl} \, |\alpha_i\rangle \, \langle\alpha_j| \, \langle\beta_l|\beta_k\rangle . \tag{2.129}$$

Note that this is referred to as tracing out as $\mathrm{Tr} \, |\beta_k\rangle \, \langle\beta_l| = \langle\beta_l|\beta_k\rangle$. It is not obvious from the above definition, but the partial trace is in fact invariant with respect to the basis. Let $L(\mathcal{H})$ denote the space of linear operators on $\mathcal{H}$. Then we can define the partial trace to be the unique function $\mathrm{Tr}_b : L(\mathcal{H}_a \otimes \mathcal{H}_b) \rightarrow L(\mathcal{H}_\dashv)$, further satisfying, $\mathrm{Tr}_b(A \otimes B) = \mathrm{Tr}(B)A \; \forall A \in \mathcal{H}_a$ and $\forall B \in \mathcal{H}_b$. We can now apply the partial trace to our quantum channel outlined in Figure 2.5. To do this, we take the partial trace over the environment of the final state, to leave only the main system we are concerned with. Let $\rho_e = |\beta_0\rangle \, \langle\beta_0|$ be the initial pure state and the set $\{\beta_i\}$ be some orthonormal basis for the environment's (finite) dimensional Hilbert space. Then,

$$\mathcal{E}(\rho_s) = \mathrm{Tr}_e \, U_{\varphi,\gamma}\rho_s \otimes \rho_e U_{\varphi,\gamma}^\dagger \tag{2.130}$$

$$= \Sigma_i \, \langle\beta_i| \, U_{\varphi,\gamma}\rho_s \otimes |\beta_0\rangle \, \langle\beta_0| \, U_{\varphi,\gamma}^\dagger \, |\beta_i\rangle \tag{2.131}$$

$$= \Sigma_i E_i \rho_s E_i^\dagger . \tag{2.132}$$

Where we define E_i,

$$E_i = (\mathbb{1}_s \otimes \langle e_i|)U_{\varphi,\gamma}(\mathbb{1}_s \otimes |e_0\rangle), \tag{2.133}$$

$$= \langle e_i|U_{\varphi,\gamma}|E_0\rangle , \tag{2.134}$$

further defining $\mathbb{1}_s$ to be the identity operator on the system Hilbert space and $\{|e_i\rangle\}$ to be the set of basis states for the environment. The operator E_i is known as a *Kraus operator* acting on the space of the main system. In order to maintain the trace of the final state as 1 (*closure* condition), we have that $\Sigma_i E_i^\dagger E_i = \mathbb{1}$.

There are two main noise channels that we consider in this work. The *depolarizing channel* and *dephasing channel*. We parameterise the noise strength by γ, which takes values between 0 and 1, inclusive. For the depolarizing channel, there is probability $1-\gamma$ that nothing happens to the state and γ probability that it is completely depolarized, that is, reduced to a complete mixed state $\mathbb{1}$,

$$\mathcal{E}_\gamma(\rho) = \frac{\gamma}{2}\mathbb{1} + (1-\gamma)\rho. \tag{2.135}$$

Where depolarizing noise can be seen as shrinking the Bloch sphere in all directions, dephasing noise can be seen as shrinking the Bloch sphere only along the Pauli-Z direction,

$$\mathcal{E}_\gamma(\rho) = \gamma\sigma_z\rho\sigma_z + (1-\gamma)\rho. \tag{2.136}$$

2.2.5 Measurement

One of the key differences between quantum information and classical information is the fact that we have non-commuting observables. This is something very key to this thesis. In short, the order in which we measure things does matter. The canonical example of position and momentum. With effects like non-commuting observables that impose some limit on how well we can estimate two parameters, one could be forgiven for thinking that using quantum systems for sensing is detrimental. There is however, more that distinguishes quantum information from classical. Another key uniquely quantum effect is that of entanglement. Quantum entanglement allows two or more quantum systems to become more highly correlated than would ever be possible classically. This, as will see, is a potent resource that grants us the ability to achieve tasks not possible in a purely classical setting. There is no one clear aspect that grants us a quantum advantages. This advantage does however come at a cost, sensitivity to noise. Quantum systems are far more sensitive to environmental noise than classical systems. This makes the faithful and fast manipulation and read out of quantum information a key element to full utilization of quantum systems.

The final aspect of quantum information theory (in the general) that we cover here is information extraction. Without the ability to extract the information we have gained in our quantum system, the additional power is wasted. Information is extracted from quantum systems via measurements on said system.

In the previous section where we discussed quantum noise channels, we noted that an interaction with an environment can be seen as some joint unitary dynamics. In a

similar way, quantum measurements can be seen as an additional external coupling. A measurement of a quantum system is described by a set of operators, M_i, that we shall call measurements operators. This is a set of operators that act on the space of the system that we are measuring. The measurements are indexed by the possible outcomes of the measurements, i. If we take some final pure state $|\psi\rangle$, then the probability of any given outcome, i, is given by,

$$p(i) = \langle \psi M_i^\dagger M_i \psi \rangle.$$ (2.137)

Further, the state of the system after said outcome,

$$\frac{M_i |\psi\rangle}{\sqrt{\langle \psi M_i^\dagger M_i \psi \rangle}}.$$ (2.138)

Further, the set of measurements must satisfy the completeness condition,

$$\sum_i M_i^\dagger M_i = \mathbb{1}.$$ (2.139)

There are two main classes of measurement we consider, *projective* and *general positive operator valued measure (POVM)*. A rank-1 projective measurement (hereby refered to as projective) is one where the measurement operator is given by a pure projective state. The resulting state after such a measurement will either be in the state queried or its orthogonal counterpart. A POVM is a generalisation of a projective measurement. In the same way that we can take general non-untiary dynamics and *purify* then into a larger space of unitary dynamics, we can see a POVM as being a projective measurement over a larger space. It is Naimark's dilation theorem [74] (sometimes spelt Neumark) that shows precisely how a POVM can be obtained from a projective measurement acting on a larger space. Naimark's theorem states, that for any set of POVMs $\{M_i\}$ acting over a Hilbert space $\mathcal{H}_1$, then there existing a set of projective measurements $\{\Pi_i\}$ acting on a larger Hilbert space $\mathcal{H}_2$ and a mapping T, such that $\forall\, i$,

$$M_i = T^\dagger \Pi_i T.$$ (2.140)

We are able to outline a rough proof of this statement with the direct construction of T. Let $\mathcal{H}_s$ be the Hilbert space of the system we are interested in measuring with a POVM $\{M_i\}_{i=1}^n$, further $\mathcal{H}_a$ be an ancillary Hilbert space with basis states $\{|i\rangle\}_{i=1}^n$, along with the total Hilbert space $\mathcal{H}_t = \mathcal{H}_s \otimes \mathcal{H}_a$. We now define the projective
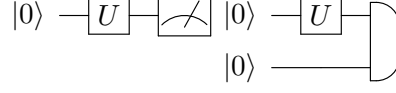
Figure 2.6: Representation of a projective measurement and a general POVM.

measurement and transformation as such,

$$\Pi_i = \mathbb{1}_s \otimes |i\rangle \langle i|_a \,, \tag{2.141}$$

$$T = \sum_{i=1}^{n} \sqrt{M_i} \otimes |i\rangle_a \,. \tag{2.142}$$

We can now explicitly show that the probability of outcome i on state $|\psi\rangle \langle\psi|_s$ when measured with POVM M_i, is the same as when using the transformed projective measurement Π_i,

$$p(i) = \mathrm{Tr}\Big[|\psi\rangle \langle\psi|_s \, T^\dagger \Pi_i T\Big], \tag{2.143}$$

$$= \mathrm{Tr}\Big[|\psi\rangle \langle\psi|_s \, T^\dagger \mathbb{1}_s \otimes |i\rangle \langle i|_a \, T\Big], \tag{2.144}$$

$$= \mathrm{Tr}\left[|\psi\rangle \langle\psi|_s \left(\sum_{j=1}^{n} = \sqrt{M_j}^\dagger \otimes \langle j|_a\right) \mathbb{1}_s \otimes |i\rangle \langle i|_a \left(\sum_{k=1}^{n} = \sqrt{M_k} \otimes |k\rangle_a\right)\right], \tag{2.145}$$

$$= \mathrm{Tr}[|\psi\rangle \langle\psi|_s \, M_i]. \tag{2.146}$$

Indeed, this is how we are able to physically implement a POVM on a physical system, by extending the mapping T, into a unitary operator U such that $T = U(\mathbb{1}_s \otimes |0\rangle_a)$, which can always be done [74]. The introduction of an arbitrary *ancilla* (or helper) system (of maximum dimension the same as the main system) and then taking a measurement over the joint system is sufficient to model a general measurement on the main system. A representation can be seen in Figure 2.6.

2.3 Magnetometry

The physical set up of interest in this thesis is that of an external magnetic field acting on a spin-1/2 system. As such we outline precisely what we mean by magnetometry for the purposes of this thesis. For some system of N qubits, a magnetic field acts independently on each qubit. Mathematically this is described by a *single-body*

Hamiltonian. Which for some one qubit Hamiltonian h and N qubit is given by,

$$\hat{H}(\hat{h}, N) = \sum_{i=1}^{N} \mathbb{1}^{\otimes(i-1)} \otimes \hat{h} \otimes \mathbb{1}^{\otimes(N-i)}. \tag{2.147}$$

Within this work we assume that the magnetic field is uniform over the qubit system. Other works have examined the case where a magnetic field varies over the qubits and gradients of a magnetic field can be estimated [10, 12]. A magnetic field can be described by three vector components and we will denote this vector $\varphi = (\varphi_x, \varphi_y, \varphi_z)$. We will examine two cases of a magnetic field, the full three parameter case and a single parameter instance where the magnetic field only acts in the Z-direction. Giving us two central Hamiltonians of interest,

$$\hat{H}_1 = \varphi_z \hat{H}(\sigma_z, N), \tag{2.148}$$

$$\hat{H}_3 = \varphi_x \hat{H}(\sigma_x, N) + \varphi_y \hat{H}(\sigma_y, N) + \varphi_z \hat{H}(\sigma_z, N). \tag{2.149}$$

Note that standard notation for $\hat{H}_1$ is L_z^N, we use this notation to distinguish between the one and three parameter Hamiltonian cleanly and only ever study the Pauli-Z one parameter Hamiltonian. For clarity we enumerate a set of definitions that fully describe the possible elements required for the theoretical study of a magnetometry problem.

The NV center [157, 202, 42] is a defect in diamond comprised of a nitrogen atom where a carbon would usually sit, along with an adjacent vacancy, or lack of atom in the lattice. An electron pair protrudes from the nitrogen atom and forms a spin-1 system, that can also be treated as a spin-1/2 system. For example, at zero magnetic field there is a degeneracy in the spin-1 system that makes two of the energy level indistinguishable, hence effectively a spin-1/2 system.

The NV center has been demonstrated as an excellent magnetometry architecture, possessing high sensitivity to magnetic fields along with long coherence times [199, 148, 180, 18, 37, 50, 63]. Microwave control, optical readout and high sensitivity even at room temperature are just a handful of further properties that make the NV center an excellent experimental set-up.

2.4 Metrology

Here we will examine the relevant topics in quantum metrology that will aid our task. Quantum metrology is a field that looks to exploit quantum resources that are not available in classical metrology. We will see that entanglement is the strongest resource at our disposal, it should be noted here though that very large entangled systems are practically very difficult to maintain and protect from noise. However, that is a problem for another time as we restrict ourselves to the much nicer noiseless setting.

It is only recently that we have reached the point that experimental measurements are quantum limited, that is to say that an experiment can gain no more sensitivity classically, but quantum metrology allows us to get more sensitivity. The most exciting examples include the LIGO search for gravitational waves [113], which actually utilities squeezing more than entanglement as well as atomic clocks. The use of squeezed light as a resource in the LIGO search has been a relatively recent upgrade to the experiment as theory and technology has improved radically in recent years. Of course magnetometry is another exciting application of quantum metrology that we are delving into here. The main advantage here is the ability to measure a magnetic field without using another one, this goes some way to eliminate the observer effect and give a truer value for the field strength. That is, using a probe to measure a magnetic field that doesn't itself generate one eliminates a potential source of systematic error. There are many very promising and exciting applications for magnetometry including the medical monitoring of heart and brain activity [200, 50] as well as GPS without the need for satellites [76]. It should here be stressed that there is no shortage of uses for magnetometry due to the ubiquity of magnetic fields [167].

It is only in the multi-parameter setting that we invoke all of the axioms of quantum mechanics, most importantly the incompatibility of observables is bought into the picture. The foundations of quantum multiparameter estimation was outlined by Helstrom [93] and Holevo [97]. Magnetometry is one of the archetypal examples in quantum enhanced estimation.

The goal of quantum enhanced multi-parameter estimation is to optimally estimate more than one parameter that is encoded into some initial state by an external process. Our optimality condition is the minimisation of the sum of variances of all parameters we are interested in estimating. This is represented by the blue segment in Figure 2.7.

Quantum enhanced metrology, is the exploration of extracting maximal information from a given physicsal system about a vector of unknown parameters. It is of great
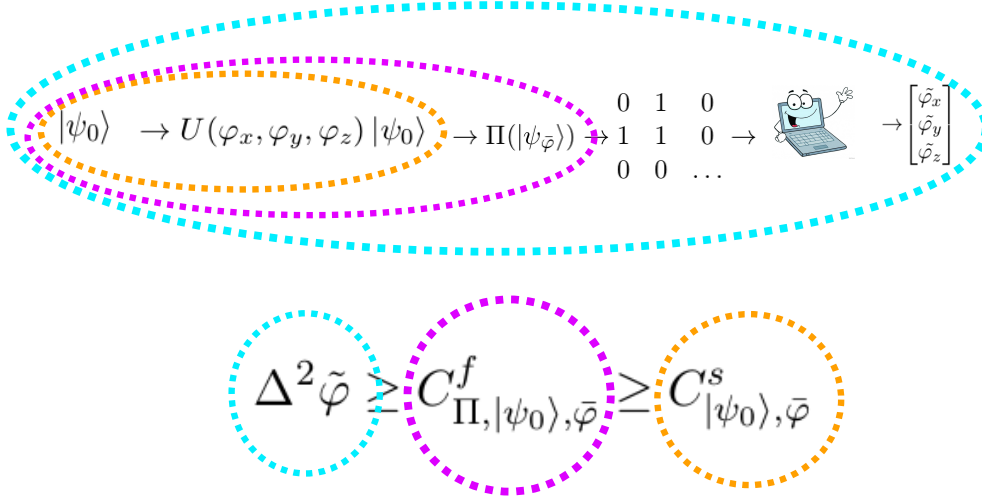
Figure 2.7: A cartoon representation of the standard quantum estimation process along with the hierarchy of bounds it introduces. The blue dotted segment represents the sum variance of your estimates, the performance figure for any actual experiment. The purple segment represent the classical Fisher information, the first Cramér-Rao bound in our hierarchy. It does not depend on the estimator or data collected, only the parameter encoded state, and a set of POVMS. Finally the orange section represents the solely parameter encoded state dependant Cramér-Rao bounds.

importance to many existing and emerging quantum technologies. In a typical linear scheme there are three stages to any metrology experiment we consider; preparation, encoding, measurement. This work will examine the relationship between the quantum bounds on the preparation stage and the classical bounds at the measurement stage. In particular, we look at how the classical bounds can asymptotically or indeed in a finite number of copies approach the quantum bounds.

Multi-parameter metrology is distinct from single-parameter metrology in several aspects. Firstly the single-parameter HCRB (reduces down to the Quantum Fisher Information (QCRB) [130]) is always saturable [31]. Whereas there is no guarantee of attainability in the multi-parameter setting. This comes from the second important distinction, incompatible observables. The inability to simultaneously diagonalise observables limits the precision of simultaneous estimation. In this way multi-parameter estimation invokes all axioms of quantum mechanics. This is what gives rise to the differing behavior in attainability for multi-parameter problems.

As well as the fundamental questions of attainability there are also interesting practical questions that can be answered at the same time. As in all emerging quantum technolo-

gies it is important to look at the question of classical/quantum state/measurement. In this way, we look to investigate where quantum advantage is most useful over noise. On the single copy level it is sufficient to determine whether or not the state/measurement are product states or not and is known for single-parameter estimation [31, 11]. The possibility of requiring multiple copies in the multi-dimensional setting adds another question to this, e.g. is it possible to gain an advantage by using an entangling measurement over multiple copies when the input state and measurement on the single copy level are product, as is the case for high noise.

2.4.1 Classical estimation theory

Estimation theory builds a framework around the problem of estimating the value of a vector of parameters $\boldsymbol{\varphi} = [\varphi_1, \ldots, \varphi_p]^T$. This vector of parameters describe some physical system, from which we are able to take measurements. These measurement outcomes contain some random component and our task is to use an estimator to attempt to approximate the true value of $\boldsymbol{\varphi}$.

There are four key components of an estimation problem. Firstly, the p parameters we wish to estimate, $\boldsymbol{\varphi} = [\varphi_1, \ldots, \varphi_p]^T$. Secondly, a statistical sample of observed outcomes, this being a vector of k outcomes $\boldsymbol{x} = [x_1, \ldots, x_k]$. Thirdly, a probability density function $p(\boldsymbol{x}|\boldsymbol{\varphi})$, that we use to describe the underlying distribution our measurements are described by. This probability density function is conditional on the values of the parameters. Finally, an estimator $\tilde{\boldsymbol{\varphi}}$, a function from the space of observed outcomes to the parameter space.

Estimation theory is also concerned with asking, how good is an estimator? In particular, we want to know how *precise* an estimator is. This section will dedicate significant time to Cramér-Rao bounds, lower bounds on the variance of an estimator. This allows for more detailed study of the individual components of an estimation problem. For example, how sensitive is a quantum state to an unknown parameter, independent of an estimator or measurement?

We now reframe classical estimation into a quantum setting. More formally, given a finite-dimensional Hilbert space $\mathcal{H}$, we consider a family of quantum states $\rho_{\boldsymbol{\varphi}}$ that depends on a vector $\boldsymbol{\varphi}$ of p real parameters. The set $\{\boldsymbol{\varphi}, \rho_{\boldsymbol{\varphi}}, \mathcal{H}\}$ is also known as a quantum statistical model. Estimation is then performed from the measurement outcomes x, with probability given by the Born rule $p(x|\boldsymbol{\varphi}) = \mathrm{Tr}[\rho_{\boldsymbol{\varphi}}\Pi_x]$, where Π_x is an element of a positive, operator-valued measure (POVM) $\Pi = \{\Pi_x \geq 0 | \sum_x \Pi_x = \mathbb{1}\}$ that describes the statistics of the measurement apparatus. In particular, we often

focus on rank-1 projective measurements $\Pi_x = |x\rangle\langle x|$, where $|x\rangle$ is an orthonormal basis; for brevity we will refer to them as projective measurements. The function of the outcomes x that gives an estimate $\tilde{\varphi}(x)$ is the estimator and its precision can be quantified by the mean square error matrix (MSEM)

Definition 2.4.1 (mean square error matrix (MSEM))**.**

$$V_{\varphi}(\Pi, \tilde{\varphi})_{i,j} = \sum_x p(x|\boldsymbol{\varphi})[\tilde{\varphi}(x)_i - \varphi_i][\tilde{\varphi}(x)_j - \varphi_j]. \qquad (2.150)$$

To compare estimation errors in a strictly ordered way we define the scalar figure of merit [1],

$$\Delta^2\tilde{\boldsymbol{\varphi}} = \text{Tr}[V_{\boldsymbol{\varphi}}(\Pi, \tilde{\boldsymbol{\varphi}})]. \qquad (2.151)$$

Furthermore, we restrict ourselves to locally unbiased estimators that satisfy for all i, j [97]

$$\sum_x p(x|\boldsymbol{\varphi})(\tilde{\varphi}(x)_i - \varphi_i) = 0, \qquad (2.152)$$

$$\sum_x \tilde{\varphi}(x)_i \frac{\partial p(x|\boldsymbol{\varphi})}{\partial \varphi_j} = \delta_{ij}. \qquad (2.153)$$

Noting that this relation holds for fixed value of $\boldsymbol{\varphi}$. Here and henceforth, all quantities are evaluated at the true value of the parameter. The MSEM in Eq. (2.150) for such estimators is just the covariance matrix, which satisfies the lower bound $V_{\boldsymbol{\varphi}}(\Pi, \tilde{\boldsymbol{\varphi}}) \geq F(\rho_{\boldsymbol{\varphi}}, \Pi)^{-1}$, in terms of the classical Fisher information (CFI) matrix [122]

Definition 2.4.2 (classical Fisher information matrix)**. ,**

$$F(\rho_{\boldsymbol{\varphi}}, \Pi)_{ij} = \sum_x p(x|\boldsymbol{\varphi}) \left(\frac{\partial \log p(x|\boldsymbol{\varphi})}{\partial \varphi_i} \right) \left(\frac{\partial \log p(x|\boldsymbol{\varphi})}{\partial \varphi_j} \right). \qquad (2.154)$$

---

[1]More generally it is common to consider the figure of merit $\text{Tr}\, W V_{\boldsymbol{\varphi}}$ depending on a positive weight matrix W; however, in this work we choose $W = \mathbb{1}$, except when explicitly stated

We will mainly focus on the corresponding *scalar* bound $C^{\mathrm{C}}(\rho_\varphi, \Pi)$ such that

---

classical Cramér-Rao bound

$$\Delta^2 \tilde{\varphi} \geq \mathrm{Tr}[F(\rho_\varphi, \Pi)^{-1}] = C^{\mathrm{C}}(\rho_\varphi, \Pi), \qquad (2.155)$$

---

where the superscript stands for classical, in contrast to quantum bounds which will depend only on the family ρ_φ and not on the measurement. The Cramér-Rao bound was orignally demonstrated and proven by Harald Cramér [49] and Calyampudi Radhakrishna Rao [164]

2.4.2 Quantum Cramér-Rao bounds

The CCRB, lower bounds the variance of an estimation problem independent of the estimator function. We now look at QCRBs, which look to lower bound the CCRB, independent of the measurement. This grants the ability to only study the input state to our estimation problem and can help reveal the deeper physical and information theoretic intuition behind quantum estimation theory.

The CFI matrix is upper bounded as $F(\rho_\varphi, \Pi) \leq J(\rho_\varphi)$ by the QFI matrix

---

Definition 2.4.3 (Quantum Fisher information matrix).

$$J(\rho_\varphi)_{ij} = \mathrm{Tr}\left[\frac{L_i L_j + L_j L_i}{2} \rho_\varphi\right], \qquad (2.156)$$

---

defined in terms of the symmetric logarithmic derivative (SLD) $\{L_i\}$ satisfying $\partial \rho_\varphi / \partial \varphi_i = (L_i \rho_\varphi + \rho_\varphi L_i)/2$ and $L_i^\dagger = L_i$. The corresponding scalar bound $C^S(\rho_\varphi)$ is [2]

Quantum Cramér-Rao bound

$$\Delta^2 \tilde{\varphi} \geq C^{\mathrm{C}}(\rho_\varphi, \Pi) \geq C^S(\rho_\varphi) = \mathrm{Tr}\big[J(\rho_\varphi)^{-1}\big]. \qquad (2.157)$$

---

[2]The superscript S denotes that the bound is obtained from the SLDs rather than other logarithmic derivatives. We will not use them in this work as they are less informative than the HCRB.

We outline of a proof for the single parameter QCRB, following [146], to give an intuitive as to where this form comes from. See Appendix H. of [121] to see a complete proof in the multiparameter picture. We begin with the following substitution,

$$\partial_\varphi p(x|\varphi) = \text{Tr}[\partial\varphi\rho_\varphi\Pi_x], \tag{2.158}$$

$$= \text{Re}(\text{Tr}[\rho_\varphi\Pi_x L_\varphi]). \tag{2.159}$$

Which we use with eq. 2.4.2 to maximise over measurements,

$$F(\rho_\varphi, \Pi) = \sum_x \frac{\text{Re}(\text{Tr}[\rho_\varphi\Pi_x L_\varphi])^2}{\text{Tr}[\rho_\varphi\Pi_x]} \tag{2.160}$$

$$\leq \sum_x \left| \frac{\text{Tr}[\rho_\varphi\Pi_x L_\varphi]}{\sqrt{\text{Tr}[\rho_\varphi\Pi_x]}} \right|^2 \tag{2.161}$$

$$= \sum_x \left| \text{Tr}\left[\frac{\sqrt{\rho_\varphi}\sqrt{\Pi_x}}{\sqrt{\text{Tr}[\rho_\varphi\Pi_x]}} \sqrt{\Pi_x}L_\varphi\sqrt{\rho_\varphi} \right] \right|^2 \tag{2.162}$$

$$\leq \sum_x \text{Tr}[\Pi_x L_\varphi\rho_\varphi L_\varphi] \tag{2.163}$$

$$= \text{Tr}\left[\rho_\varphi L_\varphi^2\right]. \tag{2.164}$$

Which gives us, $F(\rho_\varphi, \Pi) \leq J(\rho_\varphi)$. The HCRB introduced by Holevo [97], in the equivalent formulation given by Nagaoka [136], is defined as

---

Holevo-Cramér-Rao bound,

$$C^{\text{H}}(\rho_\varphi) = \min_X \text{Tr}\,\text{Re}\,Z[X] + \|\text{Im}\,Z[X]\|_1, \tag{2.165a}$$

$$\text{s.t.}\quad \text{Tr}\,X_i\frac{\partial\rho_\varphi}{\partial\varphi_j} = \delta_{ij}, \tag{2.165b}$$

$$Z[X]_{ij} = \text{Tr}[\rho_\varphi X_i X_j] \tag{2.165c}$$

---

where $X = \{X_1, \ldots X_p\}$ is a collection of p Hermitian matrices, Re and Im denote the elementwise real and imaginary part of a matrix and $\|\cdot\|_1$ denotes the trace norm (sum of the singular values). The explicit computation form of the HCRB, as

presented by Nagaoka [136], gives us a useful form for explicit computation. In order to gain more intuition from the proof of the HCRB we return to its orignal form from Holevo [97],

$$C^{\mathrm{H}} = \min_{X,V} \big(\mathrm{Tr}[V] V \geq Z[X], \mathrm{Tr}\big[\nabla \rho_\varphi X^T\big] \big), \tag{2.166}$$

where $X = [X_1, \ldots X_p]$, is a vector p (being the number of paramters we wish to estimate) of Hermitian matrices, acting on the Hilbert space of $\rho_v arphi$, V is a real square matrix of dimension p and $Z[X]$ takes the same definition as eq. 4.3. We follow the proof of [53], which in turn follows the proof of [136], with an increased emphasis on extracting a physical intuition from the proof. We begin with any measurement, $\{M_i\}$, a locally unbiased estimator $\tilde{\varphi}(i)$ of some fixed vector of parameters φ, of length p. From this, we define a vector of length p, of Hermitian matricies, $X = [X_1, \ldots, X_p]^T$,

$$X = \sum_i (\tilde{\varphi}(i) - \varphi) M_i. \tag{2.167}$$

We can gain some immediate intuition if we first look at the case where $\{M_i\}$ is projective. As we can compute the following equality,

$$V_\varphi(\Pi, \tilde{\varphi}) = \mathrm{Tr}\big[\rho_\varphi X X^T\big]. \tag{2.168}$$

In the setting where $\{M_i\}$ is not projective, this equality does not generally hold. We will now define a new extended space, that will allow us to find an inequality that will hold in general.

Let $\mathbb{C}^p$, be a complex extension to the Hilbert space $\mathcal{H}$ of ρ_φ, $\mathbb{C}^p \otimes \mathcal{H}$. We now construct a positive (implying partial traces are also positive), linear operator T on $\mathbb{C}^p \otimes \mathcal{H}$,

$$T = \sum_i [(\tilde{\varphi}(i) - \varphi)\mathbb{1} - X] M_i [(\tilde{\varphi}(i) - \varphi)\mathbb{1} - X]^T. \tag{2.169}$$

Taking the trace of this operator on the new total state space,

$$\mathrm{Tr}_{\mathcal{H}}[(\mathbb{1} \otimes \rho_\varphi)] = \sum_i (\tilde{\varphi}(i) - \varphi)\,\mathrm{Tr}[M_i \rho_\varphi](\tilde{\varphi}(i) - \varphi)^T - \mathrm{Tr}\big[\rho_\varphi X X^T\big] \tag{2.170}$$

$$= V_\varphi(\Pi, \tilde{\varphi}) - \mathrm{Tr}[\rho_\varphi] \tag{2.171}$$

$$= V_\varphi(\Pi, \tilde{\varphi}) - Z[X] \geq 0. \tag{2.172}$$

From which we can derive the following matrix and scalar bounds,

$$V_{\boldsymbol{\varphi}}(\Pi, \tilde{\boldsymbol{\varphi}}) \geq Z[X] \tag{2.173}$$

and

$$\mathrm{Tr}[V_{\boldsymbol{\varphi}}(\Pi, \tilde{\boldsymbol{\varphi}})] \geq \mathrm{Tr}[Z[X]]. \tag{2.174}$$

The intuition we see here is similar to that of Naimark's theorem. We take a POVM, extend the Hilbert space such that we have the behavior of a projective measurement and optimise over the new free parameters. Here we found a bound that depends only on the measurement and estimator through X. As such, if we are to minimise over valid vectors X, then we will obtain a universal bound. Whilst eq. 2.174, is a valid Cramér-Rao bound, it isn't as tight as it could be. The trace of a complex, symmetric matrix disregards any contribution that could stem from the complex entries of $Z[X]$. In order to mitigate this oversight, we introduce a $p \times p$ real matrix V, such that $V \geq Z[X]$, in order to obtain the form found in eq.2.166. We now have a stronger Cramér-Rao bound than before, satisfying all the same conditions.

Crucially, the HCRB is always tighter than the QCRB. Mathematically,

$$\Delta^2 \tilde{\boldsymbol{\varphi}} \geq C^{\mathrm{C}}(\rho_{\boldsymbol{\varphi}}, \Pi) \geq C^{\mathrm{H}}(\rho_{\boldsymbol{\varphi}}) \geq C^{\mathrm{S}}(\rho_{\boldsymbol{\varphi}}), \tag{2.175}$$

meaning that it takes better account of the possible incompatibility of the optimal observables while estimating multiple parameters simultaneously. It is important to note that the HCRB often collapses to other scalar quantum CRBs [7, 184]. The constrained optimisation (5.1) has recently been shown to be a convex problem [6] and can be rewritten as an SDP, which drastically reduces the cost of numerical evaluation.

The minimisation (5.1) does not guarantee the existence of a POVM acting on $\mathcal{H}$ such that $C^{\mathrm{C}}(\rho_{\boldsymbol{\varphi}}, \Pi) = C^{\mathrm{H}}(\rho_{\boldsymbol{\varphi}})$, apart from particular cases such as pure states [130]. For mixed states, the HCRB is also attainable [92, 105, 204, 207, 53], although requiring, in general, a collective measurement on an asymptotically large number of identical copies of $\rho_{\boldsymbol{\varphi}}$.

This gives another definition of the HCRB as

$$C^{\mathrm{H}}(\rho_{\boldsymbol{\varphi}}) = \lim_{k \to \infty} \min_{\Pi^{(k)}} k\, C^{\mathrm{C}}(\rho_{\boldsymbol{\varphi}}^{\otimes k}, \Pi^{(k)}), \tag{2.176}$$

where $\Pi^{(n)}$ is a POVM acting on the Hilbert space $\mathcal{H}^{\otimes n}$. We further introduce a class

of k-copies attainable bounds [3]

$$C^{(k)}(\rho_{\varphi}) = \min_{\Pi^{(k)}} k \, C^{\mathrm{C}}\left(\rho_{\varphi}^{\otimes k}, \Pi^{(k)}\right), \qquad (2.177)$$

so that formally we have $C^{(\infty)}(\rho_{\varphi}) = C^{\mathrm{H}}(\rho_{\varphi})$.

An important final note, we call a quantum statistical model *asymptotically classical* when the condition of weak commutativity is met,

$$\mathrm{Tr}[(L_i L_j - L_j L_i)\rho_{\varphi}] \ \forall \ i, j. \qquad (2.178)$$

When a quantum statisical model satisfies the above condition, the HCRB and QCRB are equal,

$$C^{\mathrm{H}}(\rho_{\varphi}) = C^{S}(\rho_{\varphi}). \qquad (2.179)$$

2.5 Control theory

In control theory, we are interested in determining what unitary evolutions and subsequently what states can be generated in a given (closed) quantum system. We assumed the Hamiltonian is of form,

$$H(t) = H_0 + \sum_k f_k(t) H_k, \qquad (2.180)$$

where H_0 is the drift Hamiltonian that we have no control over and H_k is the set of control Hamiltonians that we do have control over. The task in any quantum control problem is to determine $f_k(t)$, this represents the set of controls an experimentalist will be able to implement. The time evolution of a system is given by the Schrödinger equation,

$$\frac{\partial}{\partial t} |\psi_0\rangle = \hat{H}(t) |\psi_0\rangle, \qquad (2.181)$$

where $|\psi_0\rangle$ is our initial state. Unlike the case of a time independent Hamiltonian, no close form expression exists for the evolution of a time dependant Hamiltonian [25]. Instead, the time ordered exponential, $\exp_{\mathcal{T}}$ is used to represent the evolution of the

---

[3]This bound for $k = 1$ is also known as the *most informative* bound [136], not to be confused with the maximum between SLD and right logarithmic derivative (RLD) bounds [75].

system, given by,

$$\exp_{\mathcal{T}}\left(-i\int_0^{t'}\hat{H}(t)\mathrm{d}t\right) = \sum_{n=0}^{\infty}\frac{1}{n!}\int_0^{t'}\dots\int_0^{t'}\mathcal{T}\left(\hat{H}(t_1)\dots\hat{H}(t_n)\right), \quad (2.182)$$

$$= \sum_{n=0}^{\infty}\int_0^{t'}\int_0^{t_n}\dots\int_0^{t_2}\hat{H}(t_n)\dots\hat{H}(t_1)dt_1\dots dt_n$$

$$(2.183)$$

where $\mathcal{T}$ is the time ordering operator that ensures its arguments remain in decreasing time order going left to right when the product of its arguments is taken, e.g.

$$\mathcal{T}\left(\hat{H}(1)\hat{H}(3)\hat{H}(2)\right) = \hat{H}(3)\hat{H}(2)\hat{H}(1). \quad (2.184)$$

In the cases when no analytic form is attainable, we are able to splice the evolution into infinitesimal steps. Within each of these infinitesimal time steps, we assume that the Hamiltonian is approximately time independent and return to a closed form expression.

From this we define the idea of a reachable unitary. This is a unitary operator $U(t)$, for which there exists some $f_k(t)$ that achieves $U(t)$. More formally we define the set of reachable unitaries $\mathcal{R}$ as[59],

$$\mathcal{R} = \{U \in \mathcal{U}(d)|\exists T, f_k|U(f_k(T)) = U\}, \quad (2.185)$$

where $\mathcal{U}(d)$ is the Lie group of all unitary evolutions of dimension d and $U(f_k(t)) = e^{iH(t)t}$ is the time operator from the Schrödinger equation. Trialing every possible function $f_k(t)$ would not be an efficient method of calculating the reachable set. If we restrict ourselves to finite dimensions, then physically we will not be able to exactly achieve the desired unitary evolution. Instead we therefore examine the case of reaching a desired unitary arbitrarily well. Topologically, what we are talking about here is the closure of the set $\mathcal{R}$, denoted $\bar{\mathcal{R}}$ and defined to be [59],

$$\bar{\mathcal{R}} = \{U \in \mathcal{U}(d)|\forall\epsilon > 0 \exists V \in \mathcal{R}|\|U - V\| \leq \epsilon\}. \quad (2.186)$$

This gives us the notion of simulable Hamiltonians. We define a simulable Hamiltonian $A = -iH$, if e^{At} is reachable arbitrarily well for any $t \geq 0$. Now we are able to examine the operations that we are allowed and will keep us inside the same Hilbert space. Let us denote $\mathcal{S}$ to be the set of simulable Hamiltonians [158].

1. For $A, B \in \mathcal{S}$ then we have that $A + B \in \mathcal{S}$.

2. For $A \in \mathcal{S}$ and $\alpha > 0$, then $\alpha A \in \mathcal{S}$.

3. For $A \in \mathcal{S}$ then we have $-A \in \mathcal{S}$.

4. For $A, B \in \mathcal{S}$ then we have that $[A, B] \in \mathcal{S}$. Where denotes the commutator $[A, B] = AB - BA$.

In terms of a brief justification, 1. follows from the Trotter formula [181],

$$\lim_{n \to \infty} \left(e^{At/n} e^{Bt/n} \right)^n = e^{(A+B)t}. \tag{2.187}$$

Physically speaking the justification of 2. follows from different strengths of pulses being simulated by increasing and decreasing the time period of the pulse. We take the justification of 3. from the quantum recurrence theorem [26]. The quantum recurrence theorem states [215],

Theorem 1 (Quantum recurrence theorem). *For a finite dimensional Hilbert space, with eigenstates $\{|m\rangle\}$ and eigenvalues $\{E_m\}$, then for any initial state,*

$$|\psi_0\rangle = \sum_{m=1}^{N} a_m |m\rangle, \tag{2.188}$$

with time evolution given by,

$$|\psi(t)\rangle \sum_{m=1}^{N} a_m e^{-iE_m t} |m\rangle, \tag{2.189}$$

will return to $|\psi_0\rangle$ up to arbitrary precision infinitely many times.

The final justification for 4. comes from the Baker–Campbell–Hausdorff formula [181],

$$\lim_{n \to \infty} \left(e^{At/n} e^{Bt/n} e^{-At/n} e^{-Bt/n} \right)^{n^2} = e^{[A,B]t^2}. \tag{2.190}$$

What we find here is that these properties are in fact the same as those of a Lie group. This allows us to characterise the reachable unitaries with much greater ease.,

i.e. by taking commutations and linear combinations of the elements of H. For example if our Hamiltonian is given by, $H = X + f(t)Z$, then we can take the commutator $[X, Z] = XZ - ZX = Y$. Here we have all three Pauli matrices on a single qubit, which gives us universal control in this setting.

Chapter 3

Optimal quantum states for 3D magnetometry

> ... premature optimization is the root of all evil.
>
> ———————————————
>
> Donald Knuth

3.1 Introduction

The Quantum Fisher Information has been studied with great success from the earliest days of quantum metrology [65, 31, 120, 145, 186, 9, 16, 93, 97]. In particular for single-parameter problems where the QCRB is the ultimate bound for estimation. There have further been many 'real world' success stories of the theoretical analysis of sensing problems. The most notable is perhaps the use of squeezed light for the purposes of sensing gravitational waves [2, 113, 29, 39] (note that squeezed light was not part of the original LIGO experimental setup and came later as theory and experimental technique improved). It is in use now. With even more emerging technologies proving the power of quantum enhanced metrology [24, 213, 202, 127, 160, 21]. This initial chapter and the remainder focus on the case of magnetometry. There are multiple experimental works that have found great success in the world of quantum enhanced magnetometry, including navigation [78], medical imaging [50] and NMR [169, 188, 4, 128].

The QCRB has also been used in the analysis of multi-parameter problems [218, 118, 83, 73, 161, 8, 141, 195]. The QCRB only retains its status as the ultimate

bound for estimation when asymptotic classicality is satisfied. The single parameter magnetometry problem has been examined in great detail over the years [192, 101]. We know the optimal states for noiseless and in a noisy environment. We also know how to generate these optimal states [65, 85, 11, 101] as well as the optimal measurements. In this chapter we look to fill in some of those gaps for 3D magnetometry. Practically, it is very rare that a magnetic field is truly one dimensional. The multidimensional problem has very different geometry, optimal states and measurements.

This chapter follows on from the work of Baumgratz and Datta [19], in which it was shown that the QCRB for magnetometry depends only on the one and two body reduced density matrices. Giving much deeper analytic insight to the problem of 3D magnetometry than was previously only allowed for with the aid of numerical results. In particular it noted that maximum entanglement with respect to the two body correlations is not optimal (in fact, gives rise to a singular model) and that there is a trade-off between entanglement and QCRB. A factor of 3 improvement in performance when simultaneous estimation was employed over individual estimation was also demonstrated. The state that was considered for simultaneous estimation was the 3D-GHZ state,

$$\left|\psi_N^{\text{3D-GHZ}}\right\rangle = \frac{1}{\mathcal{N}} \sum_{k=1}^{3} |\phi_k^+\rangle^{\otimes N} + |\phi_k^-\rangle^{\otimes N}, \qquad (3.1)$$

which was shown to present Heisenberg scaling in the noiseless case [19]; $|\psi_k^{\pm}\rangle$ are the eigenvectors corresponding to the ± 1 eigenvalues of the kth Pauli matrix and $\mathcal{N}$ is the normalisation. This is a natural state to consider, for 3D magnetometry when looking for intuition from the single parameter case. For any single direction magnetic field estimation σ_i, the optimal state is the GHZ in that given direction. As such, a state which is evenly split between these 3 single parameter optimal states is considered. This state was shown to have an attainable QCRB, with explicit POVMs attaining the bound being given. The optimal state and measurement in the parallel scheme has also been identified [99]

Building from this, in this chapter we show that this proposed state is optimal for a large number of qubits (where here large is $N>8$ as we will see later, this is the point at which the geometry of the 3D-GHZ states stabilises). We will see that this stems from the particular geometry of small qubit states, not having enough degrees of freedom within the purity constraints to generate arbitrary reduced density matrices. For small numbers of qubits, the problem of finding a state that has a reduced density

matrix close to some target density matrix is largely intractable analytically (the quantum marginal problem). As such we develop a genetic inspired optimiser which searches for optimal states with respect to QCRB. The key novelty of this optimisation algorithm is its capability of finding structure . That is, we are able to write a closed form expression for the optimal state and its dependance on N.

Having developed an optimiser and calculated optimal noiseless states, the natural extension is to consider noise. Taking Pauli-Z dephasing as the example noise model we find the point at which optimal states transition. The physical system that motivates this thesis is the NV center in diamond. There are two fundamental errors that can occur in a quantum channel, bit flip error and phase errors. Bit flip errors are typically highly suppressed by the large energy gap between the 0 and 1 states. Phase errors however, occur at a much greater rate due to the coupling to other nearby spin systems. This noise characterisation has been confirmed by various studies [131, 60, 61]. In other words, for 3D magnetometry what are the low, medium and high noise thresholds, as well as what are the optimal states for those regions. It is known that the optimal states for one dimensional sensing are strictly permutational invariant, without noise and in the presence of dephasing noise. That is, the state is unaffected by the swapping of any number of qubits. This condition no longer holds for amplitude damping noise [111]. The study in [111] doesn't offer us any insight into why the assumption of optimal states being permutationally invariant for a permutationally invariant channel breaks down for amplitude damping, as it is a largely numerical study. The evidence is does present however, offers an interesting insight into a gap in our understanding into the geometry of optimal states for quantum metrology. There are many more degrees of freedom inherent to a multidimensional sensing problem, e.g. electing to put more resource into sensing one dimension in the field and leaving more error in another. With this in mind we take at look at the requirement for permutational invariance in 3D magnetometry.

The key simplification and assumption that we will make within this chapter (indeed later in this thesis too) is to work with a magnetic field in the limit of all three vector components tending to zero. As previously stated, our statistical framework already assumes local estimation, as such is it reasonable to assume we are already in a regime that can be modelled as the estimation of a small deviation of a test field from a base line one. Further, it is typically only very small magnetic fields that are of interest and where we find a quantum advantage [58, 139, 127, 132, 173].

3.2 Optimal two body reduced density operators for noiseless 3D magnetometry

With direct calculation we derive the optimal two body reduced density operator for pure state 3D magnetometry. This will give us the optimal two body reduced density matrix for any number of qubits, assuming this reduced density matrix can be reached with a pure state. Within this calculation we will find that for a low number of qubits ($N < 8$), the optimal reduced density matrix cannot always be achieved. We later use numerical techniques to find the optimal states for small numbers of qubits. We break down a two body reduced density matrix into its bloch components, compute the QCRB with respect to the coefficients of the bloch components and subsequently minimise the QCRB by computing the respective derivatives. To begin, we formulate the QFIM 2.156 taking the form [19],

$$J_{i,j} = 4NJ_{i,j}^{[1]} + 4N(N-1)J_{i,j}^{[2]}, \tag{3.2}$$

where

$$J_{i,j}^{[1]} = \mathrm{Re}\big[\mathrm{Tr}\big[\rho^{[1]}a_ia_j\big]\big] - \mathrm{Tr}\big[\rho^{[1]}a_i\big]\mathrm{Tr}\big[\rho^{[1]}a_j\big], \tag{3.3}$$

$$J_{i,j}^{[2]} = \mathrm{Tr}\big[\rho^{[2]}a_i \otimes a_j\big] - \mathrm{Tr}\big[\rho^{[1]}a_i\big]\mathrm{Tr}\big[\rho^{[1]}a_j\big] \tag{3.4}$$

and

$$a_i = \int_0^1 e^{i\alpha h}h_ie^{-i\alpha h}\mathrm{d}\alpha, \tag{3.5}$$

where h is the single particle Hamiltonian given by $h = \sum_{i=1}^3 \varphi_i\sigma_i$, where φ_i are the parameters to be estimated, which will be taken in the limit of approaching zero. Further, σ_i are the three Pauli matrices (labelled in order X, Y, Z) and $h_i = \sigma_i$. We also have $\rho^{[i]}$ is the ith reduced density matrix. We parameterise the one and two body reduced density matrix,

$$\rho^{[1]} = \frac{1}{2}\mathbb{1} + \beta_1\sigma_x + \beta_2\sigma_y + \beta_3\sigma_z \tag{3.6}$$

and

$$\rho^{[2]} = \frac{1}{4}\mathbb{1} \otimes \mathbb{1} + \sum_{i=4}^{18} \beta_i\lambda_i. \tag{3.7}$$

Where the λ_i is the $(i+3)^{th}$ element of the set $\{\sigma_x \otimes \sigma_x, \sigma_y \otimes \sigma_y, \sigma_z \otimes \sigma_z, \sigma_x \otimes \sigma_y, \sigma_y \otimes \sigma_x, \sigma_x \otimes \sigma_z, \sigma_z \otimes \sigma_x, \sigma_y \otimes \sigma_z, \sigma_z \otimes \sigma_y, \sigma_x \otimes \mathbb{1}, \mathbb{1} \otimes \sigma_x, \sigma_y \otimes \mathbb{1}, \mathbb{1} \otimes \sigma_y, \sigma_z \otimes \mathbb{1}, \mathbb{1} \otimes \sigma_z\}$. Now we can also express the a_i operators in a Pauli basis too. Noting that, a_i's are hermitian traceless operators they can be written as a sum of Pauli operators,

$$a_i = \alpha_{xi} X + \alpha_{yi} Y + \alpha_{zi} Z. \tag{3.8}$$

For a_x:

$$\alpha_{x1} = \frac{1}{\xi^2} \text{sinc}[2\xi] (\varphi_2^2 + \varphi_3^2) + \eta^2, \tag{3.9}$$

$$\alpha_{y1} = -\frac{1}{\xi^2} (\text{sinc}[2\xi] \varphi_1 \varphi_2 - \varphi_1 \varphi_2 + \text{sinc}[\xi] sin(\xi) \varphi_3 \xi), \tag{3.10}$$

$$\alpha_{z1} = -\frac{\text{sinc}[2\xi] \varphi_1 \varphi_2}{\xi^2} + \text{sinc}[\xi]^2 \varphi_2 + \frac{\varphi_1 \varphi_3}{\xi^2}. \tag{3.11}$$

For a_y:

$$\alpha_{x2} = -\frac{\text{sinc}[2\xi] \varphi_1 \varphi_2}{\xi^2} + \text{sinc}[\xi]^2 \varphi_3 + \frac{\varphi_1 \varphi_2}{\xi^2}, \tag{3.12}$$

$$\alpha_{y2} = -\frac{\text{sinc}[2\xi] \varphi_1}{\xi^2} - \frac{\text{sinc}[2\xi] \varphi_3^2}{\xi} - 2\varphi_2^2 \xi, \tag{3.13}$$

$$\alpha_{z2} = -\frac{\text{sinc}[2\xi] \varphi_2 \varphi_3}{\xi^2} - \text{sinc}[\xi]^2 \varphi_1 + \frac{\varphi_2 \varphi_3}{\xi^2}. \tag{3.14}$$

. For a_z:

$$\alpha_{x3} = \frac{\text{sinc}[2\xi] \varphi_1 \varphi_3}{\xi^2} + \text{sinc}[\xi]^2 \varphi_2 + \frac{\varphi_1 \varphi_3}{\xi^2}, \tag{3.15}$$

$$\alpha_{y3} = \frac{\text{sinc}[2\xi] \varphi_2 \varphi_3}{\xi^2} + \text{sinc}[\xi]^2 \varphi_1 + \frac{\varphi_2 \varphi_3}{\xi^2}, \tag{3.16}$$

$$\alpha_{z3} = \frac{\varphi_3^2}{\xi^2} + \frac{\text{sinc}[2\xi] (\varphi_1^2 + \varphi_2^2)}{\xi^2}. \tag{3.17}$$

We also needs to express $a_i a_j$ and $a_i \otimes a_j$ in the Pauli basis.

$$a_i \otimes a_j = (\alpha_{xi} X + \alpha_{yi} Y + \alpha_{zi} Z) \otimes (\alpha_{xj} X + \alpha_{yj} Y + \alpha_{zj} Z), \tag{3.18}$$

$$= \alpha_{xi} \alpha_{xj} X \otimes X + \alpha_{yi} \alpha_{yj} Y \otimes Y + \alpha_{zi} \alpha_{zj} Z \otimes Z$$

$$+ \alpha_{xi} \alpha_{yj} X \otimes Y + \alpha_{xi} \alpha_{zj} X \otimes Z + \alpha_{yi} \alpha_{xj} Y \otimes X$$

$$+ \alpha_{yi} \alpha_{zj} Y \otimes Z + \alpha_{zi} \alpha_{xj} Z \otimes X + \alpha_{zi} \alpha_{yj} Z \otimes Y.$$

We also have,

$$a_i a_j = (\alpha_{xi} X + \alpha_{yi} Y + \alpha_{zi} Z)(\alpha_{xj} X + \alpha_{yj} Y + \alpha_{zj} Z) \tag{3.19}$$

$$= (\alpha_{xi}\alpha_{xj} + \alpha_{yi}\alpha_{yj} + \alpha_{zi}\alpha_{zj})\mathbb{1} + i(\alpha_{xi}\alpha_{yj} - \alpha_{yi}\alpha_{xj})Z$$

$$+ i(\alpha_{xi}\alpha_{zj} - \alpha_{zi}\alpha_{xj})Y + i(\alpha_{yi}\alpha_{zj} - \alpha_{zi}\alpha_{yj})X$$

$$\tag{3.20}$$

We can now calculate the components of the QFIM. We need to calculate $\mathrm{Tr}[\rho^{[1]} a_i]$, $\mathrm{Re}[\mathrm{Tr}[\rho^{[1]} a_i aj]]$ and $\mathrm{Tr}[\rho^{[1]} a_i \otimes a_j]$. We have,

$$\mathrm{Tr}[\rho^{[1]} a_i] = \beta_1 \alpha_{xi} + \beta_2 \alpha_{yi} + \beta_3 \alpha_{zi}, \tag{3.21}$$

$$\mathrm{Re}[\mathrm{Tr}[\rho^{[1]} a_i a_j]] = \alpha_{xi}\alpha_{xj} + \alpha_{yi}\alpha_{yj} + \alpha_{zi}\alpha_{zj}, \tag{3.22}$$

$$\mathrm{Tr}[\rho^{[2]} a_i \otimes a_j] = 4 \sum_{k=4}^{12} \beta_k \tilde{\lambda}_i \tag{3.23}$$

where $\tilde{\lambda}_i$ is the set of $\alpha_{fi}\alpha_{gj}$ components, where the order matches λ's Pauli tensor products from before e.g. $\lambda_1 = \alpha_{x,1}\alpha_{x,1}$. We are interesting in measuring small magnetic fields which allows us to make some simplifications,

$$\lim_{\varphi_i \to 0} \alpha_{x1} = \lim_{\varphi_i \to 0} \alpha_{y2} = \lim_{\varphi_i \to 0} \alpha_{z3} = 1, \tag{3.24}$$

and all other α terms tend to zero. With all this we are now able to explicitly write out the QFIM,

$$J = 16N(N-1)\begin{bmatrix} \beta_4 \alpha_{x1}^2 & \beta_7 \alpha_{x1}\alpha_{y2} & \beta_9 \alpha_{x1}\alpha_{z3} \\ \beta_8 \alpha_{x1}\alpha_{y2} & \beta_5 \alpha_{y2}^2 & \beta_{11}\alpha_{z3}\alpha_{y2} \\ \beta_{10}\alpha_{x1}\alpha_{z3} & \beta_{12}\alpha_{z3}\alpha_{y2} & \beta_6 \alpha_{z3}^2 \end{bmatrix} \tag{3.25}$$

$$- (4N(4N-3))\begin{bmatrix} (\beta_1 \alpha_{x1})^2 & \beta_1 \beta_2 \alpha_{x1}\alpha_{y2} & \beta_1 \beta_3 \alpha_{x1}\alpha_{z3} \\ \beta_1 \beta_2 \alpha_{x1}\alpha_{y2} & (\beta_2 \alpha_{y2})^2 & \beta_2 \beta_3 \alpha_{y2}\alpha_{z3} \\ \beta_1 \beta_3 \alpha_{x1}\alpha_{z3} & \beta_2 \beta_3 \alpha_{y2}\alpha_{z3} & (\beta_3 \alpha_{z3})^2 \end{bmatrix}$$

$$+ 4N \begin{bmatrix} \alpha_{x1}^2 & 0 & 0 \\ 0 & \alpha_{y1}^2 & 0 \\ 0 & 0 & \alpha_{z1}^2 \end{bmatrix}.$$

$$\tag{3.26}$$

Now we wish to minimise $\text{Tr}[J^{-1}]$, it is important to note that there is still meaning to be gained from minimising $\text{Tr}[J^{-1}]$ despite its unattainability. We can gain insight into the structure of optimal states, what features in a state make it optimal for a given problem. Further, when weak-commutativity is satisfied then the bound coincides with the HCRB and is attainable. We find $\text{Tr}[J^{-1}]$ to take form,

$$\text{Tr}[J^{-1}] = \frac{1}{|J|}(J_{11}J_{22} + J_{11}J_{33} + J_{33}J_{22} - J_{23}J_{32} - J_{31}J_{13} - J_{21}J_{12}), \quad (3.27)$$

where $|J|$ is the determinant of J given by,

$$|J| = J_{11}(J_{22}J_{33} - J_{32}J_{23}) - J_{12}(J_{21}J_{33} - J_{31}J_{23}) + J_{13}(J_{21}J_{32} - J_{31}J_{22}). \quad (3.28)$$

Expanding out the above we are able to explicitly write $\text{Tr}[J^{-1}]$ as $f(\underline{\beta}) = \text{Tr}[J^{-1}] = c/d$ where,

$$
\begin{aligned}
c = &-(\beta_1\beta_2(4N-3) - 4\beta_7(N-1))^2 && (3.29) \\
&+ (\beta_1\beta_3(4N-3) - 4\beta_9(N-1))^2 \\
&+ (\beta_2\beta_3(4N-3) - 4\beta_{10}(N-1))^2 \\
&- (\beta_1^2(4N-3) - 4\beta_4(N-1) - 1)(\beta_2^2(4N-3) - 4\beta_5(N-1) - 1) \\
&- (\beta_1^2(4N-3) - 4\beta_4(N-1) - 1)(\beta_3^2(4N-3) - 4\beta_6(N-1) - 1) \\
&- (\beta_2^2(4N-3) - 4\beta_5(N-1) - 1)(\beta_3^2(4N-3) - 4\beta_6(N-1) - 1) \\
d = &\; 4N\big((\beta_3^2(4N-3) - 4\beta_6(N-1) - 1) && (3.30) \\
&* (\beta_1\beta_2(4N-3) - 4\beta_7(N-1))^2 \\
&+ (\beta_2^2(4N-3) - 4\beta_5(N-1) - 1)(\beta_1\beta_3(4N-3) - 4\beta_9(N-1))^2 \\
&+ (\beta_1^2(4N-3) - 4\beta_4(N-1) - 1)(\beta_2\beta_3(4N-3) - 4\beta_{10}(N-1))^2 \\
&- (\beta_1^2(4N-3) - 4\beta_4(N-1) - 1)(\beta_2^2(4N-3) - 4\beta_5(N-1) - 1) \\
&\; (\beta_3^2(4N-3) - 4\beta_6(N-1) - 1) \\
&+ 2(\beta_1\beta_2(3-4N) + 4\beta_7(N-1))(\beta_1\beta_3(3-4N) + 4\beta_9(N-1)) \\
&* (\beta_2\beta_3(3-4N) + 4\beta_{10}(N-1))\big).
\end{aligned}
$$

With direct (messy, hence omitted) computation of the derivative vector we are able to finalise our calculation. So for $\nabla f(\underline{\beta}) = 0$ we find the solution for the minimum to be $\beta_1 = \beta_2 = \beta_3 = \beta_7 = \beta_9 = \beta_{10} = 0$ and $\beta_4 = \beta_5 = \beta_6 \neq 0$. We can easily bound the values of $\beta_4, \beta_5, \beta_6$ because the two body reduced density matrix

is of form, $\frac{1}{4}\mathbb{1}\otimes\mathbb{1}+\sum_i\beta_i\sigma_i\otimes\sigma_i$. This is a rank-3 state so the sum of Eigenvalues is given by $3(\frac{1}{4}+\beta_i)=1$. With the additional constraint that $\nabla f(\underline{\beta})=0$ we can find a solution where all three values are equal, that is, $\beta_i=\frac{1}{12}$. Further (even messier) calculation confirms this solutions is indeed a minimum.

Putting this together, we have that for zero parameter, 3D magnetometry the optimal two body reduced density matrix for an arbitrary number of qubits is given by,

$$\frac{\mathbb{1}}{4}+\frac{1}{12}\sum_{i=1}^{3}\sigma_i\otimes\sigma_i. \qquad (3.31)$$

3.3 Genetic-inspired algorithm for input state optimisation

Having previously calculated the optimal two body reduced density matrix for 3D magnetometry, but being unable to find the optimal input states for a small number of qubits, we turn to numerical techniques. One typical issue with numerical optimisation results is that only the cost function's value has meaning or significance. The set of parameters by which the cost function is defined, which give rise to said value is often without an interpretable significance. In this section we develop an optimisation algorithm that is capable of finding not only the optimal state for estimation, but also finds a structure that holds over the number of qubits.

Genetic algorithm details

In order to obtain optimal states we will use a genetic inspired optimisation algorithm. Genetic inspired algorithms are a class of optimisation algorithms which are stochastic searches. As with all global optimisation we have no guarantee of obtaining the global maximum without doing a direct search. However, with the exponential scaling of quantum systems, this is not feasible. The inspiration for algorithms of this nature stems from genetic reproduction and mutation. Where there is some population with each member having *genes* which encode instructions on how to make that member. At each step of reproduction, mates select one another based on some selection criteria and pass on a random mix of both their gene sets. The passing on of genes is not a perfect process and random mutations also occur. We mimic this process, substituting the QCRB for the selection criteria and a heuristic set of mutations. A flow chart for the process can be seen in Figure 3.1. Once the population has been initialised with random states, the QCRB for each state is then calculated. The state with the current best QCRB is recorded. For the selection process, pairs of states are chosen randomly

from the population. The probability that any given state is chosen is proportional to the inverse of the QCRB. For each pair a random splice point is generated, that is the point which splits each state in two. The "top half" of the first state vector and "bottom half" of the second state vector are spliced togetaer to form the next state. That is, for two vectors of length m, $\boldsymbol{a}$ and $\boldsymbol{b}$, where a_i and b_i are the ith elements of the vectors. We pick a random integer $k \leq m$ and construct a new vector c in the following way,

$$c_i = \begin{cases} a_i & \text{if } i < k \\ b_i & \text{if } i \geq k. \end{cases} \tag{3.32}$$

Each new state is then mutated, for every element in the vector a mutation takes place with some probability (in practice $1/2^N$ was found to be optimal, that is approximately one mutation per iteration). There are three possible mutations:

1. Deletion: sets the element to zero (unless that would make all elements of the state 0, then do nothing),

2. Copy: sets the element to be equal to that of another random element of the vector,

3. Randomise: sets the element to a new random number.

All states are then renormalised. We now have a new population of valid quantum states. For each state we then compute its respective QCRB. If any of these new states obtain a QCRB that is lower in value than the current optimal state then we update our record of the current best state. If the current best state does not change in any given iteration then the worst performing state is replaced with the best within the population. Within the field of genetic optimisation this is known as genetic elitism, it is a technique that allows the optimiser to explore the input space freely, without constraining it too early.

Benchmarking for Genetic-inspired Optimisaer

We benchmarked this optimiser against known results. The first examples where the single parameter estimations of a 1D magnetic field over noise. In this case the analytic results are known [101, 65, 11]. The optimisation does indeed find the analytic states for low, medium and high noise over qubits (tested up to 9 qubits). The other scenario we must check is 3D magnetometry. We have previously found the analytical optimal
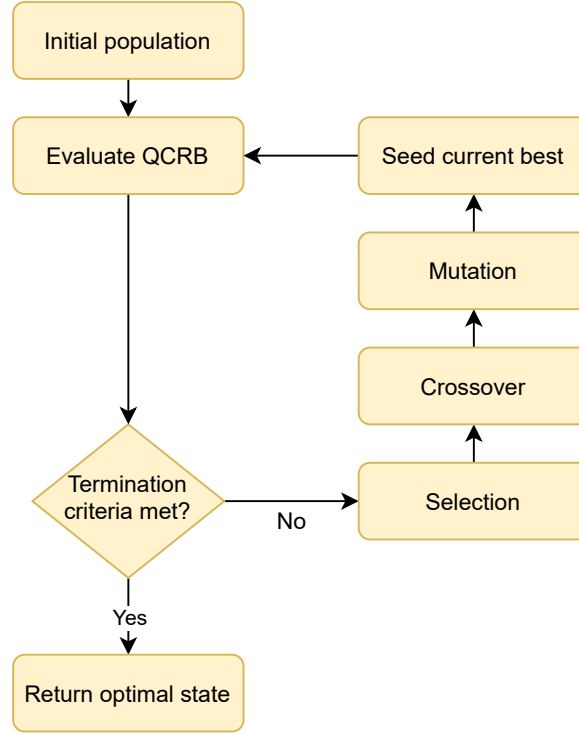
Figure 3.1: Flow chart representation of the genetic algorithm used to optimise input states for magnetometry. The population is initialised with random quantum states. Once the QCRB has been evaluated, termination conditions are checked. The termination conditions here being no improvement in the optimal result after a given number of iterations or a total number of iterations, the exact number depends on the system size. The probability of selection is then inversely proportional to a given state's QCRB. Crossover and mutation then occur, this combines features of the current population and introduces new random ones. Finally, a comparison between the new population and the current best performing state, with the best state being updated if required and reseeded into the population.

state for 8 qubits, this allows us to use a symmetric noise model to benchmark the performance of this optimisation in the presence of noise. Symmetric noise has the quantum channel given by,

$$\varepsilon_{N,\gamma}(\rho) = \frac{\gamma \mathbb{1}}{2^N} + (1 - \gamma)\rho. \tag{3.33}$$

This has QCRB of $C^{\mathrm{C}}(\varphi, \gamma) = (1 - \gamma)^2 C^{\mathrm{C}}(\varphi)$. The important feature is this QCRB is only the pure state QCRB, scaled. The scaling is state independent, as such the optimal state does not change over noise. The optimisation does indeed find the

analytic optimal state over a noise range for 8 qubits.

3.4 Results

3.4.1 Pure optimal states

To begin we run the above algorithm for noiseless systems from two, to eight qubits. In particular we look to see if the 3D-GHZ state is in fact optimal at these low qubit numbers. As an interesting secondary question we look to see if the optimal states permutationally invariant, as in the 1D counterpart.

The QCRB results are presented in Figure 3.2, that for $N < 8$, the 3D-GHZ state is not optimal. There is the exception of two qubits. This is a special case in 3D magnetometry. It does not have a two body reduced density matrix as $N > 2$, being only two qubits. This is the first case where simultaneous estimation is possible and does not fit the trend. The two qubit optimised state performs better than the 3D-GHZ state, but very marginally, less than 0.1% relative improvement.
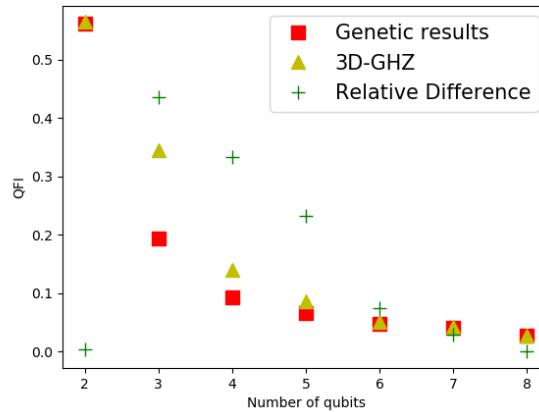
Figure 3.2: Results of genetic algorithm compared to three-directional GHZ state. The triangles representation the QCRB coming from the 3D-GHZ state, the triangles represent the QCRB coming from the result of the genetic optimisation. The green cross is the relative difference between the two results, $1 - \frac{genetic}{3D-GHZ}$. This demonstrates the genetic algorithm improving on the 3D-GHZ state up to 8 qubits, where they coincide.

Optimal states

(a)

(b)

(c)
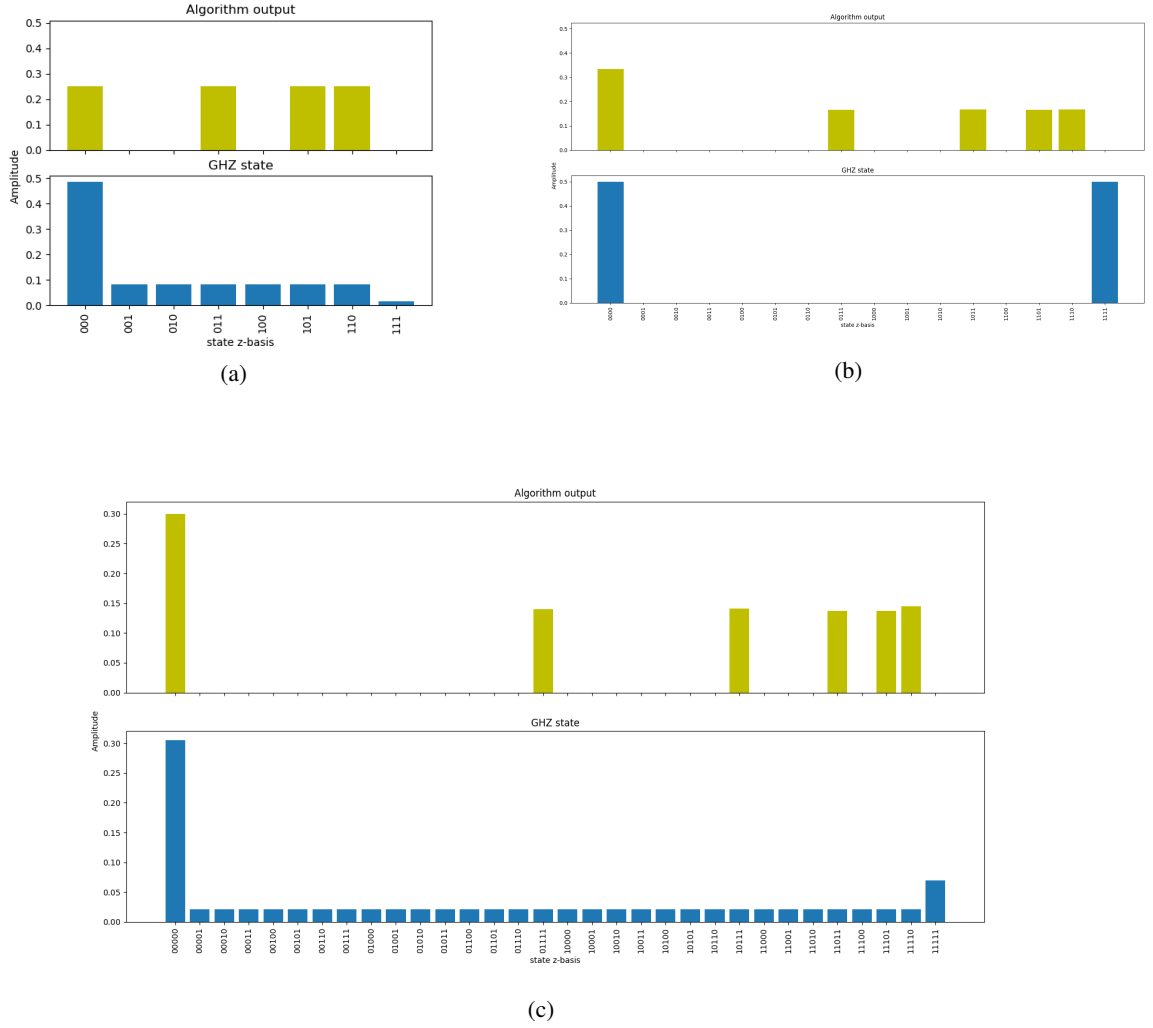
Figure 3.3: Optimal states compared to the 3D-GHZ state. With a, b, c being 3,4 and 5 qubits respectively.

The optimal states are of form,

$$|\psi\rangle = \frac{1}{a}\left(\sqrt{n-2}\,|0\rangle^{\otimes N} + \sum \pi(|0\rangle^1, |1\rangle^{N-1})\right), \tag{3.34}$$

where a is the normalisation and $\pi(|0\rangle^1, |1\rangle^{N-1})$ refers to the permutations of $|0\rangle$ and $|1\rangle$. For example $\pi(|0\rangle^1, |1\rangle^2) = \{|011\rangle, |101\rangle, |110\rangle\}$. For 4 qubits in particular this

state's two body reduced density is the same as that of the optimal derived previously. These states are visually presented in Figure 3.2, from this we can get a sense of the issue with the 3D-GHZ state at a low number of qubits. In essence, the set of three states which are being superpositioned are not necessarily linearly independent. There is destructive interference at these low qubit numbers which eliminates some useful features of the state.

Noisy results

Now that we have established the optimal pure state results, we extend our optimisation to being over noise too. In Figure 3.4 we present the values of the optimisation. Having optimised over many values of noise from 0 to 1, we find that that across all values of noise there are three different states that are optimal in different regimes. There is a state is is optimal for low noise, one for medium and a final state that is optimal for high noise. This matches what the results found for single parameter dephasing noise magnetometry [191]. To be explicit, we define low medium and high noise regimes to be the value of noise strength as being up to 0.05, 0.51 and 1, respectively. These numbers are not arbitrary, but are defined as the points at which a given state remains optimal. Further we define the pure optimal state as the state which is optimal up to a noise value of 0.05, the medium optimal state being the state that is optimal between 0.05 and 0.51 and finally the high noise state, being the state which is optimal for the remaining range of nosie 0.51 to 1. We see a very tight range in which the pure state is still optimal, the medium noise state very quickly takes over for the majority of the noise range. We focus on 4 qubits for visualisation, but the pattern holds for other qubit numbers too. This is an interesting distinction from 1D-magnetometry, where the GHZ state remains optimal for a much greater range of noise. The structure of the medium noise regime state is given by,

$$|\psi\rangle = \frac{1}{a}\left(\sqrt{n-1}\left(|0\rangle^{\otimes N} + |1\rangle^{\otimes N}\right) + \pi(|0\rangle^2, |1\rangle^{N-2})\right), \qquad (3.35)$$

where $\pi(|0\rangle^{(}j), |1\rangle^k)$ is the equal superposition of all permutations of states containing j-zeroes an k-ones. For example, the W-state is defined by the state given by $k = 1$,

$$\pi(|0\rangle^2, |1\rangle^1) = \frac{1}{\sqrt{1}}(|001\rangle + |010\rangle + |100\rangle). \qquad (3.36)$$

With the high noise regime being maximally coherent. In both noisy and pure state, the optimal states are permutationally invariant. In order to confirm this was not a bias of the optimiser developed in this chapter we also ran the optimisations with a "vanilla" scipy optimiser. This confirmed the values of the results, finding non-permutationally invariant states with the same QCRB. This is also an interesting departure from 1D-magnetometry, the optimal state is no longer unique.
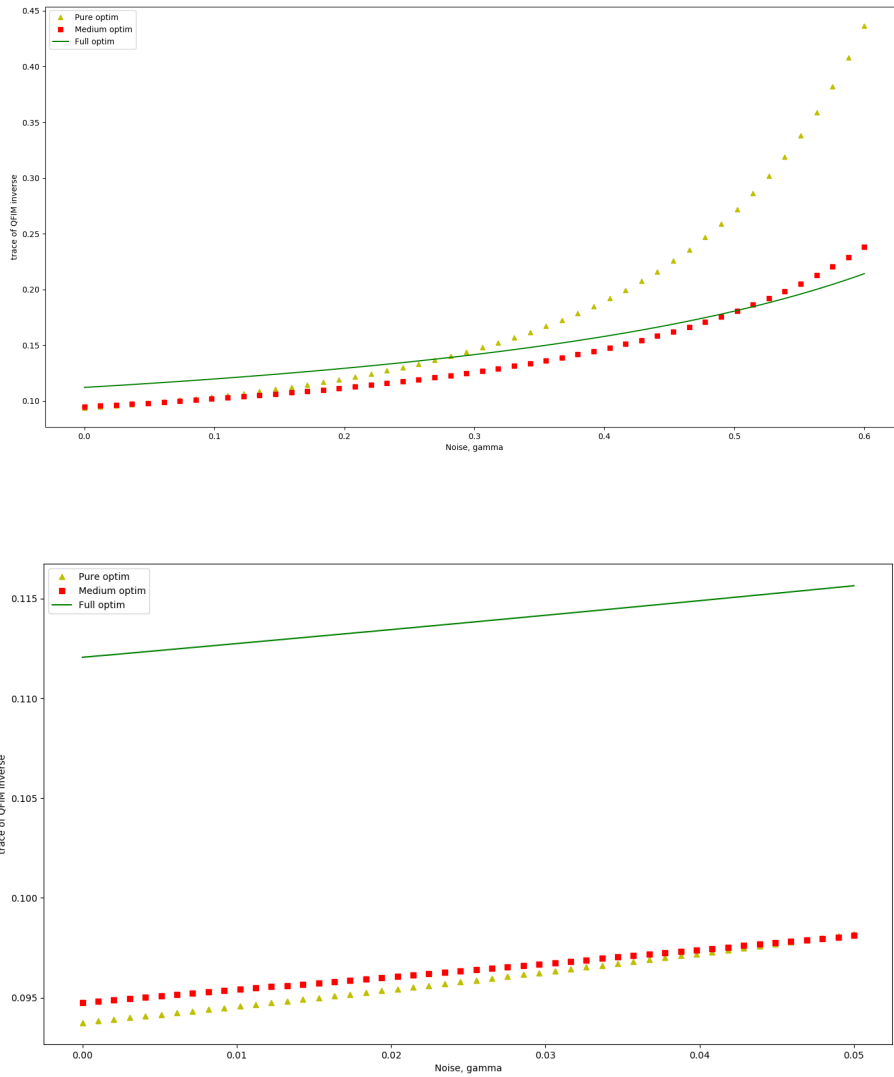
Figure 3.4: The QCRB for optimal 4-qubit states with low, medium and high noise at low noise. For all values of the noise strength we optimise the QCRB. We find there to be three different optimal states. There is a state, the low noise optimal state which remain optimal up to a noise value of 0.05. We then have a medium noise state, being the state that remains optimal until a noise value of 0.51. Finally, the high noise state is the state which is optimal until the maximum noise value of 1. We call these states, pure optim, medium optim and full optim respectively. Including a zoomed in view to add clarity to the low noise regime. Each state is plotted over all values of noise to show the thresholds at which each regime starts/ends.

3.5 Conclusions and discussions

To conclude, in this chapter we began by proving the intuition that the 3D-GHZ state was optimal for large numbers of qubits and for parameters approaching zero. More precisely, we derived the form of the optimal 2-body reduced density matrix, which for large numbers of qubits the 3D-GHZ state does indeed possess.

Further, we developed a new genetic-inspired optimisation algorithm which was capable of finding not only optimal values, but also an optimal structure. This allowed us to find optimal states for the small numbers of qubits where the 2-body reduced density matrix cannot always be in exactly the optimal form derived above. We were equally able to run our optimisation over noise and found the same structure over optimal states and noise as 1D-magnetometry. in particular, there are three regions of optimality, high, low and medium noise.

The results add further evidence to the idea that permutationally invariant states are optimal when we have a permutationally invariant channel. We numerically optimised over states and found the optimal to lie in the space of permutationally invariant states. The optimisation was not restricted to this subspace. There has been further work to support this idea [111], with the exception being amplitude damping noise. This continues to be an ongoing question that struggles to get traction due to the requirements of a spectral decomposition of impure states. It may be of interest to note that the state for 3 qubits found by the algorithm contains the Thue-Morse sequence. Also, if we use the 4-qubits Thue-Morse state then it has the same QFIM as the 3D-GHZ state, but performs better under noise. The Thue-Morse sequence can be defined in terms of bitwise negation. We begin with 0, the negation of 0 is 1, so we combine these two and the next term is 0,1. The negation of this is 1,0, so again we combine these two terms to give 0,1,1,0. Continuing,

$T_0 = 0,$

$T_1 = 01,$

$T_2 = 0110,$

$T_3 = 01101001,$

$T_4 = 0110100110010110,$

$T_5 = 01101001100101101001011001101001,$

$T_6 = 0110100110010110100101100110100110010110011010010110100110010110.$

During study of variational approaches to input state optimisation [126] it was also found that for 4 qubits, the state with the Thue-Morse pattern was a local minima that the algorithm became stuck in. There are many interesting sequences that one can find with enough time and the Online Encyclopedia of Integer Sequences, this one however is of particular interest because of how often it appears, as well as its usefulness in dynamic decoupling strategies in the field of quantum control theory.

Chapter 4

2-qubit Holevo-Cramér-Rao bound calculation

shut up and calculate

David Mermin

4.1   Introduction

The theoretical study of measuring physical quantities with quantum probes has been a successful and fruitful area of research [77, 54, 52, 150, 155]. The current era of quantum sensing with qubit probes is not one of large system sizes, where we would observe the quadratic scaling power of quantum sensing in the number of qubits. The state of the art quantum sensing experiments involve small systems pushing towards the absolute limits of estimation in particular use cases [175, 50, 37, 18]. For such use cases it is essential to fully examine systems of a fixed number of qubits in its completion. This serves as the practical motivation for the following chapter.

We study 3D-magnetometry for 2-qubits to completion (within the framework of locally unbiased estimation with maximum likelihood estimator). Multiple parameter estimation is essential for many state of the art experiments including spectroscopy, accelerometers and magnetometry. Practically speaking an experiment can always sequentially estimate the many parameters of interest. However, this may be too slow if the parameters not being observed are varying (especially if they are non-commuting) as you are estimating one. Further, there is often an advantage to simultaneous estimation [187, 122, 7, 53] which means non-optimal experimental procedure to

sequential estimation. It is pertinent to note that an experimenter could take advantage of multiple independent measurement probes. This can improve the footprint effect of measurement and give rise to conflicted estimates.

From a more fundamental quantum information perspective, incompatibility of observables is well studied through the simultaneous quantum-limited estimation of multiple parameters[89]. The goal is to study the fundamental bounds that incompatibility imposes on precision of estimators as well as the strategies to attain said bounds. More descriptively, we are trying to answer the question of how much information can be encoded and extracted onto the parameters of a quantum state. The HCRB is the fundamental of all such bound which depend on only the state and state's derivative with respect to the parameters of interest. Access to explicit measurement independent grants us complete comparison to the measurement dependant bound CCRB.

In the previous chapter 3 we exploited the analytic tractability of the QCRB to explore how the geometry of optimal states changes as the system scales in the number of qubits. We noted that for large system sizes the optimal state satisfies weak commutativity, that is to say that the QCRB and HCRB are equal. However, this did not hold for smaller system sizes (in particular $N < 8$). If our goal is optimal estimation then it is pertinent of us to further explore the Cramér Rao bounds of particular smaller systems. As previously noted, the HCRB is always attainable [96, 97, 53]. Results on how many copies of the input state are required to attain the HCRB are not known in general. Obtaining a closed form expression of the HCRB does not immediately give way to a strategy for measuring the system with the desired precision. For this reason, the work of this chapter does not only focus on the calculation of the HCRB, but also attaining it with some measurement. Hitherto, no 3-parameter model has been analytically solved for the HCRB. Without this, it is not possible to know that an estimation strategy is truly optimal.

Since the publication of the HCRB in 1976 [96] very few analytic solutions to equation 4.2 have been found in nontrivial cases [1]. These are:

1. Pure states with two parameters [130],

2. two mode Gaussian states [28],

3. one qubit models [184].

---

[1]In the context of evaluating the HCRB, with the phrase *trivial cases* we refer to those quantum statistical models for which the HCRB collapses to other bounds (SLD or RLD) that are easier to evaluate [7, 184].

This is due to the increased complexity of solving the HCRB when compared to the well studied Quantum Fisher information [145] where there is an analytic solution for any model where the Eigenvalue decomposition and derivatives are known. The constrained optimisation problem is also harder to solve, however, it was recently shown to be a convex problem [6] which drastically reduces the numerical cost of evaluation. In this chapter we find another case of an analytic HCRB solution.

For this chapter, we focus on $N = 2$, this is the smallest system size that we are able to simultaneously estimate all three parameters of a magnetic field with a pure state. This was a special case of 3-parameter magnetometry, this particular geometry will be a useful feature when calculating the HCRB analytically. As sensing a 3D magnetic field simultaneously is impossible with a single qubit, we concentrate on the smallest multi-qubit system, i.e., two qubits. Similar problems have been studied by considering the magnetic field acting on a single system with an additional ancillary system unaffected by the dynamics [51, 66, 3, 15, 43, 102, 212, 114]; in such a scenario it is sufficient to consider the QCRB matrix. On the contrary, we do not consider ancillary systems in this work. This scenario has been studied with the QCRB [112, 19, 94] as the Cramér Rao bound of choice and applied to photonic systems [81, 123]. However, the fundamental attainable bound for 3D magnetometry remains unknown.

In this chapter, we first present a closed-form analytical expression for the HCRB for 3D magnetometry for two-qubit pure states and show that it can be attained by a rank-1 projective measurement.

4.2   Mathematical setup

As seen above from the derivation, given a vector of Hermitian operators on $\mathcal{H}$, $\boldsymbol{X} = (X_1, X_2, \ldots, X_m)$ defined by,

$$\boldsymbol{X} := \left\{ \boldsymbol{X} \,|\, \forall i \,\mathrm{Tr}[\rho X_i] = 0, \forall i, j \,\mathrm{Tr}\left[\frac{\partial \rho}{\partial \boldsymbol{\varphi}_i} X_j \right] = \delta_{i,j} \right\}. \tag{4.1}$$

Then the Holevo bound is defined by (ignoring weight matrices),

$$C^{\mathrm{H}} := \min_{\boldsymbol{X}} \mathrm{Tr}[\mathrm{Re}\, Z[\boldsymbol{X}]] + \mathrm{Tr}[\mathrm{Im\, abs}\, Z[\boldsymbol{X}]], \tag{4.2}$$

where $Z_{\boldsymbol{\varphi}}[\boldsymbol{X}]$ is defined as,

$$Z_{\boldsymbol{\varphi}}[\boldsymbol{X}]_{i,j} := \text{Tr}[\rho X_i X_j]. \tag{4.3}$$

Here we are interested in the case of three parameters and so in order to try and analytically calculate the Holevo bound for our physical case of a magnetic field there are two approaches we can take. The first is a "brute force" method of calculating the constraints for our particular problem and then plugging those into the Holevo bound as an unconstrained problem where the X_i matrices are parameterised by the constraints we calculated. An alternative approach, introduced by Keiji Matsumoto [130] to calculate the bound in general for pure states with two parameters using Lagrange's method of indeterminate coefficients.

The HCRB is always attainable, in that sense we mean there is always exist a measurement such that $C^{\text{C}} = C^{\text{H}}$. However, this measurement could exists on a potentially infinite number of copies of the initial state. This gives rise to an important result of the HCRB based on CCRB,

$$C^{\text{H}} = \lim_{n \to \infty} \min_{\Pi} n C^{\text{C}}(\rho_{\boldsymbol{\varphi}}^{\otimes n}, \Pi) \tag{4.4}$$

It is important to note that the HCRB often collapses to various other Cramér-Rao bounds [6, 184]. For the system of two qubits sensing a magnetic field the HCRB does not collapse to any other bounds, see equation 4.33.

4.2.1 Pure state HCRB simplifications

For pure states $\rho_{\boldsymbol{\varphi}} = |\psi_{\boldsymbol{\varphi}}\rangle\langle\psi_{\boldsymbol{\varphi}}|$ it is possible to recast the optimisation (4.2) in terms of complex vectors [130, 91]

$$|x_i\rangle = X_i |\psi_{\boldsymbol{\varphi}}\rangle, \tag{4.5}$$

for which the matrix (4.3) becomes $Z[X]_{ij} = \langle x_i | x_j \rangle$. We can see this immediately,

$$Z[X]_{ij} = \text{Tr}(\rho X_i X_j) \tag{4.6}$$
$$= \text{Tr}(|\psi\rangle\langle\psi| X_i X_j) \tag{4.7}$$
$$= \text{Tr}(\langle\psi| X_i X_j |\psi\rangle) \tag{4.8}$$
$$= \langle x_i | x_j \rangle \tag{4.9}$$

The constraints (4.1) become

$$\mathrm{Re}\,\langle x_i|l_j\rangle = \delta_{ij}, \tag{4.10}$$

where we have introduced the vectors

$$|l_i\rangle = L_i\,|\psi\rangle = 2(|\partial_i\psi_{\boldsymbol{\varphi}}\rangle - \langle\psi_{\boldsymbol{\varphi}}|\partial_i\psi_{\boldsymbol{\varphi}}\rangle\,|\psi_{\boldsymbol{\varphi}}\rangle). \tag{4.11}$$

We can again justify this by direct calculation,

$$\mathrm{Tr}\left[X_i\frac{\partial\rho_{\boldsymbol{\varphi}}}{\partial\lambda_j}\right] = \mathrm{Tr}\left[\frac{X_i}{2}(|\partial_j\psi\rangle\,\langle\psi| + |\psi\rangle\,\langle\partial_j\psi|)\right] \tag{4.12}$$

$$= \frac{1}{2}(\langle\partial_j\psi|\,X_i\,|\psi\rangle + \langle\psi|\,X_i\,|\partial_j\psi\rangle) \tag{4.13}$$

$$= \mathrm{Re}\,\langle\partial_j\psi|\,X_i\,|\psi\rangle \tag{4.14}$$

$$= \mathrm{Re}\,\langle x_i|\partial_j\psi\rangle = \delta_{i,j}, \tag{4.15}$$

$$\implies \mathrm{Re}\,\langle x_i|l_j\rangle = \delta_{i,j}. \tag{4.16}$$

Noting that the final step is justified due to the constraint in Equation. 4.1 stating that $\langle\psi|\,X\,|\psi\rangle = 0$, which implies $\langle x_i|\psi\rangle = 0$. A crucial simplification is that the vectors $|x_i\rangle$ attaining the minimum can be always found in $\mathrm{span}_{\mathbb{C}}\{|l_i\rangle\}_{i=1}^p$ [130].

4.2.2 Magnetometry details

In this work we are interested in the estimation of the 3 components of a magnetic field, given by Hamiltonian,

$$\hat{H}(\boldsymbol{\varphi}) = \boldsymbol{\varphi}_1(\sigma_x\otimes\mathbb{1} + \mathbb{1}\otimes\sigma_x) + \boldsymbol{\varphi}_2(\sigma_y\otimes\mathbb{1} + \mathbb{1}\otimes\sigma_y) + \boldsymbol{\varphi}_3(\sigma_z\otimes\mathbb{1} + \mathbb{1}\otimes\sigma_z). \tag{4.17}$$

With subsequent evolution,

$$|\psi_{\boldsymbol{\varphi}}\rangle = e^{-i\hat{H}(\boldsymbol{\varphi})}\,|\psi_0\rangle, \tag{4.18}$$

where $|\psi_0\rangle$ is some pure input state. Importantly we also need the derivatives of the evolved state,

$$\frac{\partial\,|\psi_{\boldsymbol{\varphi}}\rangle}{\partial\varphi_i} = \frac{\partial}{\partial\varphi_i}e^{-i\hat{H}(\boldsymbol{\varphi})}\,|\psi_0\rangle = -ie^{-i\hat{H}(\boldsymbol{\varphi})}A_i(\boldsymbol{\varphi})\,|\psi_0\rangle, \tag{4.19}$$

with Hermitian operator,

$$A_i(\varphi) = \int_0^1 e^{-i\alpha\hat{H}(\varphi)}\hat{H}_i e^{i\alpha\hat{H}(\varphi)}\mathrm{d}\alpha. \tag{4.20}$$

Where $\hat{H}_i$ is $\partial_{\varphi_i}\hat{H}(\varphi)$. Here we note that we are able to write $A_i(\varphi) = \sum_{n=1}^{N} a_i^{[n]}$, where

$$a_i^{[n]} = \int_0^1 e^{-i\alpha\hat{h}(\varphi)}\hat{h}_i^{[n]} e^{i\alpha\hat{h}(\varphi)}\mathrm{d}\alpha. \tag{4.21}$$

We have that $a_i^{[n]}$ are one-body Hermitian operators that act on the nth qubit. Now, a_i's are Hermitian traceless operators and so can be written as,

$$a_i = \alpha_{xi}\sigma_x + \alpha_{yi}\sigma_y + \alpha_{zi}\sigma_z. \tag{4.22}$$

For a_x:

$$\alpha_{x1} = \frac{1}{\xi^2}\text{sinc}[2\xi]\left(\varphi_2^2 + \varphi_3^2\right) + \eta^2, \tag{4.23}$$

$$\alpha_{y1} = -\frac{1}{\xi^2}(\text{sinc}[2\xi]\varphi_1\varphi_2 - \varphi_1\varphi_2 + \text{sinc}[\xi]\text{sinc}(\xi)\varphi_3\xi), \tag{4.24}$$

$$\alpha_{z1} = -\frac{\text{sinc}[2\xi]\varphi_1\varphi_2}{\xi^2} + \text{sinc}[\xi]^2\varphi_2 + \frac{\varphi_1\varphi_3}{\xi^2}. \tag{4.25}$$

For a_y:

$$\alpha_{x2} = -\frac{\text{sinc}[2\xi]\varphi_1\varphi_2}{\xi^2} + \text{sinc}[\xi]^2\varphi_3 + \frac{\varphi_1\varphi_2}{\xi^2}, \tag{4.26}$$

$$\alpha_{y2} = -\frac{\text{sinc}[2\xi]\varphi_1}{\xi^2} - \frac{\text{sinc}[2\xi]\varphi_3^2}{\xi} - 2\varphi_2^2\xi, \tag{4.27}$$

$$\alpha_{z2} = -\frac{\text{sinc}[2\xi]\varphi_2\varphi_3}{\xi^2} - \text{sinc}[\xi]^2\varphi_1 + \frac{\varphi_2\varphi_3}{\xi^2}. \tag{4.28}$$

For a_z:

$$\alpha_{x3} = \frac{\text{sinc}[2\xi]\varphi_1\varphi_3}{\xi^2} + \text{sinc}[\xi]^2\varphi_2 + \frac{\varphi_1\varphi_3}{\xi^2}, \tag{4.29}$$

$$\alpha_{y3} = \frac{\text{sinc}[2\xi]\varphi_2\varphi_3}{\xi^2} + \text{sinc}[\xi]^2\varphi_1 + \frac{\varphi_2\varphi_3}{\xi^2}, \tag{4.30}$$

$$\alpha_{z3} = \frac{\varphi_3^2}{\xi^2} + \frac{\text{sinc}[2\xi](\varphi_1^2 + \varphi_2^2)}{\xi^2}. \tag{4.31}$$

In most of this work we will focus on the case where $\varphi_i \rightarrow 0 \; \forall \; i$. We do not make claims of being able to "move" into this parameter space as these claims seem largely unsubstantiated. However we do claim that most practical applications of magnetometry are interested in the estimation of very small magnetic fields around zero, it also makes the algebra tractable. In this regime we can see that,

$$\lim_{\varphi_i \rightarrow 0 \forall i} \frac{\partial}{\partial \varphi_i} e^{-i\hat{H}(\boldsymbol{\varphi})} \left| \psi_0 \right\rangle = -i\hat{H}_i \left| \psi_0 \right\rangle. \tag{4.32}$$

4.3 Asymptotic classicality

Asymptotically classical models, adopting the terminology of [184] are those for which $C^S = C^H$, determined by the condition $D = 0$, where $D_{ij} = \mathrm{Im}\,\mathrm{Tr}\,L_i L_j \rho_{\boldsymbol{\varphi}}$ [161]. For the problem we are considering, a sufficient condition for asymptotic classicality is to satisfy [19],

$$\mathrm{Tr}\left[\rho^{[1]} a_i a_j\right] = 0 \quad \forall i, j. \tag{4.33}$$

For zero parameter $a_i \rightarrow \sigma_i \implies \mathrm{Tr}\,\rho^{[1]} a_i a_j = \varepsilon_{i,j,k}\alpha_k$, where $\rho^{[1]} = (\mathbb{1} + \sum \alpha_i \sigma_i)/2$. The only way this is zero $\forall i, j$ is for α_i to be zero $\forall i \implies \rho^{[1]} = \mathbb{1}/2$. There are only two classes of two-qubit pure states which have this 1-body reduced density matrix,

$$\left| \psi_1 \right\rangle = \frac{1}{\sqrt{2}}(\left| 00 \right\rangle \pm e^{-\mathrm{i}\phi} \left| 11 \right\rangle) \qquad \left| \psi_2 \right\rangle = \frac{1}{\sqrt{2}}(\left| 10 \right\rangle \pm e^{-\mathrm{i}\phi} \left| 01 \right\rangle), \tag{4.34}$$

for some arbitrary phase, $e^{-\mathrm{i}\phi}$. These two classes of two-qubit states are the only ones that have a reduced 1-body density matrix of form $\mathbb{1}/2$, because $\mathbb{1}/2$ implies complete uncertainty on the 1-body level. For a two-qubit pure state, this only occurs when the state is maximally bipartite-entangled. Anything less than maximum entanglement gives some level of certainty on the 1-body reduced density matrix. These two states are unable to estimate all three parameters, since they give rise to singular statistical models, for which the QFI matrix is not invertible.

In the rest of this chapter we restrict ourselves to estimation around the true value $\boldsymbol{\varphi} = [0, 0, 0]$ to simplify algebraic expressions. This is a relevant setting in precision magnetometry, where small deviations from a known reference field are measured. Furthermore, this is usually the optimal point in parameter space and can be achieved by interspersing the evolution with adaptive control unitaries [212, 40], although a formal proof is lacking for the HCRB.

4.4 Evaluation of the HCRB

We start with a real valued two-qubit state,

$$|\psi_0\rangle = \begin{bmatrix} r_1 \\ r_2 \\ r_3 \\ r_4 \end{bmatrix}, \tag{4.35}$$

such that $r_i \in \mathbb{R}$ and $\sum_i r_i^2 = 1$. This assumption is motivated primarily by algebraic simplicity. In order to ensure this assumption does not undermine has intuition we gain from this result we are able to do two numerical checks for confirmation. First, we generate a random quantum state and compute its HCRB, then numerically search for a state with the same HCRB. No cases were found that contradicted this assumption. Secondly, we use brute force numerical optimisation with and without the restriction to real values for the state. No difference was found in the optimal state HCRB with or without the real value restriction. More generally, the question of "how real" is quantum metrology has yet to be answered rigorously [1]. In other words, is the complex nature of a quantum state an exploitable resource?

For this problem the vectors (4.11), stacked as columns of a matrix, are

$$(|l_1\rangle \; |l_2\rangle \; |l_3\rangle) \tag{4.36}$$

$$= \begin{pmatrix} 2(2r_1 r_{1,4}^+ - 1)(r_{2,3}^+) & 2ir_{2,3}^+ & 4r_1\left(r_{1,4}^+ r_{1,4}^- - 1\right) \\ 2r_{1,4}^+(2r_2 r_{2,3}^+ - 1) & -2ir_{1,4}^- & 4r_2 r_{1,4}^- r_{1,4}^+ \\ 2r_{1,4}^+(2r_3 r_{2,3}^+ - 1) & -2ir_{1,4}^- & 4r_3 r_{1,4}^- r_{1,4}^+ \\ 2(2r_4 r_{1,4}^+ - 1)r_{2,3}^+ & -2ir_{2,3}^+ & 4r_4\left(r_{1,4}^+ r_{1,4}^- + 1\right) \end{pmatrix},$$

where we have introduced

$$r_{1,4}^\pm = r_1 \pm r_4, \quad r_{2,3}^\pm = r_2 \pm r_3. \tag{4.37}$$

As $\dim \operatorname{span}_{\mathbb{R}}\{|l_i\rangle\} = 3$ and $\dim \operatorname{span}_{\mathbb{C}}\{|l_i\rangle\} = 2$,

$$\begin{aligned} \operatorname{span}_{\mathbb{C}}\{|l_i\rangle\} &= \operatorname{span}_{\mathbb{C}}\{|l_1\rangle, |l_2\rangle\} \\ &\cong \operatorname{span}_{\mathbb{R}}\{|l_1\rangle, |l_2\rangle, i\,|l_1\rangle, i\,|l_2\rangle\} \\ &\cong \operatorname{span}_{\mathbb{R}}\{|l_1\rangle, |l_2\rangle, |l_3\rangle, |v\rangle\}, \end{aligned} \tag{4.38}$$

where $|v\rangle$ is a complex linear combination of $|l_1\rangle$ and $|l_2\rangle$ satisfying $\mathrm{Re}\,\langle l_i|v\rangle = 0$. Explicitly,

$$|v\rangle = -\frac{\mathrm{i}\left((r_{1,4}^-)^2 + (r_{2,3}^+)^2\right)}{r_{1,4}^+ r_{1,4}^-}\,|l_1\rangle - |l_2\rangle\,. \tag{4.39}$$

By substituting the constraints (4.10) we get to

$$|x_i\rangle = \sum_j (J^{-1})_{ji}\,|l_j\rangle + \alpha_i\,|v\rangle\,, \tag{4.40}$$

where now for pure states the QFIM is given by $J_{ij} = \mathrm{Re}\,\langle l_i|l_j\rangle$. Crucially, we now have an unconstrained optimisation on the three real parameters α_i, that is, $C^{\mathrm{H}} = \min_\alpha \mathrm{Tr}\,\mathrm{Re}\,Z[\alpha] + \|\mathrm{Im}\,Z[\alpha]\|_1$. The same approach of explicitly substituting the constraints was initially applied to mixed states [184], being instrumental in obtaining closed-form results for qubits [185]. Before continuing with the calculation, we must confirm that this new unconstrained formulation of the HCRB remains convex. We begin with,

$$|x_i\rangle = \sum_j (J^{-1})_{ji}\,|l_j\rangle + \alpha_i\,|v\rangle\,, \tag{4.41}$$

where α_i is the vector of 3 real parameters that we minimise over. This form of $|x_i\rangle$ remains in the span of $ketl_j$, as $|v\rangle$ belongs to this span. We have reformulated this span to limit the degrees of freedom that we need to optimise over. Restated, $C^{\mathrm{H}} = \min_\alpha \mathrm{Tr}\,\mathrm{Re}\,Z[\alpha] + \|\mathrm{Im}\,Z[\alpha]\|_1$. Firstly, denoting $|\tilde{l}_i\rangle = \sum_j (J^{-1})_{ji}\,|l_j\rangle$,

$$\mathrm{Tr}\,\mathrm{Re}\,Z[\alpha] = \sum_i \alpha_i^2\,\langle v|v\rangle + \alpha_i(2\,\mathrm{Re}\,\langle\tilde{l}_i|v\rangle) + \langle\tilde{l}_i|\tilde{l}_i\rangle\,, \tag{4.42}$$

which is quadratic, hence convex in α_i.

Secondly,

$$\|\mathrm{Im}\,Z[\alpha]\|_1 = \frac{1}{2}\sqrt{\langle x_1|x_2\rangle^2 + \langle x_1|x_3\rangle^2 + \langle x_3|x_2\rangle^2}. \tag{4.43}$$

In order to show this is convex with respect to α_i we show that the Hessian of this function is positive semi-definite (PSD), namely,

$$y\begin{bmatrix} \frac{\partial^2 \|\mathrm{Im}\,Z[\alpha]\|_1}{\partial \alpha_1^2} & \frac{\partial^2 \|\mathrm{Im}\,Z[\alpha]\|_1}{\partial \alpha_1 \partial \alpha_2} & \frac{\partial^2 \|\mathrm{Im}\,Z[\alpha]\|_1}{\partial \alpha_1 \partial \alpha_3} \\ \frac{\partial^2 \|\mathrm{Im}\,Z[\alpha]\|_1}{\partial \alpha_2 \partial \alpha_1} & \frac{\partial^2 \|\mathrm{Im}\,Z[\alpha]\|_1}{\partial \alpha_1^2} & \frac{\partial^2 \|\mathrm{Im}\,Z[\alpha]\|_1}{\partial \alpha_2 \partial \alpha_3} \\ \frac{\partial^2 \|\mathrm{Im}\,Z[\alpha]\|_1}{\partial \alpha_3 \partial \alpha_1} & \frac{\partial^2 \|\mathrm{Im}\,Z[\alpha]\|_1}{\partial \alpha_3 \partial \alpha_2} & \frac{\partial^2 \|\mathrm{Im}\,Z[\alpha]\|_1}{\partial \alpha_3^2} \end{bmatrix} y^\dagger \geq 0, \tag{4.44}$$

for an arbitrary real-valued vector, $y = (y_1, y_2, y_3)$. A necessary and sufficient condition for the above to be true is all eigenvalues of the Hessian are non-negative. Indeed we find the eigenvalues λ_i to be

$$\lambda_1 = 0, \tag{4.45}$$

$$\lambda_2 = \frac{(r_{2,3}^+)^2}{(4r_{1,4}^- r_{1,4}^+)^2}, \tag{4.46}$$

$$\lambda_3 = \frac{64(r_{2,3}^+)^4 \delta((\alpha_3 r_{2,3}^+ + \alpha_1 r_{1,4}^-)^2 + \alpha_2^2 \delta) + (r_{1,4}^-)^2}{(2r_{1,4}^- r_{1,4}^+)^4}, \tag{4.47}$$

where $\delta = 1 - 2(r_1 r_4 - r_2 r_3)$. Since $2|r_1 r_4 - r_2 r_3|$ is the concurrence of a pure two-qubit state [201], which takes value in the range $[0, 1]$, we see that $\delta \geq 0$. Given the eigenvalues of the Hessian are non-negative, $\|\mathrm{Im}\, Z[\alpha]\|_1$ is a convex function of the parameters α_i. As $\mathrm{Tr}\, \mathrm{Re}\, Z[\alpha]$ is also convex with respect to α_i, and the sum of two convex functions is convex, $\mathrm{Tr}\, \mathrm{Re}\, Z[\alpha] + \|\mathrm{Im}\, Z[\alpha]\|_1$ is convex with respect to α_i and the global minimum is found for $\alpha_i = 0 \; \forall \, i$ since the gradient vanishes there.

This function is minimised by $\boldsymbol{\alpha} = [0, 0, 0]$ as can be explicitly checked by the vanishing of the gradient and the positive semidefiniteness of the Hessian as previously shown.

In other words, the optimal vectors $|x_i\rangle$ lie in the real subspace generated by the vectors $|l_i\rangle$ so we have

$$C^{\mathrm{H}} = C^S + \left\| (J^s)^{-1} D (J^s)^{-1} \right\|_1, \tag{4.48}$$

where $D_{ij} = \mathrm{Im}\, \mathrm{Tr}[L_i L_j \rho_{\boldsymbol{\varphi}}] = \mathrm{Im}\, \langle l_i | l_j \rangle$. More explicitly, the HCRB for 3D magnetometry without the presence of noise is

$$C^{\mathrm{H}} = \frac{1}{8} \left(\frac{1}{(r_{1,4}^+)^2 + (r_{1,4}^-)^2 - 2(r_{1,4}^- r_{1,4}^+)^2 + (r_{2,3}^+)^2(1 - 2(r_{1,4}^+)^2)} \right. \tag{4.49}$$

$$\left. + \left(\frac{1}{\sqrt{(r_{1,4}^-)^2 + (r_{2,3}^+)^2}} + \frac{1}{(r_{1,4}^+)} \right)^2 \right). \tag{4.50}$$

In order to touch on the significance of this result, we first must explain what is meant by a coherent (or D-invariant) bound. A quantum statistical model is called coherent at φ, if SLD-tangent space at φ is an invariant subspace of the commutation

superoperator [8]. Mathematically,

$$\forall \boldsymbol{X} \in \mathrm{span}_{\mathbb{R}}\{\boldsymbol{l_\varphi}\} \rightarrow \mathcal{D}_{|\psi_\varphi\rangle}(\boldsymbol{X}) \in \mathrm{span}_{\mathbb{R}}\{\boldsymbol{l_\varphi}\}, \tag{4.51}$$

where the commutation superoperator $\mathcal{D}_{|\psi\rangle_\varphi}(\boldsymbol{X})$ is defined to be the superoperator satisfying the following equation [95],

$$|\psi_\varphi\rangle \langle\psi_\varphi| \boldsymbol{X} - \boldsymbol{X} |\psi_\varphi\rangle \langle\psi_\varphi| \tag{4.52}$$
$$= i\left(|\psi_\varphi\rangle \langle\psi_\varphi| \mathcal{D}_{|\psi\rangle_\varphi}(\boldsymbol{X}) + \mathcal{D}_{|\psi\rangle_\varphi}(\boldsymbol{X}) |\psi_\varphi\rangle \langle\psi_\varphi|\right)$$

If the above condition holds, then equation (4.48) holds. In general, equation (4.48) an upper bound to the HCRB and only equal for any weight matrix if and only if the model is coherent, as shown [185].

For pure states and an even number of parameters, such models are called coherent as their tangent space has a symplectic structure [70]. For two-qubit 3D magnetometry we find (4.48) to hold for any diagonal weight matrix but not for a general one (See Section 4.6 for details). This is consistent with the fact that it is not a coherent model. We propose to call these models odd-coherent and that their properties warrant further study.

Before moving onto the attainability of this bound we briefly comment on the role of entanglement in the initial state. We find a one-to-one relationship between the entanglement of the input state and HCRB, with both separable and maximally entangled states leading to a singular model, meaning that they do not allow for the simultaneous estimation of all three parameters (See Section 4.5 and Ref. [19]).

4.5 Role of entanglement

The role of entanglement as a resource in quantum metrology is a question that has been well studied for single parameter problems [191, 170, 56]. With thanks to the closed form expression for the degree of entanglement for pure two qubit states we can fully study this question for this model too. We can see in figure 4.1 that there is a one to one relation between the level of entanglement and the CRB.

As seen in figure 4.1 we can see that there exists a one to one relationship between the entanglement of the initial state and its scalar bound. Also as predicted in [19] there is a trade-off relationship between entanglement and a state's performance. Both separable and maximally entangled states are singular. The important point to note is

that the HCRB and QCRB optimal points differ. That is to say the additional terms in the HCRB properly account for the entanglement of a given state.
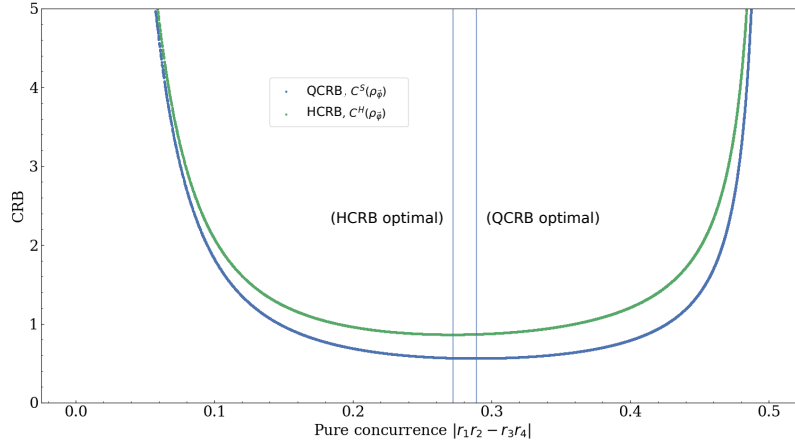
Figure 4.1: parametric plot of entanglement $|r_1 r_4 - r_2 r_3|$ vs CRB, here either QCRB or HCRB. The vertical line to the left hand side is the optimal HCRB point and the line to the right is the optimal QCRB point. We note the surprising implication that only the bipartite entanglement is required in order to infer how well a given state performs for 3D-magnetometry. The implication of which being, if we prepare an entangled state, before the parameter unitary is applied, a Cramér-Rao bound (CRB) is invariant under local transformations that occur after entangled state preparation and before parameter encoding. Noting that local transformations do not impact entanglement.

4.6 HCRB for diagonal weight matrices

Hitherto, we have ignored the inclusion of a weight matrix W. This is due to $W = \mathbb{1}$ being the case that corresponds to the MSEM. We can however, elect to manipulate the weighting of parameters or their correlations. For example, $W = 2,1,1$ corresponds to doubling the impact of sensitivity to the first parameter. We will here examine weight matrices other than identity. Suzuki [183] showed that for a full-rank state coherent model, the HCRB is equal to the coherent bound for all positive weight matrices. Given the previous comparisons made to coherent models, we further examine weight matrices in order to determine if the intuitions hold from coherent models to this model.

We introduce the weight matrix W, a $p \times p$ real-valued positive matrix. The corresponding HCRB is obtained by generalizing Eq. (5.1) to

$$\operatorname{Tr} W V_{\varphi}(\Pi, \tilde{\varphi}) \geq C^{\mathrm{H}}(|\psi\rangle\langle\psi|) = \min_X \operatorname{Tr} \operatorname{Re} W Z[X] + \left\| \sqrt{W} \operatorname{Im} Z[X] \sqrt{W} \right\|_1, \tag{4.53}$$

with the same constraints (4.1) and the same definition (4.3). We identify two natural classes of weight matrices. The first is a diagonal $W = \operatorname{diag}(w_1, w_2, w_3)$, $w_i \geq 0$, $w_i \in \mathbb{R}$. This corresponds to modifying the proportion to which we estimate each parameter. The second class is the general non-diagonal matrix $W \geq 0$, which corresponds to taking linear combinations of the parameters. For 3D magnetometry with diagonal weight matrices,

$$C^{\mathrm{H}}(|\psi\rangle\langle\psi|) = \operatorname{Tr} W J^{S-1} + \left\| \sqrt{W} J^{S-1} D J^{S-1} \sqrt{W} \right\|_1. \tag{4.54}$$

In particular,

$$\operatorname{Abs} \operatorname{Im} \sqrt{W} (J^s)^{-1} D (J^s)^{-1} \sqrt{W} = \frac{1}{4} \sqrt{\frac{w_1 w_2 (r_{1,4}^-)^2 + w_2 w_3 (r_{2,3}^+)^2}{(r_{1,4}^+)^2 \left((r_{1,4}^-)^2 + (r_{2,3}^+)^2 \right)^2}} \tag{4.55}$$

$$8 \operatorname{Re} W Z[X] = \frac{\alpha}{\beta}. \tag{4.56}$$

Where

$$\alpha = w_2 \frac{1}{(r_{1,4}^-)^2 + (r_{2,3}^+)^2} + w_3 (((r_{1,4}^+)^2 + (r_{2,3}^+)^2 (1 - 2(r_{1,4}^+)^2))) \tag{4.57}$$

$$+ w_1 \left((r_{1,4}^+)^2 (r_1^2 + r_4^2) \left((r_1^2 + r_4^2)(r_2^2 + r_3^2 - 2) + \left(r_{1,4}^- r_{1,4}^+ \right)^2 + 1 \right) \right),$$

$$\beta = 2(r_{1,4}^+)^2 \left(r_1^2 \left(-r_1^2 (r_4^2 + 2) + r_1^4 + 4r_4^2 (r_2 r_3 + 1) - r_4^4 + 1 \right) + r_4^2 (r_4^2 - 1)^2 \right) \tag{4.58}$$

$$+ (r_{2,3}^+)^2 \left(2(r_{1,4}^+)^2 \left(2(r_{1,4}^+)^2 + r_2^2 + r_3^2 - 2 \right) + 1 \right).$$

However, the form of Eq. (4.54) for the HCRB does not hold for a general weight matrix.

4.7 Attainability of the HCRB for the model

The HCRB for all pure state models are attainable with a POVM, without the need of measuring multiple copies collectively [130]. However, ancillas may be required to implement the optimal measurement. The HCRB is attainable with a projective measurement if $\dim \mathcal{H} > 2p + 1$ [89, Chap. 20, Corollary 23]. For two-qubit 3D magnetometry, $\dim \mathcal{H} = 4 < 2p + 1 = 7$. Thus, known results offer no suggestion of projective attainability of the HCRB for 3D magnetometry with two-qubit pure states. Fujiwara showed projective attainability for a 2-parameter coherent model [70]. This model's bound may take the form of a coherent model's bound but the odd number of parameters means it is not a coherent model. From these known results we have no guarantee of projective attainability.

We now show the projective attainability of the HCRB for 3D magnetometry with two-qubit real pure states. To that end, recall that a projective measurement (and a locally unbiased estimator) with $V(\Pi, \tilde{\varphi})_{ij} = F(|\psi_{\varphi}\rangle, \Pi)_{ij}^{-1} = \langle x_i | x_j \rangle$ exists if and only if $\operatorname{Im} \langle x_i | x_j \rangle = 0$ for vectors also satisfying the local unbiasedness condition (4.10) [130]. Since we have already found the HCRB, to prove its projective attainability we need to find a set $\{|x_i\rangle\}$ satisfying (4.10) as well as $C^{\mathrm{H}} = \operatorname{Tr} \operatorname{Re} Z[X]$ and $\operatorname{Im} Z[X] = 0$. Unlike the evaluation of the HCRB, it is not possible to solve this system by restricting to $|x_i\rangle \in \operatorname{span}_{\mathbb{C}} \{|l_1\rangle, |l_2\rangle\}$. This space does not have the required degrees of freedom to satisfy the additional constraints imposed by also seeking projective attainability, this is why we return to the full Hilbert space. Thus, we have 24 real parameters (coming from the 3 complex 4-dimensional vectors) with 6 linear constrains, 3 bi-linear constraints and 1 quadratic constraint. Indeed we are able to satisfy all these constraints; a family of X operators that attains the HCRB for 3D magnetometry with two-qubit real pure states, as we demonstrate. We first require the following lemma,

Lemma 2. If there exists an unbiased projective measurement such that,

$$V[M] = \operatorname{Re} X^* X, \tag{4.59}$$

where X is the ordered pair,

$$X = [M^1(M, |\psi\rangle), \dots M^m(M, |\psi\rangle)], \tag{4.60}$$

then,

$$\text{Im } X^*X = 0 \tag{4.61}$$

holds true. Conversely, if we have $ImX^*X = 0$, then there exists a projective measurement such that 4.59 holds.

The proof of which is given in [136] (theorem 4). The implication of this being, if we are able to construct a vector X such that $\text{Im } X^*X = 0$ and $V[M] = \text{Re } X^*X$ then there must exist a project measurement that attains the HCRB. We have previously computed the HCRB, utilizing a reduced space in order to simplify the calculation. This reduced space does not possess all the properties of the full vector space. Namely, there are not enough degrees of freedom in order to satisfy the HCRB constraints as well as $\text{Im } X^*X = 0$. We will in the following therefore, return to the full vector space in order to satisfy the constraints.

Theorem 3. *For a real valued 2-qubit state with a zero value magnetic field acting in the three Pauli directions has a Holevo Cramér-Rao bound that is attainable with a projective measurement.*

Proof. In order to prove Theorem 3 we construct a set of complex vectors $|x_i\rangle$ which satisfy,

$$\langle x_i | \partial_j \psi \rangle = \delta_{i,j} \tag{4.62}$$

$$\text{Im } \langle x_j | x_j \rangle = 0. \tag{4.63}$$

If we can satisfy these constrains, as well as finding X such that $V[M] = \text{Re } X^*X$, then by lemma 2 we know that there exists a projective measurement that attains the HCRB. We therefore attain the HCRB with a single copy. The key element of simplifying the proof is that we already have the HCRB, so we are able to re-write the minimisaiton,

$$C^{\text{H}} = \min_{\alpha} \text{Tr} \text{Re } Z + \text{Abs} \text{Im } Z \tag{4.64}$$

as an additional quadratic constraint, including the fact that we constrain $\text{Abs} \text{Im } Z = 0$. From this we have,

$$\min_{\alpha} \text{Tr} \text{Re } Z = \sum_{i=1}^{3} \langle x_i | x_i \rangle \tag{4.65}$$

$$= C^{\text{H}} \quad (\text{equation} \quad 4.49). \tag{4.66}$$

In this system of equations we have 24 real parameters (coming from the 3 complex 4-dimensional vectors) with 6 linear constrains, 3 bi-linear constraints and 1 quadratic constraint. Indeed we are able to satisfy all these constraints. In order to explicitly give the X-operators we begin by taking the simplified form of the HCRB pure states and calculating it terms of the 24 real parameters that construct X,

$$C^{\mathrm{h}}(|\psi\rangle) = \min_X \mathrm{Re}\, Z[X] + \mathrm{Abs}\,\mathrm{Im}\, Z[X], \tag{4.67}$$

$$Z[X] = XX^{\dagger}. \tag{4.68}$$

Where $X = \{|x_1\rangle, |x_2\rangle, |x_3\rangle\}$ is a matrix of vectors

$$X_i = \tilde{X}_i |\psi\rangle = |x_i\rangle. \tag{4.69}$$

The operator $\tilde{X}_i$ is an arbitrary Hermitian operator. The arbitrary complex vectors $|x_i\rangle$ satisfy the local-unbiased condition as well as the condition that their inner products are strictly real-valued,

$$\mathrm{Re}\,\langle x_i|\partial_j\psi\rangle = \delta_{i,j}. \tag{4.70}$$

$$\mathrm{Im}\,\langle x_i|x_j\rangle = 0. \tag{4.71}$$

we parameterise our X operators

$$X = \{|x_1\rangle, |x_2\rangle, |x_3\rangle\} \tag{4.72}$$

$$= \begin{bmatrix} x_{1,1}^r + x_{1,1}^i i & x_{2,1}^r + x_{2,1}^i i & x_{3,1}^r + x_{3,1}^i i \\ x_{1,2}^r + x_{1,2}^i i & x_{2,2}^r + x_{2,2}^i i & x_{3,2}^r + x_{3,2}^i i \\ x_{1,3}^r + x_{1,3}^i i & x_{2,3}^r + x_{2,3}^i i & x_{3,3}^r + x_{3,3}^i i \\ x_{1,4}^r + x_{1,4}^i i & x_{2,4}^r + x_{2,4}^i i & x_{3,4}^r + x_{3,4}^i i \end{bmatrix} \tag{4.73}$$

Now we look for solutions to the above conditions. We have 24 real parameters with 9 linear constrains, 3 bi-linear constraints and 1 quadratic constraints, which leaves us with 11 arbitrary parameters. We set these remaining parameters to 0 or 1 for ease, one could spend more time looking for parameters which give similar X operators, but

this is sufficient for our purposes. First we satisfy $\sum_{i=1}^{3} \langle x_i | x_i \rangle = C^{\mathrm{H}}$, which gives,

$$x_{2,2}^r = \big(C^{\mathrm{H}} - \langle x_1 | x_1 \rangle - \langle x_3 | x_3 \rangle \tag{4.74}$$

$$- [(x_{2,1}^i)^2 + (x_{2,1}^r)^2 + (x_{2,2}^i)^2 + (x_{2,3}^i)^2 + (x_{2,3}^r)^2 + (x_{2,4}^i)^2 + (x_{2,4}^r)^2] \big)^{1/2} \tag{4.75}$$

Substituting the above in, we then satisfy $\langle x_i | \partial_j \psi \rangle = \delta_{i,j}$, which gives us,

$$x_{1,3}^r = -(1/(r_{1,4}^+)) - ((r_{2,3}^+)x_{1,1}^r)/r_4 - x_{1,2}^r, \tag{4.76}$$

$$x_{1,4}^r = (r_1 x_{1,1}^r)/r_4, \tag{4.77}$$

$$x_{1,4}^i = x_{1,1}^i - ((r_{1,4}^-)x_{1,2}^i)/(r_{2,3}^+) - ((r_{1,4}^-)x_{1,3}^i)/(r_{2,3}^+), \tag{4.78}$$

$$x_{2,3}^r = -(((r_{2,3}^+)x_{2,1}^r)/r4) - x_{2,2}^r, \tag{4.79}$$

$$x_{2,4}^r = (r1 x_{2,1}^r)/r_4, \tag{4.80}$$

$$x_{2,4}^i = -(1/(r_{2,3}^+)) + x_{2,1}^i - ((r_{1,4}^-)x_{2,2}^i)/(r_{2,3}^+) - ((r_{1,4}^-)x_{2,3}^i)/(r_{2,3}^+), \tag{4.81}$$

$$x_{3,3}^r = -((r_{2,3}^+)/(2r4(r_{1,4}^+))) - ((r_{2,3}^+)x_{3,1}^r)/r4 - x_{3,2}^r, \tag{4.82}$$

$$x_{3,4}^r = 1/(2r4) + (r1 x_{3,1}^r)/r_4, \tag{4.83}$$

$$x_{3,4}^i = x_{3,1}^i - ((r_{1,4}^-)x_{3,2}^i)/(r_{2,3}^+) - ((r_{1,4}^-)x_{3,3}^i)/(r_{2,3}^+). \tag{4.84}$$

Again, substituting, we next satisfy $\operatorname{Im} \langle x_j | x_j \rangle = 0$,

$$x_{1,1}^r = ((r_{2,3}^+)r4(x_{1,1}^i x_{3,1}^r + (((r_{2,3}^+)x_{1,1}^i - (r_{1,4}^-)(x_{1,2}^i + x_{1,3}^i))(1 + 2r1 x_{3,1}^r))/(2(r_{2,3}^+)r4) \tag{4.85}$$

$$- ((r_{2,3}^+)x_{1,3}^i(1 + 2(r_{1,4}^+)x_{3,1}^r))/(2r4(r_{1,4}^+)) - x_{1,2}^r x_{3,2}^i + x_{1,2}^i x_{3,2}^r - x_{1,3}^i x_{3,2}^r$$

$$+ x_{3,3}^i/(r_{1,4}^+) + x_{1,2}^r x_{3,3}^i))/(-r1^2(x_{3,2}^i + x_{3,3}^i) + (r_{2,3}^+)(r4 x_{3,1}^i - (r_{2,3}^+)x_{3,3}^i)$$

$$+ r1((r_{2,3}^+)x_{3,1}^i + r4(x_{3,2}^i + x_{3,3}^i))),$$

$$x_{2,1}^i = 1/(r_{2,3}^+) \tag{4.86}$$

$$x_{1,1}^i = -((2r4)/(r_{1,4}^+)), \tag{4.87}$$

Finally, substituting and setting the remaining arbitrary elements to 1 or 0 to avoid singularities.

$$x^i_{1,2} = x^r_{1,2} = x^i_{1,3} = x^r_{2,1} = x^i_{2,2} = x^i_{2,3} = x^r_{3,1} = x^r_{3,2} = 0, \qquad (4.88)$$

$$x^i_{3,3} = x^i_{3,1} = x^i_{3,2} = 1, \qquad (4.89)$$

In this way, we have been able to satisfy all constraints of our system, giving rise to a real valued $Z[\boldsymbol{X}]$ that attains the HCRB. This implies that there exists a set of projective measurements which have CCRB = HCRB. With lemma 2 this concludes the proof. □

We omit presenting an explicit example of the projective measurements. We chose arbitrary free parameters which avoided singularities, but give no intuition into the explicit structure of the projective measurements. Further work includes investigating physically relevant parameters in the place of these free values in order to give simpler and physically meaningful measurements.

4.8 Conclusions and discussions

In this chapter we calculated the HCRB for 2-qubit, 3D magnetometry, for zero parameter and real valued states. Further, we demonstrated its attainability with a single-copy projective measurement. Finally we calculated the HCRB for an arbitrary diagonal weight matrix and demonstrate a 1-1 relationship between the entanglement of a given state and its corresponding HCRB.

The calculation of the HCRB was the first 3-parameter analytic calculation of the HCRB (that does not collapse to either the QCRB or RLD-Cramér-Rao bound (CRB)). This results highlights that for particular state structures (here, pure states) there are simplifications and previously known results that are capable of unlocking new insights and analytic solutions.

Asymptotic classicality is often cited and used in the multi-parameter quantum metrology literature. That is to show the QCRB is equal to the HCRB and such the QCRB represents the fundamental bound, bypassing the need to calculate the HCRB. It is equally often used to avoid discussion of the CCRB by showing the unattainability of the QCRB. However, this result highlights that asymptotic classicality fails to capture any of the subtleties of attainability. Here we showed that there exists a projective measurement on a single copy of the input state such that the CCRB is equal to the HCRB with that given measurement. We stress the point that lack of asymptotic

classicality does not necessarily mean that multiple copies are required to attain the most informative bound on estimation.

Entanglement as a resource in quantum metrology is one of the overarching questions [191]. Is it where quantum advantage comes from, is there a trade-off, how hard are the entangled states to prepare? The 1-1 relationship we demonstrated in this chapter has some interesting implications. If we briefly think about 1-parameter estimation then we know the optimal state for Pauli-Z magnetic field estimation is the GHZ state that is formed by the eigenvectors of the Pauli-Z magnetic field Hamiltonian. This state exhibits maximum entanglement in a multi-partite sense. However, 'rotating' this state and using the GHZ state generated by the Pauli-X magnetic field Hamiltonian is completely insensitive to the Pauli-Z magnetic field and gives rise to a singular QCRB. The point is made to emphasise that the 'direction' of the quantum state typically is of great significance when it comes to sensing. This particular case demonstrates a novel and surprising way in which multiparameter estimation deviates from intuitions gains from single parameter estimation. That is, it is possible in a quantum multiparameter estimation problem for only the quantity of bipartite entanglement to be of concern when it comes to a state's given performance in sensing.

On a practical point, the main result of this chapter (that being the calculation of the HCRB) was made simpler by initially calculating the HCRB for a simpler class of states. Explicitly the HCRB for a weighted GHZ state,

$$|\psi\rangle = \begin{bmatrix} a \\ 0 \\ 0 \\ \sqrt{1-a^2} \end{bmatrix}, \tag{4.90}$$

for which the algebra was greatly simplified.

4.8.1 Further work

The model possesses many similar properties to the coherent model [71]. We propose such models be refered to as *odd-coherent*. Further work that would be of great interest would be to examine how many other properties of a true coherent model hold in the odd number of parameters case we examine here. In particular, do all models satisfying coherent-ness other than having an odd number of parameters take the same form of the HCRB above and are attainable with single copy projective

measurements?

Different mathematical tools will need to be employed in order to solve the HCRB for system sizes greater than $N = 2$ as the particular difference in complex and real span of the horizontal lifts is a quirk of 2-qubit geometry. A natural extension of this work would be to find a more general solution for the HCRB that holds in general for increasing system sizes. As noted above, even solving the simplest systems algebraically can offer great insight into the general case. One of the central results of [19], was that the QCRB depends only on the one and two body reduced density matrices of the input state. The question of 2-body dependance on the HCRB is one that would be very exciting to solve. At least part of the motivation for answering this question would be to investigate how far down convexity goes! We have a convex cost function in the state as a whole, that depends quadratically on the Hamiltonian we wish to estimate. Is it possible to further impose convexity on the elements of the input state, thus, optimising the input state as a convex problem? Some initial calculations into this problem exploring the avenue of geodesic convexity [196] showed early promise. However, the complexity of calculating geodesics of quantum states as system size increases was prohibitive.

Chapter 5

Quantum limits of 3D magnetometry

In art, as in biology, there is a phenomenon that can be described as mutation, in which appearances radically change at a tempo much more rapid than that at which they normally proceed.

Mark Rothko

5.1 Introduction

In the previous chapter, we gained new insights into 3D-magnetometry through analytic calculation of the HCRB. In this chapter we look for new insights that arise with the addition of dephasing noise for 3D-magnetometry. We use this one example noise model as this is the main concern for an NV center magnetometry experiment. The sensitivity of an NV center magnetometer is limited by the dephasing time (T_2) [87, 205]. There has been many successful strides in improving the coherence times of NV centers [180, 116, 156, 82, 176]. These efforts have further translated into improvements in NV magnetometry [148, 41, 87, 98, 18, 199, 177, 124]

Quantum-enhanced metrological schemes that are capable of utilising uniquely quantum features, such as entanglement, coherence and squeezing, have found experimental success. [77, 54, 52, 150, 30, 152, 22]. Further, multi-parameter quantum

sensing experiments have seen great recent success experimentally [195, 165, 166, 147, 154]. A complete analysis is vital for pushing the boundaries of sensing. For example, a novel quantum-mechanical analysis has led to new techniques for super-resolution [194, 44, 218, 190, 147, 211, 137].

The unifying factor of all quantum sensing experiments is environmental noise. It is not possible to escape the detrimental effects of interaction with external perturbations. When looking to optimise experiments, these detrimental effects must be taken into careful consideration. The optimal state for a given experiment depends heavily on the particular noise acting on the experimental setup. Mathematically speaking, noise takes us from pure states (rank-1 matrices or vectors) into the space of density operators, a completely different geometry. The main example of noise that we consider here is dephasing noise, or Pauli-Z noise. The effect of which is to degrade a state's off-diagonal coherences to zero. This *destroys* the information that would have been contained within those coherences. It is worth noting that Pauli X and Y single body Hamiltonians are still capable of imparting information onto a state that is diagonal in the Pauli-Z basis.

When it comes to a complete analysis of a quantum multi-parameter estimation problems, the HCRB gives the ultimate bound to estimation. Although the HCRB and the scalar CRB obtained from the QCRB matrix differ by no more than a factor of two [36, 193], the former provides insights into the optimal measurements for attainability, as we will show. However, our analysis is *practically* incomplete without the consideration of noise. We aim to address this missing component of our previous analysis in this chapter.

Unlike pure states, the HCRB for mixed states is, in principle, attained asymptotically in the number of identical copies of the state, which must be measured collectively [86, 53]. As this is prohibitive in practice we study the contribution of a few (two and three) copies of the two-qubit state towards reaching the asymptotic limit, by numerical optimisation of the CCRB over collective measurements. We analyse how the attainability of 3D-magnetometry varies over noise whilst adding multiple copies of the input state.

We also use the HCRB to take a deeper look at asymptotic classicality. If a model is asymptotically classical, it means that the HCRB and QCRB are equal. This means that if the QCRB is the metric being calculated, then it can be attained. Conversely, if a model is not asymptotically classical, then the QCRB can never be attained, regardless of how many copies of your system you have. Asymptotic

classicality is often inaccurately used in discussions of attainability. As we previously noted, just because a model does not possess asymptotic classicality, it does not mean that any more than 1-copy of the input state is needed. Equally, when a model is asymptotically classical, it could take an infinite number of input states in order to attain the HCRB/QCRB. In this chapter we look at the difference between the HCRB and QCRB when the model is not asymptotically classical.

When using a noisy quantum channel repeatedly for transmitting classical or quantum information [198], it is possible to employ quantum entanglement at different stages of the estimation process. Entanglement can be deployed only at the preparation stage in a quantum-classical (QC) strategy, only at the measurement stage in a classical-quantum (CQ) strategy, or at both ends in a quantum-quantum (QQ) strategy. The QC and CQ strategies are depicted in figure 5.1, where we can see the structure of the measurements and input state. A similar approach to quantum estimation strategies shows that for single parameter estimation CQ strategies are never useful [79, 89]. The same is not true for multiple parameters, as exemplified by the fact that collective measurements are needed to attain the HCRB. Thus, we investigate the performance of a QC strategy by numerically optimising the CCRB over initial $2k$-qubit states and over k independent measurements over 2-qubits systems. Our third result is that for $k = 2$ in the high noise regime, the CQ strategy (which approaches the HCRB for high noise) outperforms the QC strategy.

Moving further towards practical implementation, we present numerically-optimised, shallow quantum circuits executing CQ strategies for quantum-limited two-qubit 3D magnetometry with up to three copies using up to six qubits. The circuits were optimised independently from the previous numerical optimisation of the CCRB over collective measurements. That they both provide commensurate results provides additional reassurance on the validity of our numerical results.

5.1.1 Computing the HCRB with a semidefinite-program

The perennial issue of global optimisation is that of local minima. How is it possible to know if the minimum value we find for some input is actually the best that is possible? In short, it is not possible. For a general optimisation problem we are unable to tell if a given solution is the true global minimum or we are in a local minima. In other words, is it possible for us to do better? For many practical problems, this is not necessarily an issue. Often a 'good enough' solution will suffice. In the case of the HCRB, obtaining a true global minima is essential, otherwise we are not calculating
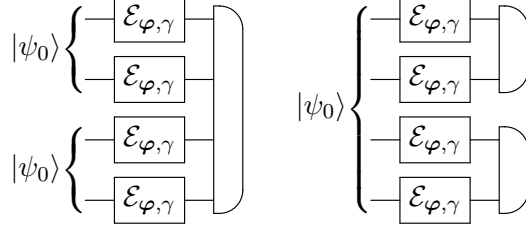
Figure 5.1: Classical-quantum (CQ) (left) vs quantum-classical (QC) (right) schemes for $k = 2$ two-qubit systems. A qubit is represented by a wire. The channel $\mathcal{E}_{\varphi,\gamma} = \Lambda_\gamma \circ \mathcal{U}_\varphi$ represents a process of noise and parameter encoding on each qubit. Both noise and encoding act independently on each qubit.

the bound, instead just an approximation.

This is what makes the formulation of an optimisation problem as a convex problem so desirable. A convex optimisation has the property that any minimum is a global one.

It was previously shown by Bradshaw et.al [28] that for displacement estimation with Gaussian states the HCRB could be computed with a semidefinite-program.

It was further shown [6] that the HCRB is indeed an SDP for all problems. A slight reformulation of the typical HCRB we have been using will be useful in this section. The HCRB can be computing with the follow minimisations[97, 91]:

$$C_{\boldsymbol{\theta}}^{\mathrm{H}}(\rho_{\boldsymbol{\theta}}; W) = \min_{V \in \mathbb{S}^n, \boldsymbol{X} \in \mathcal{X}_{\boldsymbol{\theta}}} \left(\mathrm{Tr}[WV] \mid V \succeq Z[\boldsymbol{X}] \right), \tag{5.1}$$

with the Hermitian $n \times n$ matrix $Z[\boldsymbol{X}]_{ij} = \mathrm{Tr}[X_i X_j \rho_{\boldsymbol{\theta}}]$ and the collection $\boldsymbol{X}$ of operators $X_i \in \mathcal{L}_{\mathsf{h}}(\mathcal{H})$ in the set

$$\mathcal{X}_{\boldsymbol{\theta}} = \{ \boldsymbol{X} = (X_1, \ldots, X_n) \mid \mathrm{Tr}[X_i \partial_j \rho_{\boldsymbol{\theta}}] = \delta_{ij} \}. \tag{5.2}$$

A useful numerical simplification is in essence, to ignore the eigenvectors that correspond to the 0-valued eigenvalues. Those vectors are known as the kernal of an operator. If the density matrix $\rho_{\boldsymbol{\theta}}$ is rank deficient (i.e. has rank $r < d$) we can restrict the operators X_i to the quotient space. We define the quotient space to be,

Definition 5.1.1 (Quotient space). $\mathcal{L}_{\mathsf{h}}^r(\mathcal{H}) = \mathcal{L}_{\mathsf{h}}(\mathcal{H})/\mathcal{L}_{\mathsf{h}}(\ker(\rho_{\boldsymbol{\theta}}))$, with dimension $\tilde{d} = 2dr - r^2$.

The diagonal block of any $X \in \mathcal{L}_{\mathsf{h}}(\mathcal{H})$, that corresponds to its kernel is irrelevant in any scalar quantities calculated in the eigenbasis of $\rho_{\boldsymbol{\theta}}$ [97, 72].

A quantum state induces an inner product on $\mathcal{L}_{\mathsf{h}}^{\mathsf{r}}(\mathcal{H})$ via

$$Z[\boldsymbol{X}]_{ij} = \mathrm{Tr}[X_i X_j \rho_{\boldsymbol{\theta}}] = \boldsymbol{x}_i^{\mathsf{T}} S_{\boldsymbol{\theta}} \boldsymbol{x}_j, \tag{5.3}$$

where $S_{\boldsymbol{\theta}} \succeq 0$ is the Hermitian matrix representing the inner product in the chosen basis. This choice allows us to re-write $Z[\boldsymbol{X}] = \boldsymbol{X}^{\mathsf{T}} S_{\boldsymbol{\theta}} \boldsymbol{X}$ so that the matrix inequality on the r.h.s of Eq. (5.1) reads $V \succeq \boldsymbol{X}^{\mathsf{T}} S_{\boldsymbol{\theta}} \boldsymbol{X}$. The final crucial step is to convert this matrix inequality into a *linear* matrix inequality (LMI). We achieve this by employing the Schur complement condition for positive semidefiniteness [214]:

$$V - B^{\dagger} B \succeq 0 \iff \begin{pmatrix} V & B^{\dagger} \\ B & \mathbb{1} \end{pmatrix} \succeq 0, \tag{5.4}$$

for any matrix B and identity matrix $\mathbb{1}$ of appropriate size. Combining the above we can reformulate the minimization problem in Eq. (5.1) as

$$\begin{aligned} \underset{V \in \mathbb{S}^n, \boldsymbol{X} \in \mathbb{R}^{\tilde{d} \times n}}{\text{minimize}} \quad & \mathrm{Tr}[WV] \\ \text{subject to} \quad & \begin{pmatrix} V & \boldsymbol{X}^{\mathsf{T}} R_{\boldsymbol{\theta}}^{\dagger} \\ R_{\boldsymbol{\theta}} \boldsymbol{X} & \mathbb{1}_{\tilde{r}} \end{pmatrix} \succeq 0, \\ & \boldsymbol{X}^{\mathsf{T}} \frac{\partial \boldsymbol{s}_{\boldsymbol{\theta}}}{\partial \boldsymbol{\theta}} = \mathbb{1}_n \end{aligned} \tag{5.5}$$

where the matrix $R_{\boldsymbol{\theta}}$ can be *any* $\tilde{r} \times \tilde{d}$ matrix (with $rd = \mathrm{rank}(S_{\boldsymbol{\theta}}) \leq \tilde{r} \leq \tilde{d}$) satisfying $S_{\boldsymbol{\theta}} = R_{\boldsymbol{\theta}}^{\dagger} R_{\boldsymbol{\theta}}$. Here $\partial \boldsymbol{s}_{\boldsymbol{\theta}}/\partial \boldsymbol{\theta}$ is a matrix with the vector components of the operators $\partial \rho_{\boldsymbol{\theta}}/\partial \theta_i = \partial_i \rho_{\boldsymbol{\theta}}$ as columns. The minimisation problem (5.5) can be identified as a convex minimization problem [27]. We can see this because the set of solutions to an LMI is convex and the objective function is linear. The above can be solved numerically in an efficient manor with assurance of global optimality by various SDP solvers such as CVX [84] or YALMIP [125].

5.1.2 Channel bounds

In order to allow for a clear analysis of an initial state's $|\psi_0\rangle$ performance, it is often separated from the parameter encoding quantum channel $\mathcal{E}_{\boldsymbol{\varphi}}$, such that $\rho_{\boldsymbol{\varphi}} = \mathcal{E}_{\boldsymbol{\varphi}}[|\psi_0\rangle\langle\psi_0|]$. This implicitly assumes that state preparation is significantly faster than the parameter encoding. We will later look to remove this assumption and include the parameter encoding simultaneously with state preparation. Separating the dependence
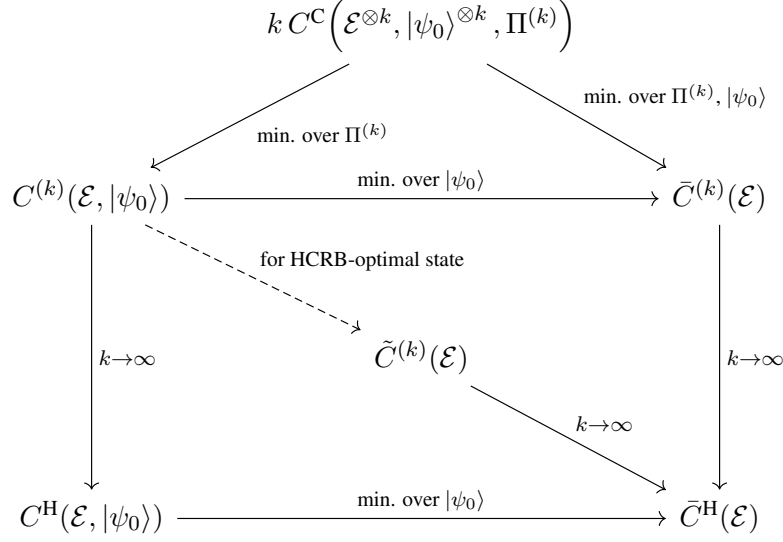
Figure 5.2: Graphical representation of the relationships that exist between the attainable scalar bound for multiparameter estimation. These relationships are defined over k identical copies of the initial system. Solid arrows point towards the object that is less than or equal to the origin of the arrow. The inequality $\tilde{C}^{(k)}(\mathcal{E}) \geq \bar{C}^{(k)}(\mathcal{E})$ is not represented in the figure. If a quantity is the result of the minimisation over the set of POVMs, then there also exists the sub-case where the measurement in questions is projective. This is denoted with a $*$ in the subscript.

on the encoding and the initial state in the various CRBs, e.g., $C^{\mathrm{C}}(\mathcal{E}, |\psi_0\rangle, \Pi)$ and $C^{(k)}(\mathcal{E}, |\psi_0\rangle)$, allows for a clean analysis of the various channel bounds in a consistent manor.

Having a scalar figure of merit allows for not only quantification of estimation error but also direct comparison of two values. It is now natural to define *channel bounds* by minimizing over the initial state. Single parameter estimation general results are well known [68, 170, 69, 90, 55, 106], however the multiparameter case is still largely unexplored. With this in mind, we define the optimised HCRB

$$\bar{C}^{\mathrm{H}}(\mathcal{E}) = \min_{|\psi_0\rangle} C^{\mathrm{H}}(\mathcal{E}, |\psi_0\rangle), \tag{5.6}$$

for which the optimal state is denoted as $|\tilde{\psi}_0\rangle = \arg\min_{|\psi_0\rangle} C^{\mathrm{H}}(\mathcal{E}, |\psi_0\rangle)$. To study how this asymptotic quantity is approached, we introduce both the fully optimised

k-copy channel bound

$$\bar{C}^{(k)}(\mathcal{E}) = \min_{|\psi_0\rangle, \Pi^{(k)}} k\, C^{\mathrm{C}}\Big(\mathcal{E}^{\otimes k}, |\psi_0\rangle^{\otimes k}, \Pi^{(k)}\Big), \qquad (5.7)$$

and the k-copy bound of the HCRB-optimal initial state

$$\tilde{C}^{(k)}(\mathcal{E}) = C^{(k)}\Big(\mathcal{E}, |\tilde{\psi}_0\rangle\Big), \qquad (5.8)$$

for which in general $\tilde{C}^{(k)}(\mathcal{E}) \geq \bar{C}^{(k)}(\mathcal{E})$, even though they both tend to $\bar{C}^{\mathrm{H}}(\mathcal{E})$ as $k \to \infty$. The relationships between the various bound considered in this work is schematically summarised in Fig. 5.2.

5.2 Numerical techniques

Before the discussions of new results we describe the details involved in the numerical optimisations. There are two main numerical optimisation techniques that were used for the results of this chapter, the first being a swarm based technique for unitary optimisation and a newly developed genetic inspired method for circuit optimisation. Particle swarm, we use to optimise the space of measurements and/or input states for 3D magnetometry. We use a swarm inspired optimisation because it covers large areas of the search space and is highly paralellisable. This is the best case scenario when faced with an optimisation problem that does not present itself with any analytic or geometric simplifications. One of the difficulties when it comes to circuit optimisation is the mixed geometry. That is, the circuit's gates have some binary encoding, being on or off where as the parameters of a given gate are continuous. This split in geometries motivates us to split the optimisation in a similar vein. We utilise a genetic inspired optimiser for the discrete part of the circuit and then optimise the continuous parameters given the proposed gate structure.

5.2.1 Unitary optimisation

Parameterisation and permutational invariance

We utilise a Pauli Bloch-vector parameterisation of a Hamiltonian, the exponential of which gives rise to a unitary operator. That is, the exponential of the linear combination of $SU(n)$ generators. This set of generators, $\{\mathbb{1}, \sigma_x, \sigma_y, \sigma_z\}^{\otimes n}$, along with a set of coefficients $\hat{\alpha} = \{\alpha_{i,...,k}\}, i,...,k = 1,...4, \alpha_{1,...,1} = 0$ form our Hamiltonian. This

gives rise to our unitary operator,

$$U(n, \hat{\alpha}) = \exp\left(\sum_{i,...,k=1}^{4} \alpha_{i,...,k} \sigma_i \otimes ... \otimes \sigma_k \right). \tag{5.9}$$

For state optimisation the initial state is given by $U(n, \hat{\alpha}) |0\rangle$ and the set of projective measurements $\Pi = \{U(n, \hat{\alpha}) |i\rangle\}_{i=1,...,2^n}$.

Here we note that over multiple copies our global state is permutationally invariant over the c-copy tensor structure. Explicitly, the input state is c-copies of itself, this implies that we have permutational invariance over the structure of these states, swapping any pair will have no impact on our optimisation. We use this same structure in our POVM structure, whilst still allowing for entanglement over the global state. We use this fact when optimisating the measurements to reduce the number of parameters needed. For example on the two-copy level Hamiltonian parameterisation we have that,

$$\alpha_{i,j,k,l} = \alpha_{k,l,i,j}. \tag{5.10}$$

This invariance does not hold on the $i - j$ level as we do not require the single copy states to be permutationally invariant (although for this problem we do find the permutational-invariant space to containt the optimal states). In this way we restrict our POVMs to also being permutationally invariant, which allows us to work with fewer parameters to optimise.

The number of parameters is the character of $SU(2^{n*c})/SU(2^n)^{\otimes c}$. The dimension of this Hilbert space for q-qubits and c-copies is given by,

$$\dim \mathcal{H}(q, c) = \frac{1}{(4^q - 1)!} \Pi_{i=1}^{4^q-1}(c + i). \tag{5.11}$$

Which goes from exponential in q and c to a polynomial of order $4^q - 1$ in c. Precisely, this invariance on the Hamiltonian generator is given by,

$$\alpha_{i,j,k,l} \sigma_i \otimes \sigma_j \otimes \sigma_k \otimes \sigma_l = \alpha_{k,l,i,j} \sigma_k \otimes \sigma_l \otimes \sigma_i \otimes \sigma_j \tag{5.12}$$

Particle Swarm

particle swarm optimisation (PSO) is a meta-heuristic global optimiser which takes multiple particles (points in the input space) and moves them through the search space given a local and global current best known answer [109]. We imbue each particle

with not just a position but a velocity too. Over each iteration a particle's position is updated by a velocity which is weighted between the local and global currently known best solution. PSO is intended to mimic the collective behavior of animals such as schooling fish or ants, where the animals are free to move along their own path but within the confines of some collective behavior.

The PSO algorithm is a bio-inspired algorithm. The orignal authors took inspiration from collective behavior of swarming animals, ants searching for food, flocks of birds, school of fish [109]. In their words, "an individual can profit from the experience of all other members", that is to say that sharing the knowledge of many memebers of a group and moving collectively with the best current solution ensures the ant finds the food and we can optimise our functions.

Let $x_i \in \mathbb{R}^m$ be the ith particle's position, with velocity $v_i \in \mathbb{R}^m$. We also need to track to current best known position y_i for the ith particle along with $\tilde{y}$, the global best known position. We also have three meta-parameters ω, c_1, c_2, which are the inertia factor, local solution bias and global solution bias respectively. Each position x_i is updated in the following way,

$$x_i(t+1) = x_i(t) + v_i(t+1), \tag{5.13}$$

$$v_i(t+1) = \omega * v_i(t) + c_1[y_i(t) - x_i(t)] + c_2[\tilde{y}(t) - x_i(t)], \tag{5.14}$$

and the optimal solutions are updated if needs be. This procedure is repeated until a termination condition is met. In this case, if optimising the measurement for CFI then that would be the HCRB. But if a minimum is not known the termination condition will be a number of iterations or wall time. This is a natural issue with non-gradient based approaches where termination lacks a clear criterion. However, for this case the gradient is well defined so we are at least able to numerically check the gradients of the final solution are small. There are many more possibilities that can be added to the update step, including some random perturbations to increase the exploration of the search space.

Genetic-Gradient Piecewise Optimisation of a Quantum Circuit

Here we will examine the variational quantum circuit (VQC) parameterisation. The fundamental idea of this set-up is to break down the circuit optimisation problem into a discrete part and a continuous part. The choice of having gates "on" or "off" constitutes the discrete part and the single qubit rotations, the continuous part. We

can see an example of a 2-qubit VQC in figure 5.3. The key idea is to parameterise the gates of some arbitrary quantum circuit. In this setting we have a piecewise discrete-continuous optimisation process. Each single qubit gate has three continuous parameters to be optimised, given by,

$$R_{i,j} = \exp(-i(\alpha_{i,j,x}\sigma_x + \alpha_{i,j,y}\sigma_y + \alpha_{i,j,z}\sigma_z)). \tag{5.15}$$

The discrete component is parameterised by two bit strings, one representing the single-qubit gates and the other the two-qubit gates. If the bit string is 1, the gate is "on" and 0 is "off" conversely. While it is true that strictly there is no need to have the single qubit gates have on-off states too, as we could set all coefficients to 1 and get the same effect we choose to leave that option in. This is because if we want this to become the blueprint for some experiment then we want to leave in the possibility of minimising the total number of gates. It also lessens the numerical burden.

The circuit is parameterised by a layer of single-qubit gates then a layer of CNOT gates. Within each layer of CNOT gates the control qubit is fixed and we apply a CNOT to each other possible target qubit. Then after the next layer of single-qubit gates we move the control qubit down by one. This gives us $n(n+1)$ single-qubit gates and $n(n-1)$ two-qubit gates. We call this collection of gates a gadget and also allow for gadgets to be concatenated.
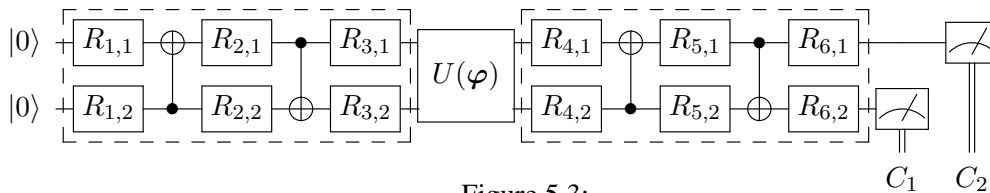
Figure 5.3:
General 2-qubit circuit for estimation of multi-dimensional field.

The flowchart for the algorithm used can be seen in Figure 5.4. It follows a typical genetic algorithm with genetic elitism, except the evaluation of the cost function involves the optimisation of the continuous single-qubit gate parameters. This can, of course be done with any continuous optimisation technique, in this work we have found a simple gradient descent to perform well. As there are typically a small number of parameters (when compared to the PSO case above), gradient descent is capable of performing well. For example, if the circuits that are being optimisation are deeper then returning to a PSO would perform better.

5.3 Asymptotic classicality in 3D magnetometry

Here, we highlight the necessity of using the HCRB for the analysis of 3D magnetometry using M qubits in the presence of dephasing noise. The parameters to be estimated $\boldsymbol{\varphi} = (\varphi_1, \varphi_2, \varphi_3)$ appear via the single-qubit Hamiltonian $H^{(j)}(\boldsymbol{\varphi})$ outlined in Sec. 2.

We use as probe states the family of 3D-GHZ states

$$|\psi_M^{\text{3D-GHZ}}\rangle = \frac{1}{\mathcal{N}} \sum_{k=1}^{3} |\phi_k^+\rangle^{\otimes M} + |\phi_k^-\rangle^{\otimes M}, \tag{5.16}$$

which was shown to present Heisenberg scaling in the noiseless case [19]. The states, $|\psi_k^\pm\rangle$ are the eigenvectors corresponding to the ± 1 eigenvalues of the kth Pauli matrix and $\mathcal{N}$ is the normalisation. The final state is given by, $\rho_{\boldsymbol{\varphi}} = \mathcal{E}_\gamma^{\otimes M}[U_{\boldsymbol{\varphi}}|\psi_M^{\text{3D-GHZ}}\rangle\langle\psi_M^{\text{3D-GHZ}}|U_{\boldsymbol{\varphi}}^\dagger]$, choosing equal parameter values $\varphi_i = 1$. This is the family of states for which we compute the relevant bounds.

The results in Fig. 5.5 demonstrate a non-trivial relationship between the three key values, HCRB, SLD-CRB and incompatibility for 3D magnetometry over a range of dephasing strengths.

The Frobenius norm $\|D_{\boldsymbol{\varphi}}\|_{\text{F}}^2 = \sum_{ij} |(D_{\boldsymbol{\varphi}})_{ij}|^2$ is the scalar metric we use to capture the violation of the weak commutativity condition.

Panel (a) shows that the relative difference $1 - C^{\text{S}}/C^{\text{H}}$ is monotonically decreasing for 2 and 3 qubits, while it has a non-monotonic behaviour for 5 or more qubits. Panel (b) shows that this behaviour is not always reflected at the level of incompatibility; this is remarkably different from the simple monotonic relationship found for 2-parameter pure state models [130]. Furthermore, whilst the matrices $D_{\boldsymbol{\theta}}$ have a comparable magnitude for different number of qubits, the relative differences do not, e.g., being around 0.2% for 5 qubits and around 30% for 2-qubits.

A single qubit will always give rise to a singular statistical model when estimating all components of $\boldsymbol{\varphi}$ [19]. We therefore look to $M = 2$ as the smallest qubit number. In Fig. (5.5) we see that around $\gamma = 0$ for 2-qubits there that there is a considerable relative difference of around 30%. Recalling that in the previous chapter 4, we demonstrated that this bound is in fact attainable with a single projective measurement, the simplest possible case of attainability.

From this example we see that the pair of matrices J^{S} and $D_{\boldsymbol{\theta}}$ are not sufficient for a complete description of a given state's performance for multi-parameter estimation from a practical view point. The size of a state's incompatibility does not yield

any information on its performance when compared to the ultimate attainability. Further, there is no guarantee that for a state with non-zero incompatibility there is any advantage to using additional copies of said state to improve its sensing performance.

5.4 Attainability of 3D-magnetometry in the presence of dephasing noise

Following on from our examinations of asymptotic classicality into how it is not a useful metric when assessing the attainability of a model we go into more detail into the attainability of 3D-magnetometry. In this section we are interested in the asymptotic nature of the attainability of the HCRB. In order to explore this feature of the bound we begin by taking the optimal state for the HCRB and optimise the CFI for many copies.

The known results on the attainability of mixed-state estimation are summarised in [8], most of these results are built around classic models that we are not able to take advantage of. We utilise numerical optimisation for the main results and make some analytic conjectures from these results.

In the real world, quantum-limited 3D magnetometry will be noisy, making an initially pure probe mixed. Attaining the HCRB for mixed states is intimately tied to collective POVMs across multiple copies of the states [53]. Furthermore, the optimal asymptotic collective measurement identified by the theory of quantum local asymptotic normality is not projective [53]. This implies the need for noiseless ancillas which is theoretically typical [56, 100, 174, 217, 197, 171, 83] but practically impossible.

5.4.1 The effects of multiple copies

In the absence of any feasible analytic techniques for evaluating the HCRB for 3D magnetometry in the presence of dephasing noise, we look to numerical techniques for insights. We consider multiple fixed values of noise (γ) between 0 and 0.9 in jumps of 0.1. We stick to 1, 2 and 3 copies of the input state and $\varphi = (0, 0, 0)$. Our explorations begin by computing the bounds $\bar{C}^{\mathrm{H}}\big(\mathcal{E}_{\varphi,\gamma}^{\otimes 2}\big)$ and $\tilde{C}_{*}^{(k)}\big(\mathcal{E}_{\varphi,\gamma}^{\otimes 2}\big)$, (see figure 5.2). In words, we begin by finding the optimal state with respect to the HCRB for each value of noise. Then for each HCRB optimal state at a given γ value we optimise the CFI over projective measurements for k-copies.

We begin by parameterising the set of projective measurements or initial state for the optimisation. Since we work with a multi-qubit system, we utilise a Bloch-vector parameterisation of a Hamiltonian. That is, the Hamiltonian is formed from a linear combination of $\mathrm{SU}(4k)$ generators obtained by taking the tensor produce of $2k$ $\mathrm{SU}(2)$ generators. In particular, $\lambda(k) = \{\mathbb{1}, \sigma_x, \sigma_y, \sigma_z\}^{\otimes 2k} \setminus \mathbb{1}^{\otimes 2k}$. This gives rise to a unitary matrix of form,

$$U(k, \tilde{\boldsymbol{\alpha}}) = \exp\left(\mathrm{i} \sum_{i=1}^{16^k-1} \tilde{\alpha}_i \lambda(k)_i \right). \tag{5.17}$$

An initial single-copy pure state is then given by $U(1, \tilde{\boldsymbol{\alpha}}_\psi)\,|0\rangle$, starting from a zero two-qubit state $|0\rangle \in \mathbb{C}^4$. We then optimise over the coefficients $\tilde{\boldsymbol{\alpha}}_\psi$ to find the optimal state $|\tilde{\psi}_0\rangle$. This is the only state we seek to optimise here. A k-copy projective measurement is then parameterised by $\Pi = \{U(k, \tilde{\boldsymbol{\alpha}})|i\rangle\langle i|U(k, \tilde{\boldsymbol{\alpha}})^\dagger\}_{i=1,\dots,4^k}$, with canonical basis states in the computational basis $\{|i\rangle\}$ of $\mathbb{C}^{4k}$. In the same way as previously mentioned for the input state we optimise the coefficients $\tilde{\boldsymbol{\alpha}}$. To recall, quantity $\bar{C}^{\mathrm{H}}\big(\mathcal{E}_{\boldsymbol{\varphi},\gamma}^{\otimes 2}\big)$ which depends on $|\tilde{\psi}_0\rangle$ is found by minimizing $C^{\mathrm{H}}\big(\mathcal{E}_{\boldsymbol{\varphi},\gamma}^{\otimes 2}, U(1, \tilde{\boldsymbol{\alpha}}_\psi)\,|0\rangle\big)$. The state $|\tilde{\psi}_0\rangle$ is then used to find the optimal k-copy projective measurement by minimizing $k\,C^{\mathrm{C}}\Big(\mathcal{E}_{\boldsymbol{\varphi},\gamma}^{\otimes 2k}, |\tilde{\psi}_0\rangle^{\otimes k}, \{U(k, \tilde{\boldsymbol{\alpha}})|i\rangle\langle i|U(k, \tilde{\boldsymbol{\alpha}})^\dagger\}\Big)$ as the objective function. This leads to $\tilde{C}^{(k)}\big(\mathcal{E}_{\boldsymbol{\varphi},\gamma}^{\otimes 2}\big)$. The detail of this optimisation process are in section 5.2.

The results from the numerical optimisation (the dashed 'quantum-classical' line will be examined later) are shown as the solid lines in Fig. 5.6. The red, blue and light green solid lines show the quantity $\tilde{C}_*^{(k)}\big(\mathcal{E}_{\boldsymbol{\varphi},\gamma}^{\otimes 2}\big)$ for $k = 1, 2, 3$ respectively. The channel HCRB $\bar{C}^{\mathrm{H}}\big(\mathcal{E}_{\boldsymbol{\varphi},\gamma}^{\otimes 2}\big)$, is compared against these results, shown by the green line. In the low-noise regime, we see that there is almost no advantage coming from the addition of a second and third copy of the input state. On the other hand, at the high-noise end of the scale adding a second copy of the state effectively attains the HCRB, with a third copy offering no additional advantage. The intermediate value ranges show a distinct advantage being offered with each additional copy of the input state. These three distinct cases of low, medium and high noise fit in with the single parameter case and appears to be one of the intuitions that carries over.
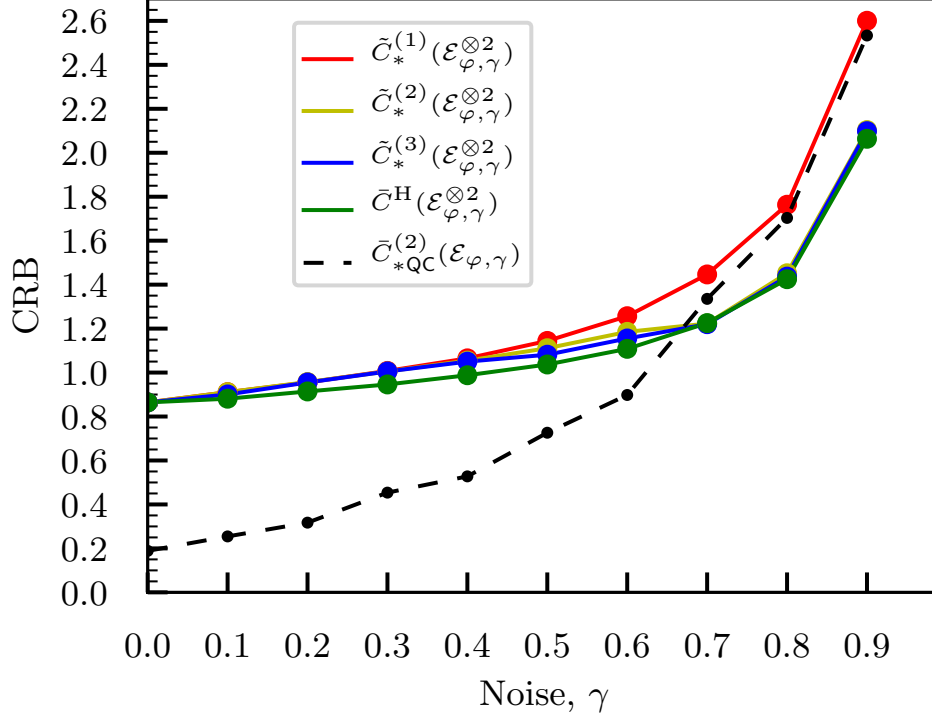
Figure 5.6: The solid lines represent the the CQ strategy portion of this analysis (left diagram in Fig. 5.1 for $k = 2$), and the dashed lines, the QC strategy. The solid green line, the channel HCRB $\bar{C}^{\mathrm{H}}\big(\mathcal{E}_{\varphi,\gamma}^{\otimes 2}\big)$ is the optimised initial state over noise. With the red, yellow and blue lines representing the k-copy projective bounds $\tilde{C}_*^{(k)}\big(\mathcal{E}_{\varphi,\gamma}^{\otimes 2}\big)$. Where projective measurements are optimised for the initial state from the corresponding channel HCRB for that value of γ. See Fig. 5.2). The dashed line CRB channel bound defintion from figure 5.2 is given by, $\bar{C}_{*\mathrm{QC}}^{(2)}(\mathcal{E}_{\varphi,\gamma})$. We note the dashed line approaching the solid line. This occurs because as entanglement at the state preparation stage becomes too strong the optimal state approaches that of $\tilde{C}_*^{(1)}\big(\mathcal{E}_{\varphi,\gamma}^{\otimes 2}\big)$. This happens due to the lack of entanglement over the copies on the measurement stage.

Low and high noise analytic conjecture

Low noise regime- Following the numerical results, we conjure that in the low noise-regime where $\gamma \approx 0$,

$$\tilde{C}_*^{(1)}\big(\mathcal{E}_{\varphi,\gamma}^{\otimes 2}\big) \approx \tilde{C}_*^{(2)}\big(\mathcal{E}_{\varphi,\gamma}^{\otimes 2}\big). \tag{5.18}$$

That is to say, for low-noise there is no advantage to adding a second copy of the input state. Based on our numerical observations, we further conjecture that

$$\tilde{C}_*^{(2)}\big(\mathcal{E}_{\boldsymbol{\varphi},\gamma}^{\otimes 2}\big) > \bar{C}^{\mathrm{H}}(\mathcal{E}_{\boldsymbol{\varphi},\gamma}^{\otimes 2}). \tag{5.19}$$

That is, a gap remains between $\tilde{C}_*^{(2)}$ and $\bar{C}^{\mathrm{H}}$. This is distinct from the high-noise case that we will discuss shortly. Some intuition may be obtained by noting that for $\gamma \approx 0$, the two-copy state $\rho_{\boldsymbol{\varphi},\gamma}^{\otimes 2}$ is approximately close to being pure for which the HCRB is attainable with a projective measurement as found in chapter 4. From this, the intuition follows that one additional copy provides little benefit. However, as the number of copies k is increased, the mixedness of $\rho_{\boldsymbol{\varphi},\gamma}^{\otimes k}$ also monotonically increases. As a rough mathematical outline, we would like to show, letting $\delta > 0$ be given,

$$F_{i,j}(\rho_{\lambda,\gamma},\Pi) \approx F_{i,j}(|\psi\rangle\langle\psi|^{\otimes 2},\Pi) + \gamma F_{i,j}'(\rho_{\lambda,\gamma},\Pi)|_{\gamma=0} \tag{5.20}$$

$$= (1+\delta)F_{i,j}(|\psi\rangle\langle\psi|^{\otimes 2},\Pi). \tag{5.21}$$

In words, that is to say if we were to Taylor expand the CFI around $\gamma = 0$ then we would find the derivative of the CFI with respect to γ was small and the CFI could be approximated as some perturbation of the initial pure state.

High Noise regime We conjecture that for $\gamma \approx 1$,

$$\tilde{C}_*^{(2)}\big(\mathcal{E}_{\boldsymbol{\varphi},\gamma}^{\otimes 2}\big) \approx \bar{C}^{\mathrm{H}}(\mathcal{E}_{\boldsymbol{\varphi},\gamma}^{\otimes 2}). \tag{5.22}$$

That is, only 2-copies are required in order to attain the HCRB with a projective measurement. An additional implication of this conjecture would be, $\tilde{C}_*^{(2)}(\mathcal{E}_{\boldsymbol{\varphi},\gamma}^{\otimes 2}) \approx \bar{C}_*^{(2)}(\mathcal{E}_{\boldsymbol{\varphi},\gamma}^{\otimes 2}) \approx \bar{C}^{(2)}(\mathcal{E}_{\boldsymbol{\varphi},\gamma}^{\otimes 2})$. In words, we also conjecture that non-projective measurements for $k \geq 2$ would not be required in order to attain the channel bound $\bar{C}^{(k)}$.

5.4.2 Quantum vs classical

In order to answer questions on the asymptotic attainability of 2-qubit 3D magnetometry we looked at adding multiple independent copies of the input state and performing collective measurements. In order to implement a collective measurement over a $2k$ qubit system we would have to implement one large entangling unitary operation. This case is the classical-quantum case (left hand side of figure 5.1), because the input is classical on the copies level. We now turn out attention to the quantum-classical case

(the right hand side of figure 5.1), that is when the input state is found by optimising some global entangling unitary and the measurement at the end is performed over some classically separable space. In particular we choose to explore a 4 qubit input with measurements over 2 copies of 2-qubits a piece. Looking into where entanglement offers most advantage can be motivated in two ways. Firstly, in practice it is often the case than an experimentalist is only capable of performing one large entangling operation before the dephasing and noise interactions cause too much harm to the experiment. It would be of great interest to such experimentalists where best to put their entangling resources. Secondly, the question of where a quantum advantage comes from in metrology is one of the perennial questions of quantum enhanced metrology.

The QC bound,

$$\bar{C}^{(2)}_{\mathsf{QC}}(\mathcal{E}_{\varphi,\gamma}) = \min_{|\psi_0\rangle,\Pi} 2\, C\big(\mathcal{E}^{\otimes 4}_{\varphi,\gamma}, |\psi_0\rangle, \Pi^{\otimes 2}\big), \qquad (5.23)$$

is not explicitly presented in Fig. 5.2. The initial state $|\psi_0\rangle$ is over 8 qubits ($\mathbb{C}^8$) and the measurement is 2 copies of a 2-qubit measurement ($\mathbb{C}^4$). This is directly compared against $\tilde{C}^{(2)}$. This direct comparison is made as $\tilde{C}^{(2)}$ corresponds to the unitary encoding over 4 qubits. It is important to note that an ideal comparison for $\bar{C}^{(2)}_{\mathsf{QC}}(\mathcal{E}_{\varphi,\gamma})$ would be done against $\bar{C}^{(2)}$. Preliminary numerical checks found no effective difference between $\bar{C}^{(2)}$ and $\tilde{C}^{(2)}$, as is to be expected. As such, we use $\bar{C}^{(2)}$ as our comparison point, lessening the computational demand.

The quantity (5.23) is plotted in Fig. 5.6, represented by the black dashed line. In both the low and medium noise regimes, the QC strategy outperforms a CQ strategy. In the low noise regime at least this was exactly what we would expect. Recalling the assumption that the state is approximately a pure state with some small perturbation, then we are able to lean on the purely unitary case [19] for some intuition. This is not the case as γ reaches 1. The impact of the noise brings the bound almost to the level of the single copy bound. There is almost zero advantage in this regime from entanglement at the input state level, however it can be strongly felt at the measurement stage. Demonstrating this advantage coming from a collective measurement reveals a new unique aspect to quantum multiparameter estimation.

5.5 Attaining Cramér-Rao bounds with shallow circuits.

In order to take the results presented in this chapter and bring them to experimentalists we must give some recipe on how these bounds could be generated in some experimental setting. In particular we look to target noisy intermediate-scale quantum devices (NISQ) [138], the current state of the art. The key feature of NISQ devices is their suseptability to noise, as such the number of operations (especially 2-qubit and beyond) must be minimised. With this in mind, we use programable quantum circuits as a representation of a general unitary operation. The study of parameterised quantum circuits have already found success in single parameter quantum metrology and quantum machine learning, using various different parameterisations [143, 206, 182, 133]. Incorporating the ideas from [143] of using a genetic algorithm for experiment design in the photonic setting and fixed structure circuits for optimising a set of continuous parameters we minimise both the total number of gates and the CRB within the cost function. We base our circuits on the programmable universal quantum circuit proposed by Sousa and Ramos [179].

We begin by splitting the circuit into a discrete and continuous representation. The discrete part is further split into two bit strings. One bit string represents the on/off state of single qubit gates and the second bit string represents the on/off state of the CNOT gates. The continuous part is a vector of floating point values (3 per gate in the "on" state) which represent some single qubit Pauli rotation. The numerical optimisation is performed by combining a genetic-inspired algorithm and a gradient-descent algorithm. Originally design for discrete optimisation [203], a genetic-inspired algorithm makes an excellent optimiser over bit strings. We then perform a local search over the continuous space using a gradient descent algorithm. Details on the numerical methods used to be found in Sec. 5.2. The key additional feature is to incorporate the number of gates into the CFI cost function. As with all heuristic optimisation algorithms, cost function design is subtle and contributes heavily to the performance of the optimiser. We found through initial experimentation that,

$$\left(\left(\sum_i SQ_i \right) + 2 * \left(\sum TQ_i \right) + 1 \right) * CFI, \qquad (5.24)$$

gave the best results qualitatively. Where SQ and TQ represent the single and two qubit bit string respectively.

The results from this process are presented in Fig. 5.7. They show that with one,

two and three copies of the input state, the final circuits remain relatively shallow in depth. With a modified cost function it is important to make explicit that the CFI of these circuits came within 10^{-4} relative difference with the results obtained in Fig. 5.6. These results are promising for an experimentalist with a NISQ device wishing to perform optimal 3D magnetometry experiments, for example, only a single two qubit gate is required for the generation of the input states. We can gain some intuition into this result by recalling the results presented in figure 3.3. Given the one to one relationship between the amount of entanglement and QCRB, this implies that simple circuits could be employed for state generation, as we can easily tune the amount of entanglement with one qubit rotations followed by a CNOT gate.
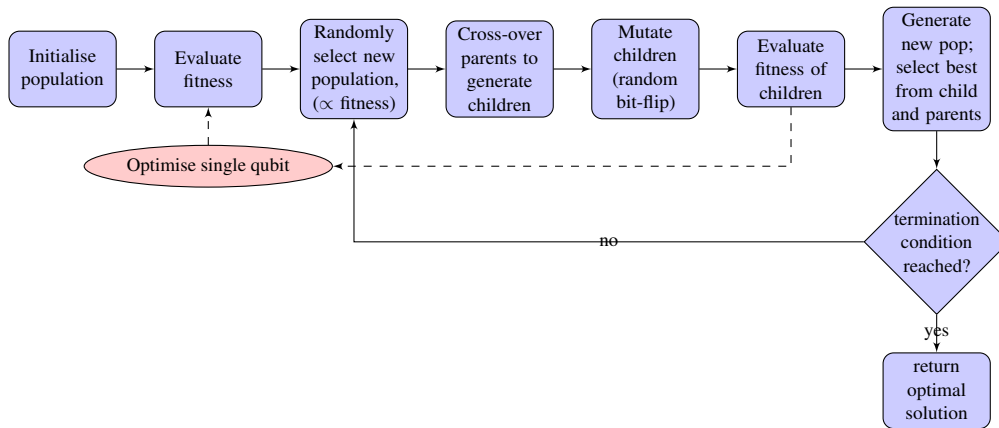
Figure 5.4: Flowchart for the genetic algorithm utilised in this chapter. An initial population is first generated, this consists of generating a set of random vectors required to construct the gadgets described in figure 5.3. Following this, the fitness is computed. In order to compute the fitness we construct the quantum circuit from figure 5.3 and use a gradient based optimiser to optimise the single qubit rotation angles against the CFI. At this stage, each member of the population each now has an associated fitness, i.e. the CFI of the circuit it generates. The next series of stages generate the population of the next iteration. This begins with randomly selecting two members from the population, these are the 'parents'. The probability that an individual member is selected is proportional to the inverse of of its fitness (as we are trying minimise our cost function). A new potential member of the population is then generated (the 'child'), for each element in the input vector, an element is randomly selected from one of its parents. Following this, the child's vector is mutated, this involves some small probability of randomly manipulating an element of its input vector. Finally in this step, the fitness of the child is computed. The member that is selected to be part of the next iteration population is the member is the best fitness out of the two parents and the child. This process is repeated until the termination condition is met and best member of the population returned. A common termination condition in non-gradient based optimisation is to check how many iterations it has been since the best value has been updated. This is the termination condition we use, no change in best value for 100 iterations.
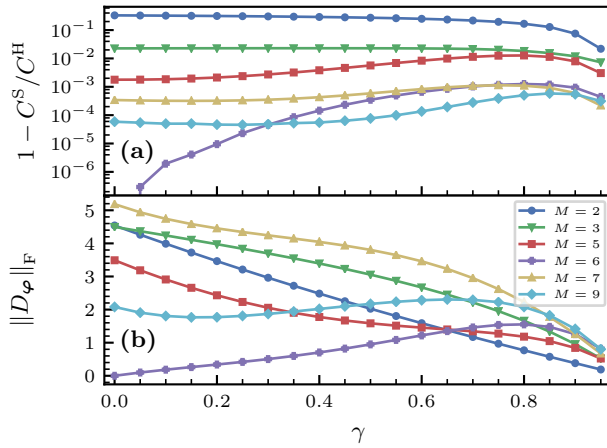
Figure 5.5: Comparison of the SLD-CRB, the HCRB and incompatibility for a M-qubit for 3D magnetometry using the 3D-GHZ state as the initial sate. The magnetic field components all taking the same value, $\varphi_i = 1$. This parameter encoding is then followed by local dephasing of strength γ in the z-direction. **(a)** Relative difference $1 - C^S/C^H$ between the SLD-CRB and HCRB. **(b)** The Frobenius norm of the matrix $(D_{\boldsymbol{\varphi}})_{ij} = \mathrm{Im}(\mathrm{Tr}[L_j L_i \rho_{\boldsymbol{\varphi}}])$, which defines the incompatibility of the model. The values for $M = 6$ and $\gamma = 0$) are omitted along with $M = 4, 8$, since such models are asymptotically classical.
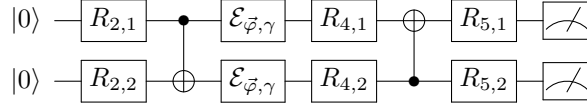
(a) One copy circuits
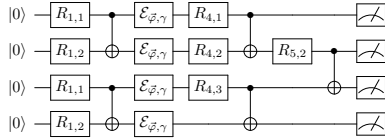
(b) Two copy circuits for medium noise
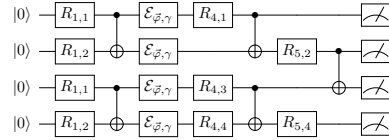
(c) Two copy circuits for high noise
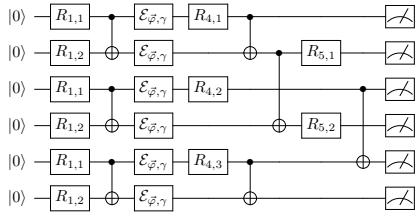
(d) Three copy circuits for medium noise
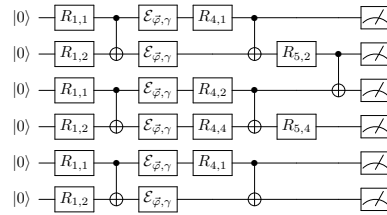
(e) Three copy circuits for high noise

Figure 5.7: Optimal quantum circuits for 3D magnetometry across noise strengths and number of copies. We first note that the state creation circuits are much simpler than the measurement circuits as every two qubits marks an input state that is repeated 1, 2 and 3 times. The measurement circuits span this global state. The meter boxes at the end of each circuit represent standard projection onto the σ_z eigenstates measurement. The values for γ chosen are 0.1, 0.5 and 0.8 for low, medium and high noise respectively. The general structure on a single copy does not deviate from (a) over any noise value. Beyond the relatively shallow depth of these circuits, we note that for both (b),(c) and (d) we have entangling CNOTs between the two the copies. Further, in (e), the lack of a CNOT to the third copy demonstrates the lack of benefit from collective measurement in adding an addition copy. The above serves as an independent reinforcement of another conclusion of Fig. 5.6.

Chapter 6

Magnetic field estimation on a spin chain

> Don't for heaven's sake, be afraid of talking nonsense! But you must pay attention to your nonsense.
>
> ———————————————
> Ludwig Wittgenstein

6.1 Introduction

In this chapter we present preliminary investigations into beating the classical sensing limit with estimation of a 1D magnetic field on a spin chain. Hitherto we have considered the case in which state preparation and measurement are completely decoupled from the encoding Hamiltonian. Whilst this is a very useful assumption to make in order to find tight analytic results it is not necessarily always justified. In this chapter we will explore the scenario where we are unable to freely decouple our probe state from an external magnetic field that we wish to measure. With this motivation we will use controls for state preparation and measurement that are more feasible with particular experimental set-ups.

There are parallels between the approach we take in this chapter and the early days of CCD cameras. In the early days of CCD camera technology, we did not have the ability to individually address a pixel. Only the edges could be accurately detected. As such, when a photon hit somewhere in the middle of the CCD detection and generated a signal, it is the timing information to the edge that gave us positional information.

Camera technology is now sufficiently advanced that such techniques are no longer required. Similarly, quantum technologies are not at the point where we have perfect single qubit addressing or arbitrary two qubit gate operations. As such, restricting the number of these operations required and only applying them to an easily accessible edge node could prove to be greatly advantageous.

The experimental work of Cappellaro and coworkers is of particular inspiration [35, 107, 163] who has repeatedly demonstrated experimental viability of long spin-chains for their use in quantum information processing. A further promising experimental design could center around the NV^- in diamond [57]. Demonstrations of practical NV^- spin chains have been made [117, 151] as well as the development of some theoretical models under noisy conditions [208].

This work builds on the previous work [110] where a ZZ Hamiltonian was studied. Only the first site could be controlled or measured whilst the final site was coupled to an external magnetic field. In that work they were interested in the case of remote estimation, when only the final site on a spin-chain is coupled to some magnetic field. They demonstrated the problem's equivalence to state transfer and were able to demonstrate quadratic scaling of sensitivity in time as well as stable control over large spin chains. For an intuitive picture, prepare a $|+\rangle$ state on the first site, transfer it to the end of the chain, hold it there to collect phase of the external magnetic field and finally transfer it back for measurement. This work has since been further developed [134, 135], where they allow local control on each site and a period boundary conditioned chain. These works demonstrated the importance of the driving force of controls in many body systems, bringing together ideas of driven enhanced estimation [119] and more general many-body control theory [34, 33].

Beyond the specific scope of quantum control theory the interaction of many-body physics and magnetic field estimation has been a fruitful area of research. Heisenberg scaling was shown possible with an Ising spin chain by utilising the GHZ state [178], given the interaction strength is known. Magnetic field gradient estimation along a spin-chain [12, 140] as well as the study of particular spin-chain properties such as anisotropy [129] have also been active areas of interest.

Here we attempt to bring together previous ideas of many-body control and estimation on a spin chain by proposing a simplified model which is experimentally feasible and demonstrates an advantage in magnetic field estimation.

6.2 Mathematical setup

We consider the Hamiltonian given by,

$$\hat{H} = \frac{1}{2} \sum_{n=1}^{N-1} c_n((1+\gamma)XX + (1-\gamma)YY)_{n,n+1} + \lambda \sum_{n=1}^{N} Z_n + f(t)X_1 + g(t)Z_1.$$
(6.1)

This describes a spin chain of next-nearest neighbour interacting electrons. The $\lambda \sum_{n=1}^{N} Z_n$ term describes an external magnetic field with strength λ and $\gamma \in [-1,1]$. We aim to estimate λ with control and measurement on the first site in the chain, only. The initial state is given by $|\underline{0}\rangle = |0\rangle^{\otimes N}$. The controls given by $\{f(t)X_1, g(t)Z_1\}$ are local operations on the first site, the unknown functions $f(t)$ and $g(t)$ are the pulse sequences we will be optimising in order to optimise the estimation of λ. The generation of a GHZ state is known to be optimal for estimation of a single direction magnetic field [191], it is known to give the quantum speed up with respect to the classical estimation. Further, the GHZ state is an eigenstate of the drift Hamiltonian can be stabilized without control [153].

The first step is to simplify the control design by making the Jordan-Wigner (JW) transformation [142, 45]. The JW transformation is defined by a_n and a_n^+, the annihilation and creation operators of fermionic modes, i.e., spin. The anit-commuator is defined as $\{A, B\} = AB + BA$. These operators satisfy the fermion anti-commutator relations given by [142],

$$\{a_n, a_m^+\} = \delta_{n,m}\mathbb{1},$$
(6.2)

$$\{a_n, a_m\} = 0.$$
(6.3)

The JW transformation is given by,

$$a_n = \bigotimes_{m<n} Z_m \otimes \sigma_n^-,$$
(6.4)

$$a_n^+ = \bigotimes_{m<n} Z_m \otimes \sigma_n^+.$$
(6.5)

Where $\sigma_n^{+/-}$ are defined as,

$$\sigma_n^+ := \frac{X + iY}{2}, \tag{6.6}$$

$$\left(\sigma_n^+\right)^\dagger = \sigma_n^- := \frac{X - iY}{2}. \tag{6.7}$$

It is prudent here that we confirm that this transformation satisfies the anti-commutator relations.

$$\{a_n, a_k\} = \{a_n^+, a_k^+\} = 0, \text{ wlog } n > k, \tag{6.8}$$

$$= \{\bigotimes_{m<n} Z_m \otimes \sigma_n^-, \bigotimes_{m<k} Z_m \otimes \sigma_k^-\}, \tag{6.9}$$

$$= \left(\bigotimes_{m<k} Z_m \otimes Z_k \otimes \bigotimes_{k<m<n} Z_m \otimes \sigma_n^-\right)\left(\bigotimes_{m<k} Z_m \otimes \sigma_k^- \otimes \bigotimes_{k<m<n} \mathbb{1}_m \otimes \mathbb{1}_n\right), \tag{6.10}$$

$$+ \left(\bigotimes_{m<k} Z_m \otimes \sigma_k^- \otimes \bigotimes_{k<m<n} \mathbb{1}_m \otimes \mathbb{1}_n\right)\left(\bigotimes_{m<k} Z_m \otimes Z_k \otimes \bigotimes_{k<m<n} Z_m \otimes \sigma_n^-\right), \tag{6.11}$$

$$= \left(Z_k \sigma_n^- \otimes \bigotimes_{k<m<n} Z_m \otimes \sigma_n^-\right) + \left(\sigma_n^- Z_k \otimes \bigotimes_{k<m<n} Z_m \otimes \sigma_n^-\right), \tag{6.12}$$

$$= \left(Z_k \sigma_n^- \otimes \bigotimes_{k<m<n} Z_m \otimes \sigma_n^-\right) - \left(Z_k \sigma_n^- \otimes \bigotimes_{k<m<n} Z_m \otimes \sigma_n^-\right), \tag{6.13}$$

$$= 0. \tag{6.14}$$

The operator is also fermionic for $\{a_n, a_m^+\} = \delta_{n,m}\mathbb{1}$, by similar reasoning. Now we are able to express the Pauli operators in terms of the fermionic operators,

$$X_n = \left(\bigotimes_{m<n} [a_m, a_m^+]\right)(a_n + a_n^+), \tag{6.15}$$

$$Y_n = \left(\bigotimes_{m<n} [a_m, a_m^+]\right)(a_n - a_n^+), \tag{6.16}$$

$$Z_n = \mathbb{1} - 2a_n^+ a_n. \tag{6.17}$$

For simplicity let us consider the case $c_n = 1$ and $\gamma = 0$. Finally, the Hamilto-

nian 6.1 is now transformed into the JW picture.

$$H = \sum_{n=1}^{N-1} \left(a_n^+ a_{n+1} + a_{n+1}^+ a_n \right) + \lambda \sum_{n=1}^{N} \left(1 - 2a_n^+ a_n \right)$$
$$+ f(t)(a_1 + a_1^+) + g(t)(1 - 2a_1^+ a_1).$$

(6.18)

6.2.1 Lie algebra calculation

The natural next step is to compute the Lie algebra of our physical model. We do this in order to confirm our assumption that whilst the setup we have limited ourselves to may not be universal, it has enough complexity to generate good states for magnetic field estimation. With a Lie algebra calculation we are no concerned with coefficients on each term, as highlighted in section 2.5. We therefore, take $\lambda = 1$ for the sake simplifying ou following computation. We compute this Lie algebra in order to demonstrate that this system is non-universal, but does demonstrate 2-body terms and 1-body rotations. This gives us the intuition that the system has enough features for single parameter magnetic field estimation. The Lie algebra of our physical model is defined by, $\mathfrak{L} = \left\langle i\left(a_n^+ a_{n+1} + a_{n+1}^+ a_n\right) + i(1 - 2a_n^+ a_n), i(1 - 2a_1^+ a_1), i(a_1 + a_1^+) \right\rangle = \langle h_1, h_2, h_3 \rangle.$

$$\begin{aligned}
h_4 = [h_1, h_2] &= i^2 \left[a_n^+ a_{n+1} + a_{n+1}^+ a_n, 1 - 2a_1^+ a_1 \right], \\
&= -\left[a_1^+ a_2 + a_2^+ a_1, a_1^+ a_1 \right] + 0 \text{ for } n > 1, \\
&= \underbrace{a_1^+ a_2 a_1^+ a_1}_{0} + a_2^+ a_1 a_1^+ a_1 - \left(a_1^+ a_1 a_1^+ a_2 + \underbrace{a_1^+ a_1 a_2^+ a_1}_{0} \right), \\
&= a_2 a_1^+ + a_2^+ a_1, \\
&= a_2^+ a_1 - a_1^+ a_2.
\end{aligned}$$

Here we must make note of some short-cuts that have been made in this initial calculation. In a Lie algebra, we are permitted to take linear combination of elements, this is what allows us to neglect constants. We have also used $a_n^+ a_n a_n^+ = a_n^+$ and $a_n a_n^+ a_n = a_n$. This can be seen with a simple matrix calculation, however if we allow ourselves to think physically for a moment, then flipping a spin, up, down and then up, will have the same effect as just a single up and visa versa. Finally, we have

$$a_n a_n = a_n^+ a_n^+ = 0.$$

$$h_5 = [h_4, h_2] = i\Big(a_2^+ a_1 a_1^+ a_1 - \cancelto{0}{a_1^+ a_2 a_1^+ a_1} - \big(\cancelto{0}{a_1^+ a_1 a_2^+ a_1} - a_1^+ a_1 a_1^+ a_2 \big)\Big),$$

$$= i\big(a_2^+ a_1 a_1^+ a_1 + a_1^+ a_1 a_1^+ a_2 \big),$$

$$= i\big(a_2^+ a_1 + a_1^+ a_2 \big).$$

These terms correspond to $(XY - YX)_{1,2}$ and $(XX + YY)_{1,2}$ respectively in the Pauli picture.

$$h_6 = [h_4, h_5] = \big[a_2^+ a_1 - a_1^+ a_2, i(a_2^+ a_1 + a_1^+ a_2) \big],$$

$$= i\Big(a_2^+ a_1 a_1^+ a_2 - \cancelto{0}{a_1^+ a_2 a_1^+ a_2} + \cancelto{0}{a_2^+ a_1 a_2^+ a_1} - a_1^+ a_2 a_2^+ a_1 ,$$

$$- \big(a_1^+ a_2 a_2^+ a_1 + \cancelto{0}{a_2^+ a_1 a_2^+ a_1} - \cancelto{0}{a_1^+ a_2 a_1^+ a_2} \big)\Big),$$

$$= 2i\big(a_2^+ a_2 + a_2^+ a_2 a_1^+ a_1 - a_1^+ a_1 - a_2^+ a_2 a_1^+ a_1 \big),$$

$$= 2i\big(a_2^+ a_2 - a_1^+ a_1 \big) \implies i(a_2^+ a_2).$$

Seeing as we already have $a_1^+ a_1$, we are able to take linear combinations to remove it from the h_6 term. This is equivalent to Z_2 in the Pauli picture. So we start over, with Z_2 this time.

$$h_7 = [h_1, h_6] = \big[i\big(a_n^+ a_{n+1} + a_{n+1}^+ a_n \big) + i\big(\mathbb{1} - 2a_n^+ a_n \big), i a_2^+ a_2 \big],$$

$$= \big[a_1^+ a_2 + a_2^+ a_1, a_2^+ a_2 \big] + \big[a_2^+ a_3 + a_3^+ a_2, a_2^+ a_2 \big] + 0 \text{ for } n > 2,$$

$$= a_1^+ a_2 - a_2^+ a_1 + \big[a_2^+ a_3 + a_3^+ a_2, a_2^+ a_2 \big],$$

we already have $a_1^+ a_2 - a_2^+ a_1$ and so it can be removed,

$$= \cancelto{0}{a_2^+ a_3 a_2^+ a_2} + a_3^+ a_2 a_2^+ a_2 - \big(a_2^+ a_2 a_2^+ a_3 + \cancelto{0}{a_2^+ a_2 a_3^+ a_2} \big),$$

$$= a_3^+ a_2 - a_2^+ a_3.$$

$$h_8 = [h_7, h_6] = \big[a_3 a_2^+ - a_2^+ a_3, i a_2^+ a_2 \big],$$

$$= i\Big(a_3^+ a_2 a_2^+ a_2 - \cancelto{0}{a_2^+ a_3 a_2^+ a_3} - \big(\cancelto{0}{a_2^+ a_2 a_3^+ a_2} - a_2^+ a_2 a_2^+ a_3 \big)\Big),$$

$$= i\big(a_3^+ a_2 + a_2^+ a_3 \big)$$

$$h_8 = [h_7, h_8] = \left[a_3 a_2^+ - a_2^+ a_3, i(a_3^+ a_2 + a_2^+ a_3)\right]$$

$$= -i\left(\cancelto{0}{a_3^+ a_2 a_3 a_3^+} - a_3^+ a_2 a_3^+ a_3 + a_2^+ a_3 a_4^+ a_2 - \cancelto{0}{a_2^+ a_3 a_2 a_3}\right)$$

$$= -i\left(a_2 a_2^+ a_3^+ a_3 - a_2^+ a_2 a_3 a_3^+\right)$$

$$= i\left(a_2^+ a_2 + a_3^+ a_3\right) \implies i a_3^+ a_3$$

By induction we can generate $a_{n+1}^+ a_n + a_n^+ a_{n+1}$, $a_{n+1}^+ a_n - a_n^+ a_{n+1}$ and $a_n + a_n$, as well as their linear combinations. Again, if we look to the Pauli picture this gives us, $X_n X_{n+1} + Y_n Y_{n+1}$, $X_n Y_{n+1} - Y_n X_{n+1}$ and Z_n. Here we only have next nearest neighbour interactions, we can now also show that we can generate interaction between qubits of arbitrary distance. We have,

$$h_k = \left[a_n^+ a_{n+1} + a_{n+1}^+ a_n, a_{n+1}^+ a_{n+2} + a_{n+2}^+ a_{n+1}\right],$$

$$= a_n^+ a_{n+1} a_{n+1}^+ a_{n+2} + \cancelto{0}{a_{n+1}^+ a_n a_{n+1}^+ a_{n+2}} + \cancelto{0}{a_n^+ a_{n+1} a_{n+2}^+ a_{n+1}} + a_{n+1}^+ a_n a_{n+2}^+ a_{n+1},$$

$$= \underbrace{\left(a_{n+1} a_{n+1}^+ a_{n+1}^+ a_{n+1}\right)}_{\mathbb{1}} a_n^+ a_{n+2} + \underbrace{\left(a_{n+1}^+ a_{n+1} + a_{n+1}^+ a_{n+1}\right)}_{\mathbb{1}} a_n a_{n+2}^+,$$

$$= a_n^+ a_{n+2} - a_{n+2}^+ a_n.$$

$$h_l = \left[a_n^+ a_{n+2} - a_{n+2}^+ a_n, i a_n^+ a_n\right],$$

$$= i\left(a_n^+ a_{n+2} + a_{n+2}^+ a_n\right).$$

In this way and with a little help from induction, we now have $X_n(\otimes_{n<k<m} Z_k) X_m + Y_n(\otimes_{n<k<m} Z_k) Y_m$ and $X_n(\otimes_{n<k<m} Z_k) Y_m - Y_n(\otimes_{n<k<m} Z_k) X_m$. Now, let's not neglect the fact we actully have two controls on the first site!

$$h_9 = [h_1, h_3] = -\left[a_n^+ a_{n+1} + a_{n+1}^+ a_n + (\mathbb{1} - 2a_n^+ a_n), a_1^+ + a_1\right],$$

$$= \cancelto{0}{a_1^+ a_2 a_1^+} + a_2^+ a_1 a_1^+ + a_1^+ a_2 a_1 + \cancelto{0}{a_2^+ a_1 a_1},$$

$$= -\left(\cancelto{0}{a_1^+ a_1^+ a_2} + a_1^+ a_2^+ a_1 + a_1 a_1^+ a_2 + \cancelto{0}{a_1 a_2^+ a_1}\right),$$

$$= a_2^+ \underbrace{\left(a_1 a_1^+ + a_1^+ a_1\right)}_{\mathbb{1}} - a_2 \underbrace{\left(a_1 a_1^+ + a_1^+ a_1\right)}_{\mathbb{1}},$$

$$= a_2^+ - a_2.$$

$$h_{10} = [h_9, h_6] = \left[a_2^+ - a_2, i(a_2^+ a_2) \right],$$

$$= i\left(\cancel{a_2^+ a_2^+ a_2}^{\,0} - a_2 a_2^+ a_2 - \left(a_2^+ a_2 - \cancel{a_2^+ a_2 a_2}^{\,0} \right) \right),$$

$$= i(a_2 + a_2^+).$$

Again, through the power of inductive reasoning we are able to add $a_n + a_n^+$ and $a_n^+ - a_n$ to our Lie algebra. There is a very important point here, when we look to the Pauli picture again. We do not have precisely X_n and Y_n, we actually have $(\otimes_{m<n} Z_m) Y_n$ and $(\otimes_{m<n} Z_m) X_n$. We can now collate all the terms in our Lie algebra at our disposal.

Fermionic term	Pauli term	number of terms
$i(1 - 2a_n^+ a_n)$	Z_n	N
$i(a_n^+ + a_n)$	$\otimes_{m<n} Z_m X_n$	N
$a_n^+ - a_n$	$i \otimes_{m<n} Z_m Y_n$	N
$i(a_n^+ + a_n)(a_m^+ - a_m)$	$Y_m \otimes_{m<k<n} Z_k Y_n$	$\frac{(N-1)N}{2}$
$i(a_n^+ - a_n)(a_m^+ + a_m)$	$X_m \otimes_{m<k<n} Z_k X_n$	$\frac{(N-1)N}{2}$
$(a_n^+ - a_n)(a_m^+ - a_m)$	$iX_m \otimes_{m<k<n} Z_k Y_n$	$\frac{(N-1)N}{2}$
$(a_n^+ + a_n)(a_m^+ + a_m)$	$iY_m \otimes_{m<k<n} Z_k X_n$	$\frac{(N-1)N}{2}$
	$dim(\mathcal{L})$:	$2N^2 + N$

Table 6.1: Table of all terms contained in the Lie algebra

It is from Table 6.1 that we justify the assumption that is Lie algebra is sufficient despite its lack of universality. We have close to local rotations and two qubit $X - Y$ operations, that also include a Z term. In essence, these are the key components of generating states for estimation in the Z-direction.

6.2.2 Linear space reduction

The work of Colpa [45, 46, 47] extensively developed the theory of the diagonalisation of quadratic Hamiltonians, including those with linear components.

Importantly for us, the key step to the diagonalisation of such Hamiltonians is to transform them into a linear space that only acts on a "state vector" of the linear creation and annihilation operators. If we consider a general quadratic Hamiltonian with linear part, it can be expressed in terms of complex matrices of coefficients,

$D_{i,r,r'}$ and M_r such that,

$$\hat{H} = \sum_{r',r=1}^{N} a_{r'}^{\dagger} D_{1,r,r'} a_r + a_{r'}^{\dagger} D_{2,r,r'} a_r^{\dagger} + a_{r'} D_{3,r,r'} a_r + a_{r'} D_{4,r,r'} a_r^{\dagger} \qquad (6.19)$$

$$+ \sum_{r=1}^{N} M_r a_r + M_r^* a_r^{\dagger}. \qquad (6.20)$$

In the absence of M_r, the dynamics can be written in a linear space,

$$\tilde{H} = \begin{bmatrix} D_1 & D_2 \\ D_3 & D_4. \end{bmatrix} \qquad (6.21)$$

We introduce a new Hilbert space of dimension $2(N+1)$ by the introduction of a "ghost particle" at the 0th site. By defining the transformations,

$$\tilde{a}_1 \rightarrow a_0^{\dagger} a_1 - a_0 a_1, \qquad (6.22)$$

$$\tilde{a}_1^{\dagger} \rightarrow a_1^{\dagger} a_0 - a_1^{\dagger} a_0^{\dagger}. \qquad (6.23)$$

This allows for the re-writing of our general quadratic Hamiltonian (Eq. 6.19) with a linear part, such that the elements of M_r and M_r^* fill the new 0th row and column respectively (beside the 0,0-th element as the linear ghost particle has no impact on dynamics). We can transform the Hamiltonian 6.18 into a linear space. Using the terminology of Colpa [45] we define the grand dynamical matrix,

$$\mathcal{D} = \left(\begin{array}{c|cccc|c|cccc} 0 & \frac{f}{2} & 0 & 0 & 0 & 0 & \frac{f}{2} & 0 & 0 & \ldots \\ \hline \frac{f}{2} & -g-\lambda & 1 & 0 & 0 & -\frac{f}{2} & 0 & 0 & 0 & 0 \\ 0 & 1 & -\lambda & 1 & 0 & 0 & 0 & 0 & 0 & 0 \\ 0 & 0 & 1 & -\lambda & 1 & 0 & 0 & 0 & 0 & 0 \\ \vdots & 0 & 0 & 1 & \ddots & \vdots & 0 & 0 & 0 & 0 \\ \hline 0 & -\frac{f}{2} & 0 & 0 & \ldots & 0 & -\frac{f}{2} & 0 & 0 & \ldots \\ \hline \frac{f}{2} & 0 & 0 & 0 & 0 & -\frac{f}{2} & g+\lambda & -1 & 0 & 0 \\ 0 & 0 & 0 & 0 & 0 & 0 & -1 & \lambda & -1 & 0 \\ 0 & 0 & 0 & 0 & 0 & 0 & 0 & -1 & \lambda & -1 \\ \vdots & 0 & 0 & 0 & 0 & \vdots & 0 & 0 & -1 & \ddots \end{array} \right). \qquad (6.24)$$

This matrix $\mathcal{D}$ acts as an effective Hamiltonian acting on the $2N \times 2N$ dimen-

sioned state,

$$\boldsymbol{\alpha} = \begin{bmatrix} a_0 \\ a_1 \\ \vdots \\ a_n \\ a_0^\dagger \\ a_1^\dagger \\ \vdots \\ a_n^\dagger \end{bmatrix} \tag{6.25}$$

of creation and annihilation operators.

The action of which is given by the Heisenberg equations of motion,

$$\alpha(t) = e^{-it\mathcal{D}}\alpha(0). \tag{6.26}$$

More directly,

$$a_i(t) = \sum_k [e^{-it\mathcal{D}}]_{i,k} a_k(0). \tag{6.27}$$

However, we must remember that we are not interested in $a_i(t)$, rather $\tilde{a}_i(t)$, which for $i \neq 0$ is given by,

$$\tilde{a}_i(t) = (a_0^\dagger(t) - a_0(t))a_i(t). \tag{6.28}$$

along with their respective derivatives with respect to λ,

$$\partial_\lambda \tilde{a}_i(t) = (\partial_\lambda(a_0^\dagger(t) - a_0(t)))a_i(t) \tag{6.29}$$

$$+ (a_0^\dagger(t) - a_0(t))(\partial_\lambda a_i(t)). \tag{6.30}$$

Recall the definition of the Fisher information given in terms of a state's Bloch vector [216] for pure states,

$$C^s(|\psi_\lambda\rangle) = ||\partial\boldsymbol{\alpha}||^2, \tag{6.31}$$

where α is the Bloch vector of $|\psi_\lambda\rangle$.

$$U_\lambda = e^{-it\mathcal{D}(\{,\},\lambda)}, \tag{6.32}$$

$$\partial_\lambda U_\lambda = \partial_\lambda e^{-it\mathcal{D}(\{,\},\lambda)}, \tag{6.33}$$

$$\omega_1 = \sum_{i=0}^{n+1} [U_\lambda]_{0,i} * [\partial_\lambda U_\lambda]_{1,n+1+i}, \tag{6.34}$$

$$\omega_2 = \sum_{i=0}^{n+1} [U_\lambda]_{0,i}^\dagger * [\partial_\lambda U_\lambda]_{1,i}, \tag{6.35}$$

$$\omega_3 = \sum_{i=0}^{n+1} [\partial_\lambda U_\lambda]_{0,i} * [U_\lambda]_{1,n+1+i}, \tag{6.36}$$

$$\omega_4 = \sum_{i=0}^{n+1} [\partial_\lambda U_\lambda]_{0,i}^\dagger * [U_\lambda]_{1,i}, \tag{6.37}$$

$$\langle \partial_\lambda X_1(t) \rangle = 2 * \mathrm{Re}(\omega_1 + \omega_2 + \omega_3 + \omega_4), \tag{6.38}$$

$$\langle \partial_\lambda Y_1(t) \rangle = 2 * \mathrm{Im}(\omega_1 + \omega_2 + \omega_3 + \omega_4), \tag{6.39}$$

$$\langle \partial_\lambda Z_1(t) \rangle = 2 * \left| \left(\sum_{i=0}^{n+1} [U_\lambda]_{1,i} * [\partial_\lambda U_\lambda^\dagger]_{1,i} + [\partial_\lambda U_\lambda]_{1,i}[U^\dagger]_{1,i} \right) \right|, \tag{6.40}$$

where $[.]_{i,j}$ refers to the element on the ith column and j^{th} row of the given matrix. Combining the above allows us to analytically compute the QCRB for the spin chain in Equation 6.18 in a linear computation space. Explicitly given by,

$$C^S(\lambda) = ||\partial_\lambda U_\lambda||^2 \tag{6.41}$$

$$= \langle \partial_\lambda X_1(t) \rangle^2 + \langle \partial_\lambda Y_1(t) \rangle^2 + \langle \partial_\lambda Z_1(t) \rangle^2 \tag{6.42}$$

6.3   Results

We utilise GRadient Ascent Pulse Engineering (GRAPE) [168] algorithm implemented with QUTIP [104] for the optimisation of the control functions $f(t)$ and $g(t)$. GRAPE is an algorithm originally developed in the context of NMR quantum computing in order to optimise the control sequence needed in order to implement some desired quantum logic gate. GRAPE typically uses the fidelity error as a distance metric between the desired evolution and the currently achieved one. Let U_t be our $N \times N$ dimension target unitary evolution and U_c be our current one, then the fidelity error is

defined as,

$$f_e(U_t, U_c) = \mathbb{1} - \langle U_t, U_c \rangle = \frac{tr(\mathbb{1} - (U_t U_c^\dagger))}{N}. \tag{6.43}$$

We substitute this fidelity computation for Equation 6.31 in the numerical runtime. The explicit form of the final state is not relevant, it is the process we are concerned with. By this we mean, we are not interested in a single optimal state, as we have been hitherto in this thesis. Instead, we are interested in the optimal sequence of control pulses for the complete estimation process, state preparation, parameter sensing and measurement.

Our time evolution is now split into a finite number of discrete time slots. The simplest optimisation algorithm would then take a random input control pulse sequence and then calculate the gradient of the fidelity error at each time slot. The algorithm then takes a step in the direction of the variable that has the greatest gradient in the direction which minimised the fidelity error. It does this for each time slot and iterates this process many times until one of the termination conditions is met. The strongest termination condition is termination of the fidelity error.

6.3.1 Numerical results

Initially we examine the scaling over the number of qubits with fixed time $t = 1$ and parameter value $\lambda = 1$. There is now a free choice on the number of time slots we break our problem down into. In order to strike the multi-way balance between computational complexity, reducing optimisation potential with too few time slots and introducing too many variables thus increasing the number of local minimum, we do a sweep over multiple values. The values chosen were $[1, 5, 10, 20, 50]$ time slots. A linear computational space allows us to explore much higher qubit numbers than would previously have been possible. As such we can sweep the qubit number dimension with values $[2, 3, 4, 5, 6, 7, 8, 25, 50, 100]$, in order to see trends form at low qubit numbers as well as the performance at very large spin-chain sizes. These results can be seen in Figure 6.1

The ultimate QCRB is $4N^2t^2$, is the optimal QCRB when a GHZ probe state is used. We find that the QCRB for 2-qubits approaches $\approx 98\%$ of $4N^2t^2$. This first data point is very promising as we have found a very efficient series of pulses for 2-qubits. The results for the remaining qubits however, do not increase above this value. That is to say we are unable to find a series of pulses such that there is any advantage to adding more qubits after the second.

Following the first set of results we explore the time dimension. For two qubits we indeed see the same efficiency in the results. We once again find no advantage in the higher number of qubits when additional time is given.
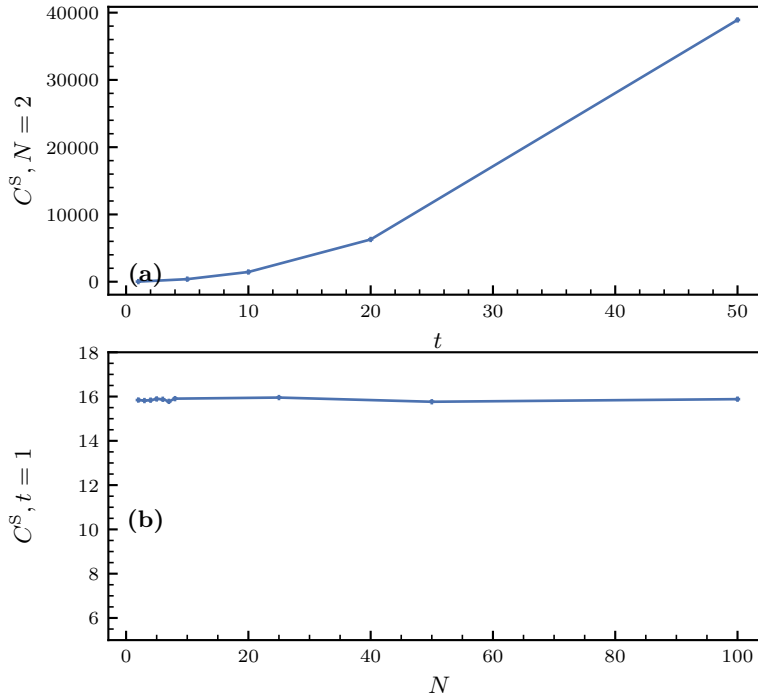
Figure 6.1: Results of optimisation of magnetic field estimation over a spin chain. In (a) we see the results for a fixed number of qubits $N = 2$ and varying over time. In (b) we see a fixed time $t = 1$ and a varying number of qubits.

6.4 Discussion and conclusions

In this chapter we sought to find an experimentally viable spin chain set up that allowed for both efficient classical simulation and an advantage in magnetic field estimation over a classical chain. A classical chain being one where there no entanglement present, only product states. The XX spin chain set up we explored in this chapter contained sufficient Lie algebra elements that intuitively allow for beneficial states to be prepared. Further to this, we were able to write the dynamics of the system and the final QCRB in a linear $(2(N + 1))$ dimensional space. For the $N = 2$ case, we found the desired quadratic scaling in time, coupled with a QCRB that approached the optimal QCRB given by a Greenberger–Horne–Zeilinger state (GHZ) state. We

did not however, find any advantage in adding any qubits after the second. There was also no advantage found with increasing time for these higher qubit numbers. The implication of this is that there is no sequence of control pulses that could be found which are able to kick-back the phase information from more than two qubits.

Whilst these initial results are disappointing, there is still much to explore in this space. A geometric wrinkle with this particular control set up is the $N = 2$ case is in fact *universal* with sub-universality only being a property of greater qubit numbers. This not only explains the success of 2-qubits, but also implies that there could be a deep local minimum at the boundary of the second qubit. This is further supported by the numerical result itself coming very close to the optimal answer even when the optimal state is directly coupled to the magnetic field. This leads to three main avenues of exploration to improve these results:

- Change the optimisation method used,

- Change the control model,

- Find better initial seed values for the control pulses.

Firstly, there are improvements that can be made to gradient based optimisation on the assumption that there are large local minimum. Often turning to stochastic gradient method are not sufficient for very large minimum, as we suspect we have in this case. One technique used in the DFT community when they are presented with such a scenario is to artificially "fill-in" the minimum. This is done with iterative modification of the cost function, taking record of the current cost function value along with its parameter values and modifying the search for the best value. This can be achieved efficiently with the fire-fly algorithm [149]. This allows the optimiser to escape such minimum points, at a computational cost. Further, moving away from gradient based optimisation techniques is possible too, such as the particle swarm method we utilised in a previous chapter.

Secondly, making adjustments to the control model is a much more nebulous solution to explore. The goal should always be to keep the set-up practical for an experimentalist to execute. There are still experimentally impractical ideas that could shed some light for our results, such as the control and measure qubit in the middle of the chain, adding another control and measure qubit at the other extreme of of the chain or keeping the control qubit at one end and the measure qubit to the other extreme end. In particular the latter should give some insight to the ability to transfer the information (even for $N = 2$) efficiently down the length of the chain.

Finally we look to seeding the initial values of the control pulses with something more meaningful than random values. Initially finding the control pulses for the GHZ state and adding them in as the first half of the values was attempted with no success. This would indicate that it is in fact the "phase-kickback" portion of the control problem that is difficult to obtain numerically. Exploring initial pulses to coax some kickback from the optimiser could prove to be very fruitful.

Chapter 7

Conclusions

> We can only see a short distance
> ahead, but we can see plenty there
> that needs to be done.
>
> ———————————————
>
> Alan Turing

7.1 Conclusions

Magnetometry is of great scientific importance. In particular NV center magnetometry, which was first proposed in 2008 [189], has demonstrated many of these key experimental successes. Since 2008, the NV center has found its uses in biological research [172, 127, 88, 23], medical application [50, 115, 17], geological [80] and condensed matter research [38]. Further, it is of great benefit to more general metrological techniques such as NMR [32, 108], magnetic field imaging [13, 103, 62] and detectors for fundamental physics [162]. These applications serve to highlight the ubiquitous and essential nature of magnetometry in fundamental physics, application and general metrology techniques.

Theoretical study of magnetometry and metrological bounds offers interesting insight into the non-commutative nature of quantum information theory [20, 48, 67, 184]. The non-commutative nature of quantum information theory is one of the core differentiators to classical information theory. Through the study of multiparameter quantum estimation problems we unlock the possibility of not only furthering technology but also our fundamental understanding of quantum information theory.

To this end, within this thesis we have explored the optimisation and attainability

of 3D-magnetometry with qubit probes. Here we enumerate the key findings contained within this thesis:

Chapter 3

- 3D-GHZ state optimal for $N > 8$

- Developed a genetic inspired optimiser capable of finding structure in the optimal results

- Numerically found optimal states for $N < 8$

- Found numerically optimal states over σ_z dephasing noise

It remains an open question how the analytic optimal state changes with parameters not around 0.

Chapter 4

- Computed the HCRB for zero-valued 3D magnetometry with real valued states, representing the first analytic computation of the HCRB for more than 2 parameters when the bound does not collapse to another

- We further calculated the bound for diagonal weight matrices

- Demonstrated the bound can be attained with a single projective measurement despite never being asymptotically classical

- Presented the 1-1 relationship between the value of the HCRB and the amount of entanglement in the initial state

Chapter 5

- Showed the non-trivial relationship between attainability of a bound at its asymptotic classicality

- Used numerical optimisation to reveal the relationship between attainability and the number of input state copies of 3D magnetometry over noise

   - In the low noise regime, where a state is approximately pure there is effectively no benefit to additional copies of the input state

   - In the middle noise regime there is an incremental improvement with each addition input copy of the input state

- – In the high noise regime the HCRB is effectively attained with two copies of the input state.

- We developed a genetic inspired algorithm that minimised circuit depth as well as minimising some additional cost function

- Using the newly developed algorithm we found circuits which attained the optimal CCRB found previously

Chapter 6

- Set up a quadratic sub-universal Hamiltonian in a linear space along with an analytic form of the QCRB for such a system

- Found that when trying to estimate a 1D magnetic field on the first site along we were unable to make improvements beyond an effective 2-site spin chain. This is despite the rich dynamics of this Lie algebra, being non-universal by only a Hadammard operation of the second site.

7.2 Discussions and further work

From chapter 3, a natural question that remains unanswered is the dependency of the reduced two-body density matrices on the QFI, with a noisy channel. The case where the input state is mixed (equivalently the noise channel commuting with the encoding channel), we can see that the QFI depends solely on the two body reduced density matrices of the input state's eigenstates. The less fundamental, but still interesting question is to explore optimal states over varying parameter values.

Chapter 4 offers some very rich veins of inquiry. In particular, do all the properties of a coherent bound extend to this apparent odd-coherent model in general? If not, then where do the similarities break down. This could extend the classes of statistical models further and give scope for simpler analytic computation of bounds. There also exist the purely technical extensions of the work from this chapter; explicitly finding the relationship between the HCRB and entanglement, extending the bound over arbitrary parameter value and exploring attainability over varying parameters.

Chapter 5 gives the outline of a recipe for an experimentalist. To take these result and tune them for an exact experimental set up would be of great interest, especially if the optimisation can be done in-situ with the experiment. Beyond this, there remains the analytic answers to the questions of where the differences in adding many copies

of a state comes from. We can formulate some loose arguments, however, they lack the required analytic rigour.

Finally, in Chapter 6 we have many lines of enquiry in order to attempt to un-stick the optimisation of sensing over a spin chain. It would be pertinent to first confirm the hypothesis that the optimiser is indeed stuck in a local minima. If this is not the case then it suggests there is some fundamental limit involved. As previously expressed. Whilst this is not expected to be the case, the investigation would still yield interesting results in the limitations of sub-universal control models.

Bibliography

[1] Scott Aaronson. *Why are amplitudes complex?* 2018. URL: `https://www.scottaaronson.com/blog/?p=4021`.

[2] Junaid Aasi et al. "Enhanced sensitivity of the LIGO gravitational wave detector by using squeezed states of light". In: *Nature Photonics* 7.8 (2013), pp. 613–619.

[3] Antonio Acín, E. Jané, and Guifré Vidal. "Optimal estimation of quantum dynamics". In: *Phys. Rev. A* 64.5 (2001), p. 050302. ISSN: 1050-2947. DOI: `10.1103/PhysRevA.64.050302`. URL: `https://link.aps.org/doi/10.1103/PhysRevA.64.050302`.

[4] Nati Aharon et al. "NV center based nano-NMR enhanced by deep learning". In: *Scientific reports* 9.1 (2019), pp. 1–11.

[5] Alexander Craig Aitken. *Determinants and matrices*. Read Books Ltd, 2017.

[6] Francesco Albarelli, Jamie F. Friel, and Animesh Datta. "Evaluating the Holevo Cramér-Rao Bound for Multiparameter Quantum Metrology". In: *Phys. Rev. Lett.* 123.20 (2019), p. 200503. ISSN: 0031-9007. DOI: `10.1103/PhysRevLett.123.200503`. arXiv: `1906.05724`. URL: `http://arxiv.org/abs/1906.05724https://link.aps.org/doi/10.1103/PhysRevLett.123.200503`.

[7] Francesco Albarelli et al. "A perspective on multiparameter quantum metrology: From theoretical tools to applications in quantum imaging". In: *Phys. Lett. A* 384.12 (2020), p. 126311. ISSN: 03759601. DOI: `10.1016/j.physleta.2020.126311`. arXiv: `1911.12067`. URL: `http://arxiv.org/abs/1911.12067https://linkinghub.elsevier.com/retrieve/pii/S0375960120301109`.

[8] Francesco Albarelli et al. "A perspective on multiparameter quantum metrology: From theoretical tools to applications in quantum imaging". In: *Physics Letters A* 384.12 (2020), p. 126311.

[9] Francesco Albarelli et al. "Restoring Heisenberg scaling in noisy quantum metrology by monitoring the environment". In: (2018). arXiv: 1803.05891.

[10] Sanah Altenburg et al. "Estimation of gradients in quantum metrology". In: *Physical Review A* (2017). ISSN: 24699934. DOI: 10.1103/PhysRevA.96.042319. arXiv: 1703.09123.

[11] Iagoba Apellaniz et al. "Detecting metrologically useful entanglement in the vicinity of Dicke states". In: *New J. Phys.* 17.8 (2015), p. 83027. ISSN: 13672630. DOI: 10.1088/1367-2630/17/8/083027. arXiv: 1412.3426. URL: http://dx.doi.org/10.1088/1367-2630/17/8/083027.

[12] Iagoba Apellaniz et al. "Precision bounds for gradient magnetometry with atomic ensembles". In: *Phys. Rev. A* 97 (5 2018), p. 053603. DOI: 10.1103/PhysRevA.97.053603. URL: https://link.aps.org/doi/10.1103/PhysRevA.97.053603.

[13] Keigo Arai et al. "Fourier Magnetic Imaging with Nanoscale Resolution and Compressed Sensing Speed-up using Electronic Spins in Diamond". In: *Nature nanotechnology* 10 (Sept. 2014). DOI: 10.1038/nnano.2015.171.

[14] Sheldon Jay Axler. *Linear algebra done right*. Vol. 2. Springer, 1997.

[15] Manuel A. Ballester. "Estimation of unitary quantum operations". In: *Phys. Rev. A* 69.2 (2004), p. 022303. ISSN: 1050-2947. DOI: 10.1103/PhysRevA.69.022303. arXiv: 0305104 [quant-ph]. URL: http://arxiv.org/abs/quant-ph/0305104{\%}5Cnhttp://link.aps.org/doi/10.1103/PhysRevA.69.022303.

[16] Ole E. Barndorff-Nielsen and Richard D. Gill. "Fisher information in quantum statistics". In: *J. Phys. A* 33.24 (2000), pp. 4481–4490. ISSN: 0305-4470. DOI: 10.1088/0305-4470/33/24/306. arXiv: 9808009v4 [arXiv:quant-ph]. URL: http://arxiv.org/abs/quant-ph/9808009http://stacks.iop.org/0305-4470/33/i=24/a=306?key=crossref.eae2af16f1fc6a72b83e285a7f28b86f.

[17] John F. Barry et al. "Optical magnetic detection of single-neuron action potentials using quantum defects in diamond". In: *Proceedings of the National Academy of Sciences* 113.49 (2016), pp. 14133–14138. DOI: `10.1073/pnas.1601513113`. eprint: `https://www.pnas.org/doi/pdf/10.1073/pnas.1601513113`. URL: `https://www.pnas.org/doi/abs/10.1073/pnas.1601513113`.

[18] John F. Barry et al. "Sensitivity optimization for NV-diamond magnetometry". In: *Rev. Mod. Phys.* 92.1 (2020), p. 015004. ISSN: 0034-6861. DOI: `10.1103/RevModPhys.92.015004`. arXiv: `1903.08176`. URL: `http://arxiv.org/abs/1903.08176http://dx.doi.org/10.1103/RevModPhys.92.015004https://link.aps.org/doi/10.1103/RevModPhys.92.015004`.

[19] Tillmann Baumgratz and Animesh Datta. "Quantum Enhanced Estimation of a Multidimensional Field". In: *Physical Review Letters* (2016). ISSN: 10797114. DOI: `10.1103/PhysRevLett.116.030801`. arXiv: `1507.02956`.

[20] Tillmann Baumgratz and Animesh Datta. "Quantum Enhanced Estimation of a Multidimensional Field". In: *Phys. Rev. Lett.* 116.3 (2016), p. 030801. ISSN: 0031-9007. DOI: `10.1103/PhysRevLett.116.030801`. arXiv: `1507.02956`. URL: `http://arxiv.org/abs/1507.02956http://link.aps.org/doi/10.1103/PhysRevLett.116.030801https://link.aps.org/doi/10.1103/PhysRevLett.116.030801`.

[21] Alessio Belenchia et al. "Quantum physics in space". In: *Physics Reports* 951 (2022), pp. 1–70.

[22] I Ruo Berchera and Ivo Pietro Degiovanni. "Quantum imaging with sub-Poissonian light: challenges and perspectives in optical metrology". In: *Metrologia* 56.2 (2019), p. 024001. ISSN: 0026-1394. DOI: `10.1088/1681-7575/aaf7b2`. URL: `http://stacks.iop.org/0026-1394/56/i=2/a=024001?key=crossref.97b62801859bcacf293b39d2eb14f664`.

[23] Ettore Bernardi et al. "A biocompatible technique for magnetic field sensing at (sub)cellular scale using Nitrogen-Vacancy centers". In: *EPJ Quantum Technology* 7 (Oct. 2020), p. 13. DOI: `10.1140/epjqt/s40507-020-00088-2`.

[24] Ettore Bernardi et al. "Nanoscale Sensing Using Point Defects in Single-Crystal Diamond: Recent Progress on Nitrogen Vacancy Center-Based Sensors". In: (2017). ISSN: 2073-4352. DOI: `10.3390/cryst7050124`. arXiv: `1704.04011`.

[25] Dominic W. Berry et al. "Time-dependent Hamiltonian simulation with L^1-norm scaling". In: *Quantum* 4 (Apr. 2020), p. 254. ISSN: 2521-327X. DOI: `10.22331/q-2020-04-20-254`. URL: `https://doi.org/10.22331/q-2020-04-20-254`.

[26] P. Bocchieri and A. Loinger. "Quantum Recurrence Theorem". In: *Phys. Rev.* 107 (2 1957), pp. 337–338. DOI: `10.1103/PhysRev.107.337`. URL: `https://link.aps.org/doi/10.1103/PhysRev.107.337`.

[27] Stephen Boyd and Lieven Vandenberghe. *Convex Optimization*. New York: Cambridge University Press, 2004. ISBN: 9780521833783. URL: `https://web.stanford.edu/{~}boyd/cvxbook/bv{\_}cvxbook.pdf`.

[28] Mark Bradshaw, Ping Koy Lam, and Syed M. Assad. "Ultimate precision of joint quadrature parameter estimation with a Gaussian probe". In: *Phys. Rev. A* 97.1 (2018), p. 012106. ISSN: 2469-9926. DOI: `10.1103/PhysRevA.97.012106`. arXiv: `1710.04817`. URL: `http://arxiv.org/abs/1710.04817https://link.aps.org/doi/10.1103/PhysRevA.97.012106`.

[29] Dominic Branford, Haixing Miao, and Animesh Datta. "Fundamental quantum limits of multicarrier optomechanical sensors". In: *Physical review letters* 121.11 (2018), p. 110505.

[30] Daniel Braun et al. "Quantum-enhanced measurements without entanglement". In: *Rev. Mod. Phys.* 90.3 (2018), p. 035006. ISSN: 0034-6861. DOI: `10.1103/RevModPhys.90.035006`. arXiv: `1701.05152`. URL: `https://link.aps.org/doi/10.1103/RevModPhys.90.035006`.

[31] Samuel L. Braunstein and Carlton M. Caves. "Statistical distance and the geometry of quantum states". In: *Phys. Rev. Lett.* 72.22 (1994), pp. 3439–3443. ISSN: 0031-9007. DOI: `10.1103/PhysRevLett.72.3439`. URL: `https://link.aps.org/doi/10.1103/PhysRevLett.72.3439`.

[32] Dominik Bucher et al. "Hyperpolarization-Enhanced NMR Spectroscopy with Femtomole Sensitivity Using Quantum Defects in Diamond". In: *Physical Review X* 10 (June 2020). DOI: `10.1103/PhysRevX.10.021053`.

[33] Daniel Burgarth and Sougato Bose. "Conclusive and arbitrarily perfect quantum-state transfer using parallel spin-chain channels". In: *Physical Review A - Atomic, Molecular, and Optical Physics* 71.5 (2005), pp. 1–6. ISSN: 10502947. DOI: `10.1103/PhysRevA.71.052315`. arXiv: `0406112 [quant-ph]`.

[34] Daniel Burgarth et al. "Scalable quantum computation via local control of only two qubits". In: *Physical Review A - Atomic, Molecular, and Optical Physics* 81.4 (2010). 10.1103/PhysRevA.81.040303, pp. 2–5. ISSN: 10502947. DOI: `10.1103/PhysRevA.81.040303`.

[35] P. Cappellaro and M. D. Lukin. "Quantum correlation in disordered spin systems: Applications to magnetic sensing". In: *Phys. Rev. A* 80 (3 2009), p. 032311. DOI: `10.1103/PhysRevA.80.032311`. URL: `https://link.aps.org/doi/10.1103/PhysRevA.80.032311`.

[36] Angelo Carollo et al. "On quantumness in multi-parameter quantum estimation". In: *J. Stat. Mech. Theory Exp.* 2019.9 (2019), p. 094010. ISSN: 1742-5468. DOI: `10.1088/1742-5468/ab3ccb`. URL: `https://iopscience.iop.org/article/10.1088/1742-5468/ab3ccb`.

[37] Francesco Casola, Toeno van der Sar, and Amir Yacoby. "Probing condensed matter physics with magnetometry based on nitrogen-vacancy centres in diamond". In: *Nat. Rev. Mater.* 3.1 (2018), p. 17088. ISSN: 2058-8437. DOI: `10.1038/natrevmats.2017.88`. URL: `http://www.nature.com/articles/natrevmats201788`.

[38] Francesco Casola, Toeno van der Sar, and Amir Yacoby. "Probing condensed matter physics with magnetometry based on nitrogen-vacancy centres in diamond". In: *Nature Reviews Materials* 3 (Jan. 2018), p. 17088. DOI: `10.1038/natrevmats.2017.88`.

[39] Carlton M. Caves. "Quantum-mechanical noise in an interferometer". In: *Phys. Rev. D* 23 (8 1981), pp. 1693–1708. DOI: `10.1103/PhysRevD.23.1693`. URL: `https://link.aps.org/doi/10.1103/PhysRevD.23.1693`.

[40] Hongzhen Chen and Haidong Yuan. "Optimal joint estimation of multiple Rabi frequencies". In: *Phys. Rev. A* 99.3 (2019), p. 032122. ISSN: 2469-9926. DOI: `10.1103/PhysRevA.99.032122`. URL: `https://link.aps.org/doi/10.1103/PhysRevA.99.032122`.

[41] Yu Chen et al. "Quantum Calibration of Multi-pixel Photon Counter and Its Application in High-Sensitivity Magnetometry With NV Center Ensemble". In: *IEEE Journal of Selected Topics in Quantum Electronics* 26.3 (2020), pp. 1–7. DOI: `10.1109/JSTQE.2020.2991432`.

[42] L Childress and R Hanson. "Diamond NV centers for quantum computing and quantum networks". In: *MRS Bulletin* 38.2 (2013). 10.1557/mrs.2013.20, pp. 134–138. ISSN: 0883-7694. DOI: `10.1557/mrs.2013.20`. URL: `http://journals.cambridge.org/download.php?file=/MRS/MRS38_02/S0883769413000201a.pdf&code=00415e54e42e6862e051a6bcc1b`

[43] Giulio Chiribella, Giacomo Mauro D'Ariano, and Massimiliano Federico Sacchi. "Optimal estimation of group transformations using entanglement". In: *Phys. Rev. A* 72.4 (2005), p. 042338. ISSN: 1050-2947. DOI: `10.1103/PhysRevA.72.042338`. arXiv: `0506267 [quant-ph]`. URL: `http://link.aps.org/doi/10.1103/PhysRevA.72.042338`.

[44] Andrzej Chrostowski et al. "On super-resolution imaging as a multiparameter estimation problem". In: *Int. J. Quantum Inf.* 15.08 (2017), p. 1740005. ISSN: 0219-7499. DOI: `10.1142/S0219749917400056`. arXiv: `1709.08392`. URL: `http://arxiv.org/abs/1709.08392http://www.worldscientific.com/doi/abs/10.1142/S0219749917400056`.

[45] J H P Colpa. "Diagonalisation of the quadratic fermion Hamiltonian with a linear part". In: *Journal of Physics A: Mathematical and General* 12.4 (1979), pp. 469–488. ISSN: 0305-4470. DOI: `10.1088/0305-4470/12/4/008`. URL: `http://stacks.iop.org/0305-4470/12/i=4/a=008?key=crossref.53deddd02739db73de860173cf31cb83`.

[46] J H P Colpa. "Diagonalisation of the quadratic fermion Hamiltonian with a linear part". In: *Journal of Physics A: Mathematical and General* 12.4 (1979). 10.1088/0305-4470/12/4/008, pp. 469–488. ISSN: 0305-4470. DOI: `10.1088/0305-4470/12/4/008`. URL: `http://stacks.iop.org/0305-4470/12/i=4/a=008?key=crossref.53deddd02739db73de860173cf31cb83.`

[47]   J. H.P. Colpa. "Diagonalization of the quadratic boson Hamiltonian with zero modes. II. Physical". In: *Physica A: Statistical Mechanics and its Applications* 134.2 (1986), pp. 417–442. ISSN: 03784371. DOI: 10.1016/0378-4371(86)90057-9.

[48]   Ivan Contreras, Elisa Ercolessi, and Michele Schiavina. "On the geometry of mixed states and the Fisher information tensor". In: *J. Math. Phys.* 57.6 (2016), p. 062209. ISSN: 0022-2488. DOI: 10.1063/1.4954328. arXiv: 1501.00054. URL: http://arxiv.org/abs/1501.00054http://aip.scitation.org/doi/10.1063/1.4954328.

[49]   Harald Cramér. *Mathematical Methods of Statistics (PMS-9)*. Princeton University Press, 1999. ISBN: 9780691005478. URL: http://www.jstor.org/stable/j.ctt1bpm9r4.

[50]   Matthew W. Dale and Gavin W. Morley. "Medical applications of diamond magnetometry: commercial viability". In: *arXiv:1705.01994* (2017). arXiv: 1705.01994. URL: http://arxiv.org/abs/1705.01994.

[51]   Giacomo Mauro D'Ariano, Paoloplacido Lo Presti, and Matteo G. A. Paris. "Using Entanglement Improves the Precision of Quantum Measurements". In: *Phys. Rev. Lett.* 87.27 (2001), p. 270404. ISSN: 0031-9007. DOI: 10.1103/PhysRevLett.87.270404. arXiv: 0109040 [quant-ph]. URL: https://link.aps.org/doi/10.1103/PhysRevLett.87.270404.

[52]   C. L. Degen, Friedemann Reinhard, and Paola Cappellaro. "Quantum sensing". In: *Rev. Mod. Phys.* 89.3 (2017), p. 035002. ISSN: 0034-6861. DOI: 10.1103/RevModPhys.89.035002. arXiv: 1611.02427. URL: http://link.aps.org/doi/10.1103/RevModPhys.89.035002.

[53]   Rafał Demkowicz-Dobrzański, Wojciech Górecki, and Mădălin Guţă. "Multi-parameter estimation beyond Quantum Fisher Information". In: *J. Phys. A* (2020), in press. ISSN: 1751-8113. DOI: 10.1088/1751-8121/ab8ef3. arXiv: 2001.11742. URL: http://arxiv.org/abs/2001.11742https://iopscience.iop.org/article/10.1088/1751-8121/ab8ef3.

[54]   Rafał Demkowicz-Dobrzański, Marcin Jarzyna, and Jan Kołodyński. "Quantum Limits in Optical Interferometry". In: *Prog. Opt. Vol. 60*. Ed. by Emil Wolf. Amsterdam: Elsevier, 2015. Chap. 4, pp. 345–435. ISBN: 9780128022849. DOI:

10.1016/bs.po.2015.02.003. URL: `http://arxiv.org/abs/1405.7703http://linkinghub.elsevier.com/retrieve/pii/S0079663815000049`.

[55] Rafał Demkowicz-Dobrzański, Jan Kołodyński, and Mădălin Guţă. "The elusive Heisenberg limit in quantum-enhanced metrology". In: *Nat. Commun.* 3 (2012), p. 1063. ISSN: 2041-1723. DOI: 10.1038/ncomms2067. arXiv: 1201.3940. URL: `http://www.nature.com/doifinder/10.1038/ncomms2067`.

[56] Rafał Demkowicz-Dobrzański and Lorenzo Maccone. "Using Entanglement Against Noise in Quantum Metrology". In: *Phys. Rev. Lett.* 113.25 (2014), p. 250801. ISSN: 0031-9007. DOI: 10.1103/PhysRevLett.113.250801. URL: `https://link.aps.org/doi/10.1103/PhysRevLett.113.250801`.

[57] Marcus W. Doherty et al. "The nitrogen-vacancy colour centre in diamond". In: (Feb. 2013). 10.1016/j.physrep.2013.02.001. DOI: 10.1016/j.physrep.2013.02.001. URL: `http://arxiv.org/abs/1302.3288http://dx.doi.org/10.1016/j.physrep.2013.02.001`.

[58] Florian Dolde et al. "Electric-field sensing using single diamond spins". In: *Nature Physics* 7.6 (2011), pp. 459–463. ISSN: 1745-2473. DOI: 10.1038/nphys1969. arXiv: 1103.3432. URL: `http://www.nature.com/doifinder/10.1038/nphys1969{\%}5Cnhttp://arxiv.org/abs/1103.3432{\%}5Cnhttp://dx.doi.org/10.1038/nphys1969`.

[59] D. Dong and Ian R. Petersen. "Quantum control theory and applications: A survey". In: *ArXiv* abs/0910.2350 (2009).

[60] A. Dréau et al. "Single-Shot Readout of Multiple Nuclear Spin Qubits in Diamond under Ambient Conditions". In: *Phys. Rev. Lett.* 110 (6 2013), p. 060502. DOI: 10.1103/PhysRevLett.110.060502. URL: `https://link.aps.org/doi/10.1103/PhysRevLett.110.060502`.

[61] Gurudev Dutt et al. "Quantum Register Based on Individual Electronic and Nuclear Spin Qubits in Diamond, Science 316". In: *Science (New York, N.Y.)* 316 (July 2007), pp. 1312–6. DOI: 10.1126/science.1139831.

[62] A. M. Edmonds et al. "Production of oriented nitrogen-vacancy color centers in synthetic diamond". In: *Phys. Rev. B* 86 (3 2012), p. 035201. DOI: `10.1103/PhysRevB.86.035201`. URL: `https://link.aps.org/doi/10.1103/PhysRevB.86.035201`.

[63] Kejie Fang et al. "High-sensitivity magnetometry based on quantum beats in diamond nitrogen-vacancy centers". In: *Physical Review Letters* (2013). ISSN: 00319007. DOI: `10.1103/PhysRevLett.110.130802`. arXiv: `1212.1495`.

[64] Jamie Friel. *Quantum Estimation Toolbox*. `https://github.com/tantrix10/QuantumEstimationToolboox`. 2022.

[65] Florian Fröwis et al. "Optimal quantum states for frequency estimation". In: *New J. Phys.* 16.8 (2014), p. 083010. ISSN: 1367-2630. DOI: `10.1088/1367-2630/16/8/083010`. arXiv: `1402.6946`. URL: `http://stacks.iop.org/1367-2630/16/i=8/a=083010?key=crossref.46fae66d53421f21ea639611698f4c61`.

[66] Akio Fujiwara. "Estimation of SU(2) operation and dense coding: An information geometric approach". In: *Phys. Rev. A* 65.1 (2001), p. 012316. ISSN: 1050-2947. DOI: `10.1103/PhysRevA.65.012316`. URL: `https://link.aps.org/doi/10.1103/PhysRevA.65.012316`.

[67] Akio Fujiwara. "Geometry of quantum information systems". In: *Geom. Present Day Sci.* (1998), pp. 1–14. URL: `http://www.math.sci.osaka-u.ac.jp/{~}fujiwara/research/Aarhus.pdf`.

[68] Akio Fujiwara. "Quantum channel identification problem". In: *Phys. Rev. A* 63.4 (2001), p. 042304. ISSN: 1050-2947. DOI: `10.1103/PhysRevA.63.042304`. URL: `https://link.aps.org/doi/10.1103/PhysRevA.63.042304`.

[69] Akio Fujiwara and Hiroshi Imai. "A fibre bundle over manifolds of quantum channels and its application to quantum statistics". In: *J. Phys. A* 41.25 (2008), p. 255304. ISSN: 1751-8113. DOI: `10.1088/1751-8113/41/25/255304`. URL: `http://stacks.iop.org/1751-8121/41/i=25/a=255304?key=crossref.2a155c4a97dd09d840b31a336e1943b1`.

[70] Akio Fujiwara and Hiroshi Nagaoka. "An estimation theoretical characterization of coherent states". In: *J. Math. Phys.* 40.9 (1999), pp. 4227–4239. ISSN: 0022-2488. DOI: 10.1063/1.532962. URL: http://aip.scitation.org/doi/10.1063/1.532962.

[71] Akio Fujiwara and Hiroshi Nagaoka. "An Estimation Theoretical Characterization of Coherent States". In: *Journal of Mathematical Physics* 40 (Sept. 1999). DOI: 10.1063/1.532962.

[72] Akio Fujiwara and Hiroshi Nagaoka. "Quantum Fisher metric and estimation for pure state models". In: *Phys. Lett. A* 201.2-3 (1995), pp. 119–124. ISSN: 03759601. DOI: 10.1016/0375-9601(95)00269-9. URL: http://linkinghub.elsevier.com/retrieve/pii/0375960195002699.

[73] Christos N Gagatsos, Dominic Branford, and Animesh Datta. "Gaussian systems for quantum-enhanced multiple phase estimation". In: *Physical Review A* 94.4 (2016), p. 042342.

[74] I. M. Gelfand and M. A. Neumark. "On the imbedding of normed rings into the ring of operators in Hilbert space". eng. In: *Matematiceskij sbornik* 54.2 (1943), pp. 197–217. URL: http://eudml.org/doc/65219.

[75] Marco G. Genoni et al. "Optimal estimation of joint parameters in phase space". In: *Phys. Rev. A* 87.1 (2013), p. 012107. ISSN: 1050-2947. DOI: 10.1103/PhysRevA.87.012107. arXiv: 1206.4867. URL: http://link.aps.org/doi/10.1103/PhysRevA.87.012107.

[76] Vladislav Gerginov, FCS da Silva, and David Howe. "Prospects for magnetic field communications and location using quantum sensors". In: *Review of Scientific Instruments* 88.12 (2017), p. 125005.

[77] Vittorio Giovannetti, Seth Lloyd, and Lorenzo Maccone. "Advances in quantum metrology". In: *Nat. Photonics* 5.4 (2011), pp. 222–229. ISSN: 1749-4885. DOI: 10.1038/nphoton.2011.35. arXiv: arXiv:1102.2318v1. URL: http://www.nature.com/articles/nphoton.2011.35.

[78] Vittorio Giovannetti, Seth Lloyd, and Lorenzo Maccone. "Quantum-enhanced positioning and clock synchronization". In: *Nature* 412.6845 (2001), pp. 417–419.

[79] Vittorio Giovannetti, Seth Lloyd, and Lorenzo Maccone. "Quantum Metrology". In: *Phys. Rev. Lett.* 96.1 (2006), p. 010401. ISSN: 0031-9007. DOI: `10.1103/PhysRevLett.96.010401`. arXiv: `arXiv:1102.2318v1`. URL: `http://link.aps.org/doi/10.1103/PhysRevLett.96.010401`.

[80] D. R. Glenn et al. "Micrometer-scale magnetic imaging of geological samples using a quantum diamond microscope". In: *Geochemistry, Geophysics, Geosystems* 18.8 (2017), pp. 3254–3267. DOI: `https://doi.org/10.1002/2017GC006946`. eprint: `https://agupubs.onlinelibrary.wiley.com/doi/pdf/10.1002/2017GC006946`. URL: `https://agupubs.onlinelibrary.wiley.com/doi/abs/10.1002/2017GC006946`.

[81] Aaron Z. Goldberg and Daniel F. V. James. "Quantum-limited Euler angle measurements using anticoherent states". In: *Phys. Rev. A* 98.3 (2018), p. 032113. ISSN: 2469-9926. DOI: `10.1103/PhysRevA.98.032113`. arXiv: `1806.02355`. URL: `https://link.aps.org/doi/10.1103/PhysRevA.98.032113`.

[82] D. Andrew Golter, Thomas K. Baldwin, and Hailin Wang. "Suppression of Spin Dephasing in Diamond NV Centers with Microwave-Dressed Spin States". In: *CLEO: 2014*. Optical Society of America, 2014, FW1B.3. DOI: `10.1364/CLEO_QELS.2014.FW1B.3`. URL: `http://www.osapublishing.org/abstract.cfm?URI=CLEO_QELS-2014-FW1B.3`.

[83] Wojciech Gorecki et al. "Quantum error correction in multi-parameter quantum metrology". In: *arXiv:1901.00896* 4 (2019), p. 288. ISSN: 2521-327X. DOI: `10.22331/q-2020-07-02-288`. arXiv: `1901.00896`. URL: `https://arxiv.org/abs/1901.00896`.

[84] Michael Grant and Stephen Boyd. *CVX: Matlab Software for Disciplined Convex Programming, version 2.1*. 2019. URL: `http://cvxr.com/cvx`.

[85] Daniel M Greenberger, Michael A Horne, and Anton Zeilinger. "Going beyond Bell's theorem". In: *Bell's theorem, quantum theory and conceptions of the universe*. Springer, 1989, pp. 69–72.

[86] Mădălin Guţă and Anna Jenčová. "Local Asymptotic Normality in Quantum Statistics". In: *Commun. Math. Phys.* 276.2 (2007), pp. 341–379. ISSN: 0010-3616. DOI: `10.1007/s00220-007-0340-1`. arXiv: `0606213`

[quant-ph]. URL: `http://link.springer.com/10.1007/s00220-007-0340-1`.

[87] L. T. Hall et al. "Ultrasensitive diamond magnetometry using optimal dynamic decoupling". In: *Phys. Rev. B* 82 (4 2010), p. 045208. DOI: `10.1103/PhysRevB.82.045208`. URL: `https://link.aps.org/doi/10.1103/PhysRevB.82.045208`.

[88] L.T. Hall, D.A. Simpson, and L.C.L. Hollenberg. "Nanoscale sensing and imaging in biology using the nitrogen-vacancy center in diamond". In: *MRS Bulletin* 38.2 (2013), 162–167. DOI: `10.1557/mrs.2013.24`.

[89] Masahito Hayashi, ed. *Asymptotic Theory of Quantum Statistical Inference: Selected Papers*. Singapore: World Scientific, 2005. ISBN: 978-981-256-015-5. DOI: `10.1142/5630`. URL: `https://www.worldscientific.com/worldscibooks/10.1142/5630`.

[90] Masahito Hayashi. "Comparison Between the Cramer-Rao and the Mini-max Approaches in Quantum Channel Estimation". In: *Commun. Math. Phys.* 304.3 (2011), pp. 689–709. ISSN: 0010-3616. DOI: `10.1007/s00220-011-1239-4`. arXiv: `1003.4575`. URL: `http://link.springer.com/10.1007/s00220-011-1239-4`.

[91] Masahito Hayashi. *Quantum Information Theory*. Berlin, Heidelberg: Springer, 2017. ISBN: 978-3-662-49723-4. DOI: `10.1007/978-3-662-49725-8`. URL: `http://link.springer.com/10.1007/978-3-662-49725-8`.

[92] Masahito Hayashi and Keiji Matsumoto. "Asymptotic performance of optimal state estimation in qubit system". In: *J. Math. Phys.* 49.10 (2008), p. 102101. ISSN: 0022-2488. DOI: `10.1063/1.2988130`. arXiv: `0411073 [quant-ph]`. URL: `http://aip.scitation.org/doi/10.1063/1.2988130`.

[93] Carl W Helstrom. "Quantum detection and estimation theory". In: *Journal of Statistical Physics* 1.2 (1969), pp. 231–252.

[94] Le Bin Ho et al. "Multiparameter quantum estimation under dephasing noise". In: *arXiv:2004.00720* (2020). arXiv: `2004.00720`. URL: `http://arxiv.org/abs/2004.00720`.

[95] Alexander S. Holevo. "Commutation superoperator of a state and its applications to the noncommutative statistics". In: *Rep. Math. Phys.* 12.2 (1977), pp. 251–271. ISSN: 00344877. DOI: `10.1016/0034-4877(77)90009-X`. URL: `http://linkinghub.elsevier.com/retrieve/pii/003448777790009X`.

[96] Alexander S. Holevo. "Noncommutative analogues of the Cramér-Rao inequality in the quantum measurement theory". In: *Proceedings of the Third Japan — USSR Symposium on Probability Theory*. Ed. by Gisiro Maruyama and Jurii V. Prokhorov. Vol. 550. Lecture Notes in Mathematics. Berlin, Heidelberg: Springer Berlin Heidelberg, 1976. ISBN: 978-3-540-07995-8. DOI: `10.1007/BFb0077479`. URL: `http://link.springer.com/10.1007/BFb0077479`.

[97] Alexander S. Holevo. *Probabilistic and Statistical Aspects of Quantum Theory*. 2nd. Pisa: Edizioni della Normale, 2011. ISBN: 978-88-7642-375-8. DOI: `10.1007/978-88-7642-378-9`. URL: `http://link.springer.com/10.1007/978-88-7642-378-9`.

[98] Sungkun Hong et al. "Nanoscale magnetometry with NV centers in diamond". In: *MRS bulletin* 38.2 (2013), pp. 155–161.

[99] Zhibo Hou et al. "Minimal tradeoff and ultimate precision limit of multiparameter quantum magnetometry under the parallel scheme". In: *Physical Review Letters* 125.2 (2020), p. 020501.

[100] Zixin Huang, Chiara Macchiavello, and Lorenzo Maccone. "Usefulness of entanglement-assisted quantum metrology". In: *Phys. Rev. A* 94.1 (2016), p. 012101. ISSN: 2469-9926. DOI: `10.1103/PhysRevA.94.012101`. arXiv: `1603.03993`. URL: `http://arxiv.org/abs/1603.03993http://link.aps.org/doi/10.1103/PhysRevA.94.012101`.

[101] Susanna F Huelga et al. "Improvement of frequency standards with quantum entanglement". In: *Physical Review Letters* 79.20 (1997), p. 3865.

[102] Hiroshi Imai and Akio Fujiwara. "Geometry of optimal estimation scheme for SU (D) channels". In: *J. Phys. A* 40.16 (2007), pp. 4391–4400. ISSN: 1751-8113. DOI: `10.1088/1751-8113/40/16/009`. URL: `http://stacks.iop.org/1751-8121/40/i=16/a=009?key=crossref.f8d601b52a434175cf0dca30e668f7b9`.

[103] Jean-Christophe Jaskula et al. "Superresolution optical magnetic imaging and spectroscopy using individual electronic spins in diamond". In: *Opt. Express* 25.10 (2017), pp. 11048–11064. DOI: 10.1364/OE.25.011048. URL: http://opg.optica.org/oe/abstract.cfm?URI=oe-25-10-11048.

[104] J R Johansson, P D Nation, and Franco Nori. "QuTiP: An open-source Python framework for the dynamics of open quantum systems". In: (). 1110.0573v2. DOI: 1110.0573v2.

[105] Jonas Kahn and Mădălin Guţă. "Local Asymptotic Normality for Finite Dimensional Quantum Systems". In: *Commun. Math. Phys.* 289.2 (2009), pp. 597–652. ISSN: 0010-3616. DOI: 10.1007/s00220-009-0787-3. URL: http://www.springerlink.com/index/10.1007/s00220-009-0787-3http://link.springer.com/10.1007/s00220-009-0787-3.

[106] Vishal Katariya and Mark M. Wilde. "Geometric distinguishability measures limit quantum channel estimation and discrimination". In: *arXiv:2004.10708* (2020). arXiv: 2004.10708. URL: http://arxiv.org/abs/2004.10708.

[107] Gurneet Kaur and Paola Cappellaro. "Initialization and readout of spin chains for quantum information transport". In: *New Journal of Physics* 14.8 (2012), p. 083005. DOI: 10.1088/1367-2630/14/8/083005. URL: https://app.dimensions.ai/details/publication/pub.1023580192andhttps://doi.org/10.1088/1367-2630/14/8/083005.

[108] Pauli Kehayias et al. "Solution nuclear magnetic resonance spectroscopy on a nanostructured diamond chip". In: *Nature Communications* 8 (Aug. 2017). DOI: 10.1038/s41467-017-00266-4.

[109] J. Kennedy. "The particle swarm: social adaptation of knowledge". In: (1997), pp. 303–308. DOI: 10.1109/ICEC.1997.592326.

[110] Jukka Kiukas, Kazuya Yuasa, and Daniel Burgarth. "Remote Parameter Estimation in a Quantum Spin Chain Enhanced by Local Control". In: *Physical Review A* 95.5 (2017). 10.1103/PhysRevA.95.052132, p. 052132. ISSN: 2469-9926. DOI: 10.1103/PhysRevA.95.052132. URL: http://arxiv.org/abs/1701.07399%5Cnhttp://link.aps.org/doi/10.1103/PhysRevA.95.052132.

[111] Bálint Koczor et al. "Variational-State Quantum Metrology". In: *New J. Phys.* (May 2020), in press. DOI: `10.1088/1367-2630/ab965e`.

[112] Piotr Kolenderski and Rafal Demkowicz-Dobrzanski. "Optimal state for keeping reference frames aligned and the platonic solids". In: *Phys. Rev. A* 78.5 (2008), p. 052333. ISSN: 1050-2947. DOI: `10.1103/PhysRevA.78.052333`. URL: `https://link.aps.org/doi/10.1103/PhysRevA.78.052333`.

[113] Shimon Kolkowitz et al. "Gravitational wave detection with optical lattice atomic clocks". In: *ArXiv* 124043 (2016), pp. 1–14. ISSN: 2470-0010. DOI: `10.1103/PhysRevD.94.124043`. arXiv: `1606.01859`. URL: `http://arxiv.org/abs/1606.01859`.

[114] Naoto Kura and Masahito Ueda. "Finite-error metrological bounds on multi-parameter Hamiltonian estimation". In: *Phys. Rev. A* 97.1 (2018), p. 012101. ISSN: 2469-9926. DOI: `10.1103/PhysRevA.97.012101`. arXiv: `1708.09556`. URL: `http://arxiv.org/abs/1708.09556https://link.aps.org/doi/10.1103/PhysRevA.97.012101`.

[115] Akihiro Kuwahata et al. "Magnetometer with nitrogen-vacancy center in a bulk diamond for detecting magnetic nanoparticles in biomedical applications". In: *Scientific Reports* 10 (Feb. 2020). DOI: `10.1038/s41598-020-59064-6`.

[116] G. de Lange et al. "Universal Dynamical Decoupling of a Single Solid-State Spin from a Spin Bath". In: *Science* 330.6000 (2010), pp. 60–63. DOI: `10.1126/science.1192739`. eprint: `https://www.science.org/doi/pdf/10.1126/science.1192739`. URL: `https://www.science.org/doi/abs/10.1126/science.1192739`.

[117] Gijs de Lange et al. "Controlling the quantum dynamics of a mesoscopic spin bath in diamond." In: *Scientific reports* 2.9 (2012). 10.1038/srep00382, p. 382. ISSN: 2045-2322. DOI: `10.1038/srep00382`. URL: `http://www.nature.com/srep/2012/120425/srep00382/full/srep00382.html%5Chttp://www.ncbi.nlm.nih.gov/pubmed/22536480%5Chttp://arxiv.org/abs/1104.4648%5Chttp://www.pubmedcentral.nih.gov/articlerender.fcgi?artid=3336181&tool=pmcentrez&rendertype=abstract`.

[118]   Jing Liu and Haidong Yuan. "Control-enhanced multiparameter quantum estimation". In: *Physical Review A* (2017). ISSN: 24699934. DOI: `10.1103/ PhysRevA.96.042114`. arXiv: `1710.06741`.

[119]   Jing Liu and Haidong Yuan. "Control-enhanced multiparameter quantum estimation". In: *Phys. Rev. A* 96 (4 2017), p. 042114. DOI: `10.1103/ PhysRevA.96.042114`. URL: `https://link.aps.org/doi/10. 1103/PhysRevA.96.042114`.

[120]   Jing Liu et al. "Quantum Fisher information for density matrices with arbitrary ranks". In: (2013). arXiv: `arXiv:1312.6910v1`.

[121]   Jing Liu et al. "Quantum Fisher information matrix and multiparameter estimation". In: *Journal of Physics A: Mathematical and Theoretical* 53 (Nov. 2019). DOI: `10.1088/1751-8121/ab5d4d`.

[122]   Jing Liu et al. "Quantum Fisher information matrix and multiparameter estimation". In: *J. Phys. A* 53.2 (2020), p. 023001. ISSN: 1751-8113. DOI: `10.1088/1751-8121/ab5d4d`. arXiv: `1907.08037`. URL: `http: //arxiv.org/abs/1907.08037https://iopscience.iop. org/article/10.1088/1751-8121/ab5d4d`.

[123]   Nana Liu and Hugo Cable. "Quantum-enhanced multi-parameter estimation for unitary photonic systems". In: *Quantum Sci. Technol.* 2.2 (2017), p. 025008. ISSN: 2058-9565. DOI: `10.1088/2058-9565/aa6fea`. arXiv: `1612. 03621`. URL: `http://stacks.iop.org/2058-9565/2/i=2/a= 025008?key=crossref.7522acfdc074f3f624b80eece2adb419`.

[124]   Yi-Xiang Liu, Ashok Ajoy, Paola Cappellaro, et al. "Nanoscale vector dc magnetometry via ancilla-assisted frequency up-conversion". In: *Physical review letters* 122.10 (2019), p. 100501.

[125]   J. Löfberg. "YALMIP : a toolbox for modeling and optimization in MATLAB". In: *2004 IEEE Int. Conf. Robot. Autom.* Taipei, Taiwan: IEEE, 2004, pp. 284–289. ISBN: 0-7803-8636-1. DOI: `10.1109/CACSD.2004.1393890`. URL: `http://ieeexplore.ieee.org/document/1393890/`.

[126]   Katarzyna Macieszczak. "Quantum Fisher Information: Variational principle and simple iterative algorithm for its efficient computation". In: 2.4 (2013). arXiv: `1312.1356`. URL: `http://arxiv.org/abs/1312.1356`.

[127] D. MacLaurin et al. "Nanoscale magnetometry through quantum control of nitrogen-vacancy centres in rotationally diffusing nanodiamonds". In: *New Journal of Physics* (2013). ISSN: 13672630. DOI: 10.1088/1367-2630/15/1/013041. arXiv: 1207.5276.

[128] HJ Mamin et al. "Nanoscale nuclear magnetic resonance with a nitrogen-vacancy spin sensor". In: *Science* 339.6119 (2013), pp. 557–560.

[129] Ugo Marzolino and Toma ž Prosen. "Quantum metrology with nonequilibrium steady states of quantum spin chains". In: *Phys. Rev. A* 90 (6 2014), p. 062130. DOI: 10.1103/PhysRevA.90.062130. URL: https://link.aps.org/doi/10.1103/PhysRevA.90.062130.

[130] Keiji Matsumoto. "A new approach to the Cramér-Rao-type bound of the pure-state model". In: *J. Phys. A* 35.13 (2002), pp. 3111–3123. ISSN: 0305-4470. DOI: 10.1088/0305-4470/35/13/307. URL: http://iopscience.iop.org/0305-4470/35/13/307.

[131] P Maurer et al. "Room-Temperature Quantum Bit Memory Exceeding One Second". In: *Science (New York, N.Y.)* 336 (June 2012), pp. 1283–6. DOI: 10.1126/science.1220513.

[132] J R Maze et al. "Nanoscale magnetic sensing using spin qubits in diamond". In: (). DOI: 10.1117/12.813802.

[133] Johannes Jakob Meyer, Johannes Borregaard, and Jens Eisert. "A variational toolbox for quantum multi-parameter estimation". In: *arXiv:2006.06303* (2020). arXiv: 2006.06303. URL: http://arxiv.org/abs/2006.06303.

[134] Utkarsh Mishra and Abolfazl Bayat. "Driving Enhanced Quantum Sensing in Partially Accessible Many-Body Systems". In: *Phys. Rev. Lett.* 127 (8 2021), p. 080504. DOI: 10.1103/PhysRevLett.127.080504. URL: https://link.aps.org/doi/10.1103/PhysRevLett.127.080504.

[135] Utkarsh Mishra and Abolfazl Bayat. *Integrable quantum many-body sensors for AC field sensing*. 2021. arXiv: 2105.13507 [quant-ph]. URL: https://arxiv.org/abs/2105.13507.

[136] Hiroshi Nagaoka. "A New Approach to Cramér-Rao Bounds for Quantum State Estimation". In: *IEICE Tech. Rep.* IT 89-42 (1989), pp. 9–14.

[137] Carmine Napoli et al. "Towards Superresolution Surface Metrology: Quantum Estimation of Angular and Axial Separations". In: *Phys. Rev. Lett.* 122.14 (2019), p. 140505. ISSN: 0031-9007. DOI: `10.1103/PhysRevLett.122.140505`. arXiv: `1805.04116`. URL: `http://arxiv.org/abs/1805.04116https://link.aps.org/doi/10.1103/PhysRevLett.122.140505`.

[138] Beatrice Nash, Vlad Gheorghiu, and Michele Mosca. "Quantum circuit optimizations for NISQ architectures". In: *Quantum Sci. Technol.* 5.2 (2020), p. 025010. ISSN: 2058-9565. DOI: `10.1088/2058-9565/ab79b1`. arXiv: `1904.01972v3`. URL: `https://iopscience.iop.org/article/10.1088/2058-9565/ab79b1`.

[139] P. Neumann et al. "High-precision nanoscale temperature sensing using single defects in diamond". In: *Nano Letters* 13.6 (2013), pp. 2738–2742. ISSN: 15306984. DOI: `10.1021/nl401216y`. arXiv: `arXiv:1304.0688v1`.

[140] H.T. Ng and K. Kim. "Quantum estimation of magnetic-field gradient using W-state". In: *Optics Communications* 331 (2014), pp. 353–358. ISSN: 0030-4018. DOI: `https://doi.org/10.1016/j.optcom.2014.06.048`. URL: `https://www.sciencedirect.com/science/article/pii/S0030401814005951`.

[141] Rosanna Nichols et al. "Multiparameter Gaussian Quantum Metrology". In: (2017). arXiv: `1711.09132`.

[142] Michael A Nielsen. "The Fermionic canonical commutation relations and the Jordan-Wigner transform". In: *Notes* (2005), pp. 1–8.

[143] L. O'Driscoll, R. Nichols, and P. A. Knott. "A hybrid machine learning algorithm for designing quantum experiments". In: *Quantum Mach. Intell.* 1.1-2 (2019), pp. 5–15. ISSN: 2524-4906. DOI: `10.1007/s42484-019-00003-8`. arXiv: `1812.03183`. URL: `http://link.springer.com/10.1007/s42484-019-00003-8`.

[144] M. G. A. Paris, G. M. D'Ariano, and M. F. Sacchi. "Maximum-likelihood method in quantum estimation". In: *AIP Conference Proceedings* 568.1 (2001), pp. 456–467. DOI: `10.1063/1.1381908`. eprint: `https://aip.scitation.org/doi/pdf/10.1063/1.1381908`. URL: `https://aip.scitation.org/doi/abs/10.1063/1.1381908`.

[145] Matteo G. A. Paris. "Quantum estimation for quantum technology". In: (2008). ISSN: 0219-7499. DOI: `10.1142/S0219749909004839`. arXiv: `0804.2981`. URL: `http://arxiv.org/abs/0804.2981`.

[146] Matteo G. A. Paris. "Quantum estimation for quantum technology". In: *Int. J. Quantum Inf.* 07.supp01 (2009), pp. 125–137. ISSN: 0219-7499. DOI: `10.1142/S0219749909004839`. URL: `http://www.worldscientific.com/doi/abs/10.1142/S0219749909004839`.

[147] Michał Parniak et al. "Beating the Rayleigh Limit Using Two-Photon Interference". In: *Phys. Rev. Lett.* 121.25 (2018), p. 250503. ISSN: 0031-9007. DOI: `10.1103/PhysRevLett.121.250503`. URL: `https://link.aps.org/doi/10.1103/PhysRevLett.121.250503`.

[148] R.L. Patel et al. "Subnanotesla Magnetometry with a Fiber-Coupled Diamond Sensor". In: *Phys. Rev. Applied* 14 (4 2020), p. 044058. DOI: `10.1103/PhysRevApplied.14.044058`. URL: `https://link.aps.org/doi/10.1103/PhysRevApplied.14.044058`.

[149] Adam Payne et al. "Optimizing the Orbital Occupation in the Multiple Minima Problem of Magnetic Materials from the Metaheuristic Firefly Algorithm". In: *Physical Chemistry Chemical Physics* 21 (Sept. 2019). DOI: `10.1039/C9CP03618K`.

[150] Luca Pezzè et al. "Quantum metrology with nonclassical states of atomic ensembles". In: *Rev. Mod. Phys.* 90.3 (2018), p. 035005. ISSN: 0034-6861. DOI: `10.1103/RevModPhys.90.035005`. arXiv: `1609.01609`. URL: `http://arxiv.org/abs/1609.01609https://link.aps.org/doi/10.1103/RevModPhys.90.035005`.

[151] Yuting Ping et al. "Practicality of Spin Chain Wiring in Diamond Quantum Technologies". In: *Phys. Rev. Lett.* 110 (10 2013), p. 100503. DOI: `10.1103/PhysRevLett.110.100503`. URL: `https://link.aps.org/doi/10.1103/PhysRevLett.110.100503`.

[152] Stefano Pirandola et al. "Advances in photonic quantum sensing". In: *Nat. Photonics* 12.12 (2018), pp. 724–733. ISSN: 1749-4885. DOI: `10.1038/s41566-018-0301-6`. arXiv: `1811.01969`. URL: `https://arxiv.org/abs/1811.01969?fbclid=IwAR35PxfmQ-GkIabzx8AzfTXWdzW7irlTq7UXpzEA//www.nature.com/articles/s41566-018-0301-6`.

[153] Martin B Plenio. "Remarks on Duality Transformations and Generalized Stabilizer States". In: (2008). 0703007v1, pp. 1–5. DOI: 0703007v1. arXiv: 0703007v1 [quant-ph].

[154] Emanuele Polino et al. "Experimental multiphase estimation on a chip". In: *Optica* 6.3 (2019), pp. 288–295.

[155] Emanuele Polino et al. "Photonic quantum metrology". In: *AVS Quantum Sci.* 2.2 (2020), p. 024703. ISSN: 2639-0213. DOI: 10.1116/5.0007577. arXiv: 2003.05821. URL: http://arxiv.org/abs/2003.05821http://avs.scitation.org/doi/10.1116/5.0007577.

[156] V.P. Popov et al. "Long dephasing time of NV center spins in diamond layers formed by hot ion implantation and high pressure high temperature annealing". In: *Diamond and Related Materials* 120 (2021), p. 108675. ISSN: 0925-9635. DOI: https://doi.org/10.1016/j.diamond.2021.108675. URL: https://www.sciencedirect.com/science/article/pii/S0925963521004386.

[157] Steven. Prawer and Igor. Aharonovich. *Quantum information processing with diamond : principles and applications*. Woodhead Publishing, 2014, p. 367. ISBN: 9780857096562.

[158] Matematica Pura and Domenico D Alessandro. "The Lie Algebra Structure and Nonlinear Controllability of Spin Systems". In: (). 0106115v2, pp. 1–22. DOI: 0106115v2. arXiv: 0106115v2 [quant-ph].

[159] I. I. Rabi. "On the Process of Space Quantization". In: *Phys. Rev.* 49 (4 1936), pp. 324–328. DOI: 10.1103/PhysRev.49.324. URL: https://link.aps.org/doi/10.1103/PhysRev.49.324.

[160] Markus Rademacher, James Millen, and Ying Lia Li. "Quantum sensing with nanoparticles for gravimetry: when bigger is better". In: *Advanced Optical Technologies* 9.5 (2020), pp. 227–239.

[161] Sammy Ragy, Marcin Jarzyna, and Rafał Demkowicz-Dobrzański. "Compatibility in multiparameter quantum metrology". In: *Phys. Rev. A* 94.5 (2016), p. 052108. ISSN: 2469-9926. DOI: 10.1103/PhysRevA.94.052108. arXiv: 1608.02634. URL: http://arxiv.org/abs/1608.02634http://link.aps.org/doi/10.1103/PhysRevA.94.052108.

[162] Surjeet Rajendran et al. "A method for directional detection of dark matter using spectroscopy of crystal defects". In: *Phys. Rev. D* 96 (3 2017), p. 035009. DOI: `10.1103/PhysRevD.96.035009`. URL: `https://link.aps.org/doi/10.1103/PhysRevD.96.035009`.

[163] Chandrasekhar Ramanathan et al. "Experimental characterization of coherent magnetization transport in a one-dimensional spin system". In: *New Journal of Physics* 13.10 (2011), p. 103015. DOI: `10.1088/1367-2630/13/10/103015`. URL: `https://app.dimensions.ai/details/publication/pub.1020434569andhttps://doi.org/10.1088/1367-2630/13/10/103015`.

[164] C. Radhakrishna Rao. *Information and the Accuracy Attainable in the Estimation of Statistical Parameters*. Ed. by Samuel Kotz and Norman L. Johnson. New York, NY: Springer New York, 1992, pp. 235–247. ISBN: 978-1-4612-0919-5. DOI: `10.1007/978-1-4612-0919-5_16`. URL: `https://doi.org/10.1007/978-1-4612-0919-5_16`.

[165] Emanuele Roccia et al. "Entangling measurements for multiparameter estimation with two qubits". In: *Quantum Sci. Technol.* 3.1 (2018), 01LT01. ISSN: 2058-9565. DOI: `10.1088/2058-9565/aa9212`. arXiv: `1704.03327`. URL: `http://arxiv.org/abs/1704.03327http://stacks.iop.org/2058-9565/3/i=1/a=01LT01?key=crossref.fdfb01c16cae8d9708632d7b68455c11`.

[166] Emanuele Roccia et al. "Multiparameter approach to quantum phase estimation with limited visibility". In: *Optica* 5.10 (2018), p. 1171. ISSN: 2334-2536. DOI: `10.1364/OPTICA.5.001171`. URL: `https://www.osapublishing.org/abstract.cfm?URI=optica-5-10-1171`.

[167] L. Rondin et al. "Magnetometry with nitrogen-vacancy defects in diamond". In: (Nov. 2013). 10.1088/0034-4885/77/5/056503. DOI: `10.1088/0034-4885/77/5/056503`. URL: `http://arxiv.org/abs/1311.5214http://dx.doi.org/10.1088/0034-4885/77/5/056503`.

[168] Benjamin Rowland et al. "Implementing quantum logic gates with GRAPE: principles and practicalities". In: (2012). 1203.6260v1. DOI: `1203.6260v1`.

[169] D. Rugar et al. "Proton magnetic resonance imaging using a nitrogen-vacancy spin sensor". In: *Nature Nanotechnology* 10.2 (2015), pp. 120–124. ISSN: 17483395. DOI: `10.1038/nnano.2014.288`. arXiv: `1406.2983`. URL: `http://dx.doi.org/10.1038/nnano.2014.288`.

[170] Mohan Sarovar and Gerard J. Milburn. "Optimal estimation of one-parameter quantum channels". In: *J. Phys. A* 39.26 (2006), pp. 8487–8505. ISSN: 0305-4470. DOI: `10.1088/0305-4470/39/26/015`. URL: `http://stacks.iop.org/0305-4470/39/i=26/a=015?key=crossref.65db86c1224c8edf8990368ef62c3755`.

[171] Marco Sbroscia et al. "Experimental ancilla-assisted phase estimation in a noisy channel". In: *Phys. Rev. A* 97.3 (2018), p. 032305. ISSN: 2469-9926. DOI: `10.1103/PhysRevA.97.032305`. arXiv: `arXiv:1707.08792v1`. URL: `https://link.aps.org/doi/10.1103/PhysRevA.97.032305`.

[172] Romana Schirhagl et al. "Nitrogen-Vacancy Centers in Diamond: Nanoscale Sensors for Physics and Biology". In: *Annual Review of Physical Chemistry* 65.1 (2014). PMID: 24274702, pp. 83–105. DOI: `10.1146/annurev-physchem-040513-103659`. eprint: `https://doi.org/10.1146/annurev-physchem-040513-103659`. URL: `https://doi.org/10.1146/annurev-physchem-040513-103659`.

[173] Simon Schmitt et al. "Submillihertz magnetic spectroscopy performed with a nanoscale quantum sensor". In: *Science* (2017). ISSN: 10959203. DOI: `10.1126/science.aam5532`. arXiv: `1706.02103`.

[174] Pavel Sekatski et al. "Quantum metrology with full and fast quantum control". In: *Quantum* 1 (2017), p. 27. ISSN: 2521-327X. DOI: `10.22331/q-2017-09-06-27`. arXiv: `1603.08944`. URL: `http://arxiv.org/abs/1603.08944http://quantum-journal.org/papers/q-2017-09-06-27/`.

[175] Robert J. Sewell et al. "Magnetic Sensitivity Beyond the Projection Noise Limit by Spin Squeezing". In: *Phys. Rev. Lett.* 109.25 (2012), p. 253605. ISSN: 0031-9007. DOI: `10.1103/PhysRevLett.109.253605`. arXiv: `1111.6969`. URL: `https://link.aps.org/doi/10.1103/PhysRevLett.109.253605`.

[176]   J. H. Shim et al. "Robust dynamical decoupling for arbitrary quantum states of a single NV center in diamond". In: *EPL (Europhysics Letters)* 99.4 (2012), p. 40004. DOI: 10.1209/0295-5075/99/40004. URL: https://doi.org/10.1209/0295-5075/99/40004.

[177]   Chang S Shin et al. "Room-temperature operation of a radiofrequency diamond magnetometer near the shot-noise limit". In: *Journal of Applied Physics* 112.12 (2012), p. 124519.

[178]   Michael Skotiniotis, Pavel Sekatski, and Wolfgang D??r. "Quantum metrology for the Ising Hamiltonian with transverse magnetic field". In: *New Journal of Physics* 17.7 (2015). 10.1088/1367-2630/17/7/073032. ISSN: 13672630. DOI: 10.1088/1367-2630/17/7/073032.

[179]   P. B. M. Sousa and R. V. Ramos. "Universal Quantum Circuit for N-Qubit Quantum Gate: A Programmable Quantum Gate". In: *Quantum Info. Comput.* 7.3 (Mar. 2007), pp. 228–242. ISSN: 1533-7146.

[180]   C. J. Stephen et al. "Deep Three-Dimensional Solid-State Qubit Arrays with Long-Lived Spin Coherence". In: *Phys. Rev. Applied* 12 (6 2019), p. 064005. DOI: 10.1103/PhysRevApplied.12.064005. URL: https://link.aps.org/doi/10.1103/PhysRevApplied.12.064005.

[181]   Vladimir M Stojanovi. "Lie algebraic aspects of quantum control in interacting spin-1/2 (qubit) chains". In: *Lecture notes* (2014).

[182]   Barnaby van Straaten and Bálint Koczor. "Measurement cost of metric-aware variational quantum algorithms". In: *arXiv:2005.05172* 2005.05172 (2020). arXiv: 2005.05172. URL: http://arxiv.org/abs/2005.05172.

[183]   Wen Yang Sun et al. "Exploration quantum steering, nonlocality and entanglement of two-qubit X-state in structured reservoirs". In: *Scientific Reports* 7.November 2016 (2017), pp. 1–9. ISSN: 20452322. DOI: 10.1038/srep39651.

[184]   Jun Suzuki. "Classification and characterization of quantum parametric models in quantum estimation theory". In: *arXiv:1807.06990* 21.7 (2018), p. 703. ISSN: 1099-4300. DOI: 10.3390/e21070703. arXiv: 1807.06990. URL: https://arxiv.org/abs/1807.06990.

[185] Jun Suzuki. "Explicit formula for the Holevo bound for two-parameter qubit-state estimation problem". In: *J. Math. Phys.* 57.4 (2016), p. 042201. ISSN: 0022-2488. DOI: 10.1063/1.4945086. arXiv: 1505.06437. URL: http://aip.scitation.org/doi/10.1063/1.4945086.

[186] Magdalena Szczykulska, Tillmann Baumgratz, and Animesh Datta. "Multi-parameter Quantum Metrology". In: ().

[187] Magdalena Szczykulska, Tillmann Baumgratz, and Animesh Datta. "Multi-parameter quantum metrology". In: *Adv. Phys. X* 1.4 (2016), pp. 621–639. ISSN: 2374-6149. DOI: 10.1080/23746149.2016.1230476. arXiv: 1604.02615. URL: http://arxiv.org/abs/1604.02615https://www.tandfonline.com/doi/full/10.1080/23746149.2016.1230476.

[188] M. Takagi and A. Kawanaka. "Estimation of static magnetic field and gradient fields from NMR image". In: *Journal of physics. E, Scientific instruments* 19.10 (1986), pp. 871–875.

[189] Jacob Taylor et al. "High-sensitivity diamond magnetometer with nanoscale resolution". In: *Nature Physics* 7 (May 2008). DOI: 10.1038/nphys1075.

[190] Weng-Kian Tham, Hugo Ferretti, and Aephraim M. Steinberg. "Beating Rayleigh's Curse by Imaging Using Phase Information". In: *Phys. Rev. Lett.* 118.7 (2017), p. 070801. ISSN: 0031-9007. DOI: 10.1103/PhysRevLett.118.070801. arXiv: 1606.02666. URL: http://arxiv.org/abs/1606.02666http://link.aps.org/doi/10.1103/PhysRevLett.118.070801.

[191] Géza Tóth. "Multipartite entanglement and high-precision metrology". In: *Phys. Rev. A* 85 (2 2012), p. 022322. DOI: 10.1103/PhysRevA.85.022322. URL: https://link.aps.org/doi/10.1103/PhysRevA.85.022322.

[192] Geza Toth and Iagoba Apellaniz. "Quantum metrology from a quantum information science perspective". In: (2014). ISSN: 17518121. DOI: 10.1088/1751-8113/47/42/424006. arXiv: 1405.4878.

[193] Mankei Tsang, Francesco Albarelli, and Animesh Datta. "Quantum Semiparametric Estimation". In: *Phys. Rev. X* 10.3 (2020), p. 031023. ISSN: 2160-3308. DOI: 10.1103/PhysRevX.10.031023. arXiv: 1906.09871. URL:

http://arxiv.org/abs/1906.09871https://link.aps.org/doi/10.1103/PhysRevX.10.031023.

[194] Mankei Tsang, Ranjith Nair, and Xiao-Ming Lu. "Quantum Theory of Superresolution for Two Incoherent Optical Point Sources". In: *Phys. Rev. X* 6.3 (2016), p. 031033. ISSN: 2160-3308. DOI: 10.1103/PhysRevX.6.031033. arXiv: 1511.00552. URL: https://link.aps.org/doi/10.1103/PhysRevX.6.031033.

[195] Mihai D. Vidrighin et al. "Joint estimation of phase and phase diffusion for quantum metrology". In: *Nat. Commun.* 5.1 (2014), p. 3532. ISSN: 2041-1723. DOI: 10.1038/ncomms4532. arXiv: arXiv:1410.5353v1. URL: http://www.ncbi.nlm.nih.gov/pubmed/24727938http://www.nature.com/articles/ncomms4532.

[196] Nisheeth K. Vishnoi. "Geodesic Convex Optimization: Differentiation on Manifolds, Geodesics, and Convexity". In: (2018). arXiv: 1806.06373 [math.OC].

[197] Kunkun Wang et al. "Entanglement-enhanced quantum metrology in a noisy environment". In: *Phys. Rev. A* 97.4 (2018), p. 042112. ISSN: 2469-9926. DOI: 10.1103/PhysRevA.97.042112. arXiv: arXiv:1707.08790v1. URL: https://link.aps.org/doi/10.1103/PhysRevA.97.042112.

[198] Mark M. Wilde. *Quantum Information Theory*. Cambridge: Cambridge University Press, 2013. ISBN: 9781139525343. DOI: 10.1017/CBO9781139525343. URL: http://www.markwilde.com/qit-notes.pdf.

[199] Thomas Wolf et al. "Subpicotesla diamond magnetometry". In: *Physical Review X* 5.4 (2015), p. 041001.

[200] James D A Wood et al. "Microwave-free nuclear magnetic resonance at molecular scales". In: *Nature Communications* 8.May (2017). 10.1038/ncomms15950, pp. 1–6. ISSN: 20411723. DOI: 10.1038/ncomms15950. URL: http://dx.doi.org/10.1038/ncomms15950.

[201] William K. Wootters. "Entanglement of Formation of an Arbitrary State of Two Qubits". In: *Phys. Rev. Lett.* 80.10 (1998), pp. 2245–2248. DOI: 10.1103/PhysRevLett.80.2245. URL: https://link.aps.org/doi/10.1103/PhysRevLett.80.2245.

[202] Jörg Wrachtrup and Fedor Jelezko. "Quantum information processing in diamond". In: (). URL: `https://iopscience.iop.org/article/10.1088/0953-8984/18/21/S08`.

[203] Shyue-Jian Wu and Pei-Tse Chow. "Steady-state genetic algorithms for discrete optimization of trusses". In: *Comput. Struct.* 56.6 (1995), pp. 979–991. ISSN: 00457949. DOI: `10.1016/0045-7949(94)00551-D`. URL: `https://linkinghub.elsevier.com/retrieve/pii/004579499400551D`.

[204] Koichi Yamagata, Akio Fujiwara, and Richard D. Gill. "Quantum local asymptotic normality based on a new quantum likelihood ratio". In: *Ann. Stat.* 41.4 (2013), pp. 2197–2217. ISSN: 0090-5364. DOI: `10.1214/13-AOS1147`. URL: `http://projecteuclid.org/euclid.aos/1382547518`.

[205] Pengcheng Yang et al. "Complete Quantum-State Tomography with a Local Random Field". In: *Phys. Rev. Lett.* 124 (1 2020), p. 010405. DOI: `10.1103/PhysRevLett.124.010405`. URL: `https://link.aps.org/doi/10.1103/PhysRevLett.124.010405`.

[206] Xiaodong Yang et al. "Probe optimization for quantum metrology via closed-loop learning control". In: *npj Quantum Inf.* 6.1 (2020), p. 62. ISSN: 2056-6387. DOI: `10.1038/s41534-020-00292-z`. arXiv: `2006.09730`. URL: `http://arxiv.org/abs/2006.09730http://www.nature.com/articles/s41534-020-00292-z`.

[207] Yuxiang Yang, Giulio Chiribella, and Masahito Hayashi. "Attaining the ultimate precision limit in quantum state estimation". In: *arXiv:1802.07587* 368.1 (2018), pp. 223–293. ISSN: 0010-3616. DOI: `10.1007/s00220-019-03433-4`. arXiv: `1802.07587`. URL: `http://arxiv.org/abs/1802.07587`.

[208] N. Y. Yao et al. "Robust quantum state transfer in random unpolarized spin chains". In: *Physical Review Letters* 106.4 (2011). 10.1103/PhysRevLett.106.040505, pp. 1–4. ISSN: 00319007. DOI: `10.1103/PhysRevLett.106.040505`.

[209] N. Young. "An Introduction to Hilbert Space". In: (1988). DOI: `10.1017/CBO9781139172011`.

[210] Thomas Young. "I. The Bakerian Lecture. Experiments and calculations relative to physical optics". In: *Philosophical transactions of the Royal Society of London* 94 (1804), pp. 1–16.

[211] Zhixian Yu and Sudhakar Prasad. "Quantum Limited Superresolution of an Incoherent Source Pair in Three Dimensions". In: *Phys. Rev. Lett.* 121.18 (2018), p. 180504. ISSN: 0031-9007. DOI: `10.1103/PhysRevLett.121.180504`. arXiv: `1805.09227`. URL: `https://doi.org/10.1103/PhysRevLett.121.180504https://link.aps.org/doi/10.1103/PhysRevLett.121.180504`.

[212] Haidong Yuan. "Sequential Feedback Scheme Outperforms the Parallel Scheme for Hamiltonian Parameter Estimation". In: *Phys. Rev. Lett.* 117.16 (2016), p. 160801. ISSN: 0031-9007. DOI: `10.1103/PhysRevLett.117.160801`. URL: `http://link.aps.org/doi/10.1103/PhysRevLett.117.160801https://link.aps.org/doi/10.1103/PhysRevLett.117.160801`.

[213] Sebastian Zaiser et al. "Enhancing quantum sensing sensitivity by a quantum memory". In: *Nature Communications* 7 (2016), p. 12279. ISSN: 2041-1723. DOI: `10.1038/ncomms12279`. URL: `http://www.nature.com/doifinder/10.1038/ncomms12279`.

[214] Fuzhen Zhang, ed. *The Schur Complement and Its Applications*. Vol. 4. Numerical Methods and Algorithms. New York: Springer-Verlag, 2005. ISBN: 0-387-24271-6. DOI: `10.1007/b105056`. URL: `http://link.springer.com/10.1007/b105056`.

[215] J.M. Zhang and Y. Liu. "Witnessing a Poincaré recurrence with Mathematica". In: *Results in Physics* 7 (2017), pp. 3373–3379. ISSN: 2211-3797. DOI: `https://doi.org/10.1016/j.rinp.2017.08.055`. URL: `https://www.sciencedirect.com/science/article/pii/S2211379717313104`.

[216] Wei Zhong et al. "Fisher information under decoherence in Bloch representation". In: *Physical Review A - Atomic, Molecular, and Optical Physics* 87.2 (2013), pp. 1–16. ISSN: 10502947. DOI: `10.1103/PhysRevA.87.022337`. arXiv: `arXiv:1212.0917v2`.

[217] Sisi Zhou et al. "Achieving the Heisenberg limit in quantum metrology using quantum error correction". In: *Nat. Commun.* 9.1 (2018), p. 78. ISSN: 2041-1723. DOI: `10.1038/s41467-017-02510-3`. arXiv: `1706.02445`. URL: `https://arxiv.org/pdf/1706.02445.pdfhttp:`

`//arxiv.org/abs/1706.02445http://www.nature.com/ articles/s41467-017-02510-3`.

[218]   Jaroslav Řeháček et al. "Multiparameter quantum metrology of incoherent point sources: Towards realistic superresolution". In: *Phys. Rev. A* 96.6 (2017), p. 062107. ISSN: 2469-9926. DOI: `10.1103/PhysRevA.96. 062107`. arXiv: `1709.07705`. URL: `http://arxiv.org/abs/1709. 07705https://link.aps.org/doi/10.1103/PhysRevA.96. 062107`.

Do not go gentle into that good
night,
Old age should burn and rave at
close of day;
Rage, rage against the dying of the
light.

_____
Dylan Thomas